LEPTON UNIVERSALITY

Michel Davier
Laboratoire de l'Accélérateur Linéaire
IN2P3-CNRS et Université de Paris-Sud
91405 Orsay
France

ABSTRACT

The topic of lepton universality is directly related to the structure of the fundamental fermion fields and the dynamics generating it. It can be investigated independently for the charged and the neutral weak interactions. The precise measurements of the neutral couplings achieved at LEP and SLC are the key ingredients for the investigation of electroweak radiative corrections and the indirect investigation of the Higgs sector. Since it is heavy enough to decay into hadrons, the τ lepton has turned into a nice source of QCD studies, including the most precise determination of the strong coupling constant.

Introduction

During recent years, a great deal has been learned about leptons through the experimental program at LEP and SLC. It is well-known that e^+e^- annihilation is a democratic supplier of leptons and quarks. In addition, the large cross section provided by the existence of the Z resonance enabled the experiments to register important statistics of leptons, hence opening a field of precision measurements unheard of before in high-energy physics.

These lectures emphasize the properties of the leptonic couplings to the gauge bosons. In the Standard Model, a universal structure is assumed for the couplings of leptons and quarks to the γ, W, and Z bosons. The new experimental data can test this structure with great accuracy.

Nobody questions today the fascinating universality of the electric charge of leptons which measures their coupling to the photon. This property is imbedded in the universal QED theory which, however, tells us nothing about the existence of quark and lepton families. The situation might be different with the electroweak interaction, whose structure could have some relation to the particle spectrum. The driving force for investigating so aggressively the problem of universality rests on the possibility that violations might be discovered, thereby unveiling some clue about the puzzling family structure of matter.

The lectures are organized as follows:

(i) **Leptonic W couplings**: Universality of the couplings in the weak charged current is investigated in order to confirm the structure assumed in the Standard Model or find departures.

(ii) **Leptonic Z couplings**: The same approach is applied to the electroweak neutral current. In addition to testing universality, precise determination of the leptonic couplings provides a fascinating tool to explore the electroweak vacuum, with information on very massive fermions like the top quark and the Higgs sector of the theory.

(iii) **The τ, a peculiar standard lepton**: The τ lepton has standard electroweak properties, as discussed in the previous lectures. But, owing to its relatively large mass, it can decay into hadrons as well as into leptons, opening a field of study of the strong interactions (QCD) in a very clean and favorable environment. The recent results from these studies will be presented and discussed.

1 Leptonic W Couplings

1.1 Structure of Leptonic Charged-Current Interaction

The general four-fermion interaction is well-described theoretically[1] under the assumptions of locality, a derivative-free Lagrangian, and lepton number conservation. The most general amplitude for the transition shown in Fig. 1(a) contains *a priori* 12 complex coupling constants:

$$M = \frac{4G}{\sqrt{2}} \sum_{\substack{\gamma=S,V,T \\ \lambda,\mu=R,L}} g^{\gamma}_{\lambda\mu} \; [\bar{l}_{\lambda}\Gamma_{\gamma}\nu_l] \; [\overline{\nu}_{l'}\Gamma^{\gamma} l'_{\mu}], \tag{1}$$

where G is the Fermi constant, γ describes the current type (scalar S, vector V, or tensor T) and λ, μ are the chiralities of the charged fermions. It should be remarked that the helicities of the neutrinos ν_l and $\overline{\nu}_{l'}$ are determined by the choice of γ, λ, and μ. Of the 12 couplings, only ten are relevant since $g^T_{RR} = g^T_{LL} = 0$, so that only(!) 19 independent real parameters are involved.

Let us introduce the probabilities $Q_{\lambda\mu}$ for a lepton l_{λ} to yield a lepton l'_{μ} in the transition. They can be simply expressed in terms of the couplings through

$$\sum_{\lambda,\mu} Q_{\lambda\mu} = 1 \tag{2}$$

with

$$Q_{RR} = \frac{1}{4}|g^S_{RR}|^2 + |g^V_{RR}|^2, \tag{3}$$

$$Q_{RL} = \frac{1}{4}|g^S_{RL}|^2 + |g^V_{RL}|^2 + 3|g^T_{RL}|^2, \tag{4}$$

$$Q_{LR} = \frac{1}{4}|g^S_{LR}|^2 + |g^V_{LR}|^2 + 3|g^T_{LR}|^2, \tag{5}$$

$$Q_{LL} = \frac{1}{4}|g^S_{LL}|^2 + |g^V_{LL}|^2. \tag{6}$$

In the Standard Model, only $V - A$ currents are involved and all the couplings vanish, except $g^V_{LL} = 1$. Consequently, $Q_{LL} = 1$ and $Q_{RR} = Q_{RL} = Q_{LR} = 0$.

1.2 Leptonic Weak Decay

Consider the electronic decay of a charged lepton,

$$l \longrightarrow \nu_l \; e \; \overline{\nu}_e, \tag{7}$$

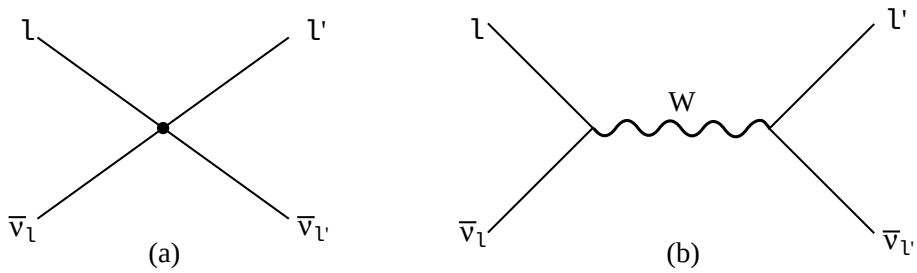

Fig. 1. *Charged-current four-fermion transition: (a) local limit in the general case, (b) Standard Model.*

according to the phenomenology of Sec. 1.1 and ignoring for the moment radiative corrections. To first order in the ratio $\frac{m_e}{m_l}$, the decay distribution of a polarized lepton is given in its center of mass by

$$\frac{d\Gamma(l^{\pm})}{d\Omega dx} = \frac{G^2 m_l^5}{192\pi^4} x^2 \{3(1-x) + \frac{2}{3}\rho(4x-3) + 6\eta \frac{m_e}{m_l}\frac{1-x}{x} \pm \xi P_l \cos\theta[1-x+\frac{2}{3}\delta(4x-3)]\}, \tag{8}$$

where θ is the angle between the electron momentum and the lepton polarization (P_l) and $x = \frac{E_e}{E_l}$. The quantities ρ, η, ξ, and δ are called Michel parameters and they can be expressed in terms of the $g^{\gamma}_{\lambda\mu}$ coupling constants. For example:

$$\rho = \frac{3}{4}\{1 - |g^V_{LR}|^2 + |g^V_{RL}|^2 + 2|g^T_{LR}|^2 + 2|g^T_{RL}|^2 + Re(g^S_{LR} g^{T^*}_{LR} + g^S_{RL} g^{T^*}_{RL})\}, \tag{9}$$

$$\eta = \frac{1}{2} Re\{6 g^V_{RL} g^{T^*}_{LR} + 6 g^V_{LR} g^{T^*}_{RL} + g^S_{RR} g^{V^*}_{LL} + g^S_{LL} g^{V^*}_{RR} g^S_{RL} g^{V^*}_{LR} + g^S_{LR} g^{V^*}_{RL}\}. \tag{10}$$

Thus, four parameters of the general matrix element can be determined. In the Standard Model, one has $\rho = \delta = \frac{3}{4}$, $\xi = 1$, and $\eta = 0$. Notice that η is an interesting quantity to study, as a small contribution from $g^{S^*}_{RR}$ could be detected through the interference with the dominant coupling $g^{V^*}_{LL}$.

The measurement of the x dependence of the electron polarization (through Möller scattering of the final state electron on a magnetized foil) allows the determination of six more parameters, leaving, however, an ambiguity between g^S_{LL} and g^V_{LL}.

To proceed further, one needs information about the final state neutrinos. This is not possible on an event-by-event basis, but fortunately the inverse β-decay process

$$\nu_l \; e \longrightarrow l \; \nu_e \tag{11}$$

is measurable in practice for $l = \mu$, thanks to the existence of intense muon neutrino beams. Experiment tells us that such ν_μ beams prepared from $\pi^+ \to \mu^+\nu_\mu$ have a well-defined helicity,[2]

$$|2\lambda_{\nu_\mu}| = |h_{\nu_\mu}| = |h_{\mu^+}| > 0.9959. \tag{12}$$

The cross section for (11) receives no contribution from g^S_{LL}. Since the measurement yields a nonzero value,[3] the dominance of g^V_{LL} over g^S_{LL} is established, thus breaking the degeneracy.

1.3 Experiments on Muon Decay

Beautiful experiments were carried out at TRIUMF and PSI in the '80s with polarized muons from π decays.[4] The shape of the electron energy spectrum determines ρ, while the decay asymmetry (the correlation between the electron momentum and the muon polarization) yields ξ and $\frac{\xi\delta}{\rho}$ at the end point ($x \simeq 1$). After measurement of the electron polarization, one obtains $Q_{LL} > 0.95$ while the other probabilities are consistent with zero. As explained in Sec. 1.2, the degeneracy between g^V_{LL} and g^S_{LL} is lifted giving

$$g^V_{LL} > 0.96, \qquad\qquad g^S_{LL} < 0.55, \tag{13}$$

at the 90% C.L. The full information on the couplings is given in Fig. 2, which displays the allowed regions for the reduced quantities

$$g'^{\gamma}_{\lambda\mu} = \frac{g^\gamma_{\lambda\mu}}{max(g^\gamma_{\lambda\mu})}, \tag{14}$$

where $max(g^\gamma_{\lambda\mu}) = 2, 1, \frac{1}{\sqrt{3}}$ for $\gamma = S, V, T$, respectively.

1.4 Experiments on τ Decays

1.4.1 The Process $e^-e^+ \to \tau^-\tau^+$

Experimental information from τ decays comes solely from e^+e^- data through the process $e^+e^- \to \tau^+\tau^-$. Two channels are kinematically open: $\tau^- \to \nu_\tau e^- \overline{\nu}_e$ and $\tau^- \to \nu_\tau \mu^- \overline{\nu}_\mu$. For both of them, Eq. (8) applies with the relevant label changes.

Data originate from two sets of experiments: *(i)* at $\sqrt{s} \simeq 10$ GeV (ARGUS, CLEO) where $P_\tau \simeq 0$ and *(ii)* at $\sqrt{s} \simeq M_Z$ (ALEPH, DELPHI, L3, OPAL, SLD)

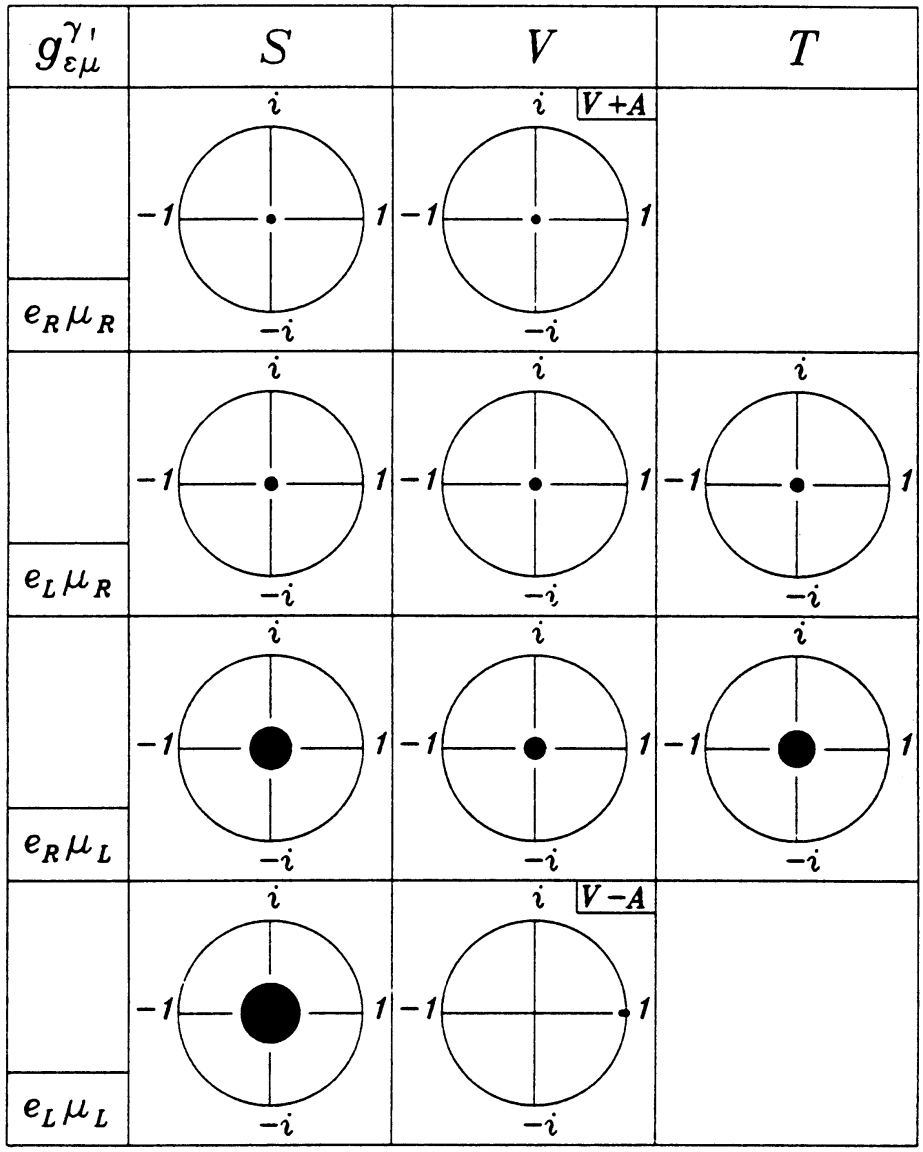

Fig. 2. 90% *C.L. limits for the reduced couplings* $g^{l\gamma}_{\lambda\mu}$ *in the decay* $\mu^- \to \nu_\mu e^- \overline{\nu}_e$ *(Ref. 5).*

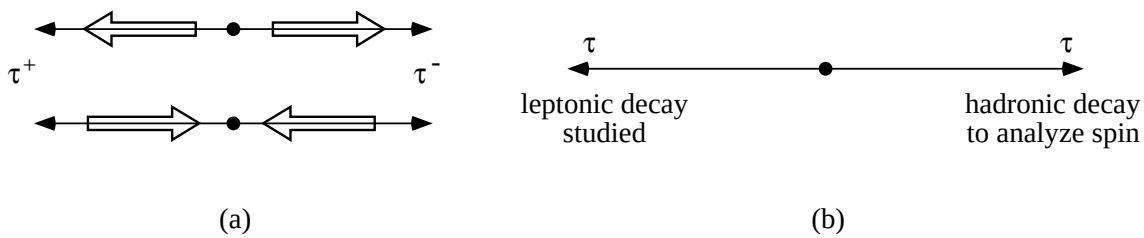

Fig. 3. *Helicity correlation in $e^-e^+ \to \tau^-\tau^+$: (a) the two contributing states at high energy, (b) the tagging helicity scheme.*

with $P_\tau \simeq -0.15$ (at LEP). The fact that the τ polarization is small, or even vanishes, can be circumvented since the two back-to-back τ's are produced with a very large correlation between their spins. This is the consequence of helicity conservation for V, A interactions in the high-energy limit, $\frac{\sqrt{s}}{m_\tau} \to \infty$.

As a consequence only $J_z = \pm 1$ states are produced in e^+e^- annihilation [Fig. 3(a)], corresponding to the two only nonzero transitions: $e^-_L e^+_R \to \tau^-_L \tau^+_R$ and $e^-_R e^+_L \to \tau^-_R \tau^+_L$. This provides an efficient way to produce polarized τ's under the scheme indicated in Fig. 3(b): The hadronic decay of one of the two τ's is used as a spin analyzer (following the method described in the next section), thereby tagging the helicity of the opposite τ, whose decay properties can then be studied.

1.4.2 τ Helicity Determination

Owing to the spin-zero pion, the simplest τ decay mode to use to analyze the τ polarization is $\tau \to \nu_\tau \pi$. Assuming the same $V-A$ structure as in $\pi \to \mu\nu$ decay, the π angular distribution in the center of mass is correlated with the τ helicity (Fig. 4).

The decay amplitude is proportional to $\cos\frac{\theta^*}{2}$ (*resp.* $\sin\frac{\theta^*}{2}$) for τ^-_R (*resp.* τ^-_L), yielding a decay rate $\sim 1+\cos\theta^*$ (*resp.* $\sim 1-\cos\theta^*$). Thus, the decay rate for a τ with helicity λ_τ is

$$\frac{1}{\Gamma}\frac{d\Gamma}{d\cos\theta^*} = 1 + 2\lambda_\tau \cos\theta^*, \tag{15}$$

yielding after a Lorentz boost

$$\frac{1}{\Gamma}\frac{d\Gamma}{dx} = 1 + 2\lambda_\tau(2x-1) \tag{16}$$

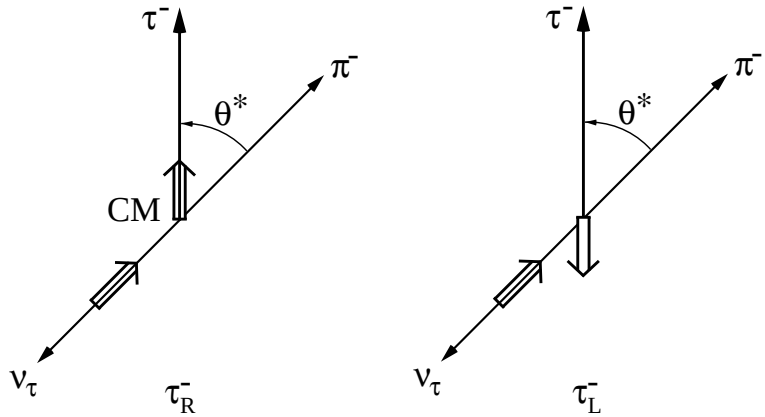

Fig. 4. *Decay of a polarized* τ, τ_R^- *or* τ_L^-, *into* $\nu_\tau \pi$.

where $x = \frac{E_\pi}{E_\tau}$. For a sample of τ leptons, the polarization is given by $P_\tau = 2 \langle \lambda_\tau \rangle$. The expected decay distributions for samples of τ_R^- or τ_L^- are given in Fig. 5.

The simplest case can be extended for any τ decay mode[6] $\tau \to \nu_\tau X$, where X decays into a final state described by a set of observables $\vec{\xi}$. Assuming only $V-A$ structure, the decay rate (16) can be generalized to

$$\frac{1}{\Gamma}\frac{d\Gamma}{d\vec{\xi}} = f(\vec{\xi}) + P_\tau g(\vec{\xi}). \tag{17}$$

At every point in $\vec{\xi}$ space, one defines the variable ω through

$$\omega = \frac{g(\vec{\xi})}{f(\vec{\xi})}. \tag{18}$$

The probability density distribution for ω

$$\frac{1}{\Gamma}\frac{d\Gamma}{d\cos\theta} = \hat{f}(\omega)\{1 + P_\tau \omega\} \tag{19}$$

shows the same linear behavior as for the π case. Thus, with no loss in sensitivity, a difficult analysis in the multidimensional $\vec{\xi}$ space is reduced to a straightforward one-dimensional problem with the variable ω which analyzes optimally the τ polarization.

One can define the sensitivity S of an observable for the determination of the τ polarization in a sample of N decay events through $S^{-1} = \sigma_{P_\tau}\sqrt{N}$, where σ_{P_τ} is the achieved statistical uncertainty on the measurement of P_τ. Table 1 gives the

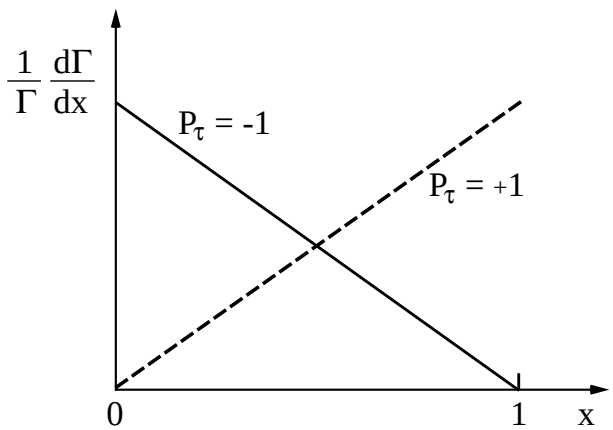

Fig. 5. *Energy spectra for τ_R^- and τ_L^- decay into $\nu_\tau \pi^-$.*

values for the sensitivity which can be achieved in the various τ decay modes. It should be emphasized that only decay channels with known dynamics [providing the functions $f(\vec{\xi})$ and $g(\vec{\xi})$] can be used, already accounting for 91% of all modes. Except for the leptonic channels, where the missing neutrinos cause a large loss of information, all the hadronic modes reach the maximal sensitivity when the full decay information is used, including the knowledge of the τ direction which can be kinematically reconstructed.

If ν_τ is not assumed to be left-handed, the parameter

$$h_\tau = 2\lambda_{\nu_\tau} \tag{20}$$

can be left free to be determined by experiment. In this case, Eq. (19) can be rewritten as

$$\frac{1}{\Gamma}\frac{d\Gamma}{d\cos\theta} = \hat{f}(\omega)\{1 - h_\tau P_\tau \omega\}. \tag{21}$$

1.4.3 Results on τ Couplings

The most complete analysis of τ decay parameters has been performed by ALEPH[7] using all polarization-sensitive states in Table 1. A global fit of the helicity correlation distributions renders values for ρ, η, ξ, $\xi\delta$, and h_τ. However, the most precise results come from a very recent work by CLEO[8] using only the $l\overline{\nu}_l - \rho$ and $\rho - \rho$ correlated states, but with large statistics. In the first pair, the ρ side is the polarization analyzer for the leptonic hemisphere, and ρ, $h_\tau\xi$, and $h_\tau\xi\delta$ are

channel X	observables $\vec{\xi}$	sensitivity S
$l\overline{\nu}_l$	x_l	0.22
π^-	x_π	0.58
$\rho^-(\to \pi^-\pi^0)$	x_ρ	0.26
	+ decay variables	0.49
	+ τ direction	0.58
$a_1^-(\to \rho\pi)$	x_{a_1}	0.03
$\hookrightarrow \pi\pi$	+ decay variables	0.44
	+ τ direction	0.58

Table 1. *Sensitivity to τ polarization which can be achieved in the τ decay channels $\tau^- \to \nu_\tau X$ with different sets of observables $\vec{\xi}$.*

deduced for decays into an electron or a muon. The second pair of decays is used for the measurement of h_τ^2. The technique is illustrated in Fig. 6. The sign of h_τ is known from previous experiments.[9] The results of CLEO given in Table 2 improve the precision of the previous world-average values by factors of two to three. When expressed in terms of the phenomenological $g^{l\gamma}_{\lambda\mu}$ couplings, they yield the allowed regions indicated in Fig. 7.

The results from leptonic τ decays are consistent with those from μ decay, although they are less precise by a factor of ~ 5 due to the much smaller available statistics. However, they allow the investigation of a larger variety of lepton pairs: $e-\tau$ and $\mu-\tau$ as compared to $e-\mu$ in μ decay. The ambiguity between g^V_{LL} and g^S_{LL} cannot be resolved for the τ because the process $\nu_\tau e \to \tau\nu_e$ has not yet been measured—a situation unlikely to change for some time!

The charged weak τ current is therefore dominantly left-handed. The probability for a transition involving a right-handed τ is

$$P^\tau_R = Q_{RR} + Q_{LR} < 0.44 \tag{22}$$

at 90% C.L.

Since the τ measurements are limited by statistics, a large potential for improvement can be obtained from high-luminosity machines, such as B factories and a dedicated τ-charm factory.

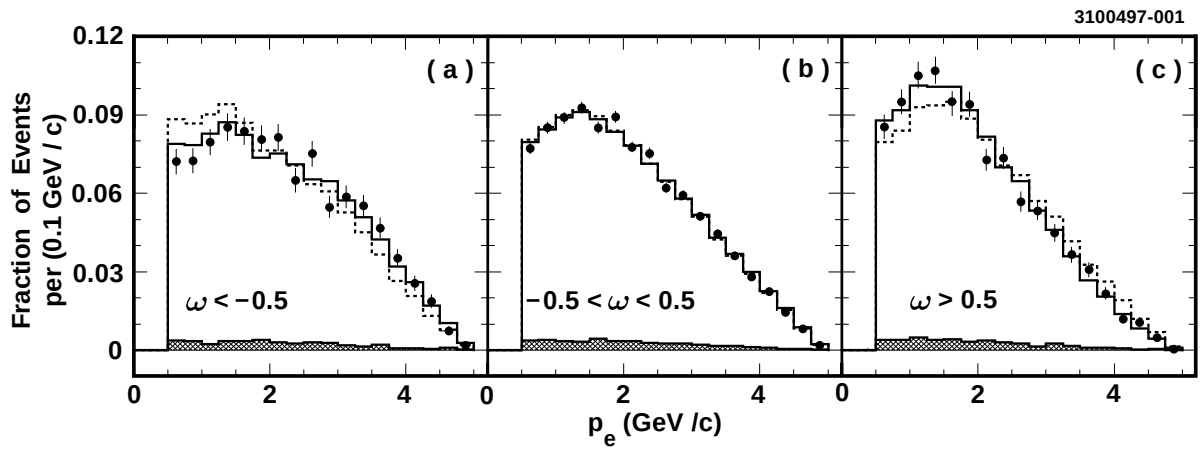

Fig. 6. *CLEO results*[8] *on hemisphere helicity correlations. The top plots show the electron energy distributions for different* ω *values of the opposite decay into a* ρ*: a clear correlation is seen. The bottom plots display the same behavior when the two hemispheres contain* ρ *decays.*

	world average[10]	CLEO[8]
h_τ	-1.011 ± 0.027	$-0.995 \pm 0.010 \pm 0.003$
ρ	0.742 ± 0.027	$0.747 \pm 0.010 \pm 0.006$
ξ	1.03 ± 0.12	$1.007 \pm 0.040 \pm 0.015$
$\xi\delta$	0.76 ± 0.11	$0.745 \pm 0.026 \pm 0.009$
ρ_e	0.736 ± 0.028	$0.747 \pm 0.012 \pm 0.004$
ξ_e	1.03 ± 0.25	$0.979 \pm 0.048 \pm 0.016$
$\xi_e\delta_e$	1.11 ± 0.18	$0.720 \pm 0.032 \pm 0.010$
ρ_μ	0.74 ± 0.04	$0.750 \pm 0.017 \pm 0.045$
ξ_μ	1.23 ± 0.24	$1.054 \pm 0.069 \pm 0.047$
$\xi_\mu\delta_\mu$	0.71 ± 0.15	$0.786 \pm 0.041 \pm 0.032$

Table 2. *Measurements of Michel parameters in leptonic* τ *decays and of the parameter* h_τ.

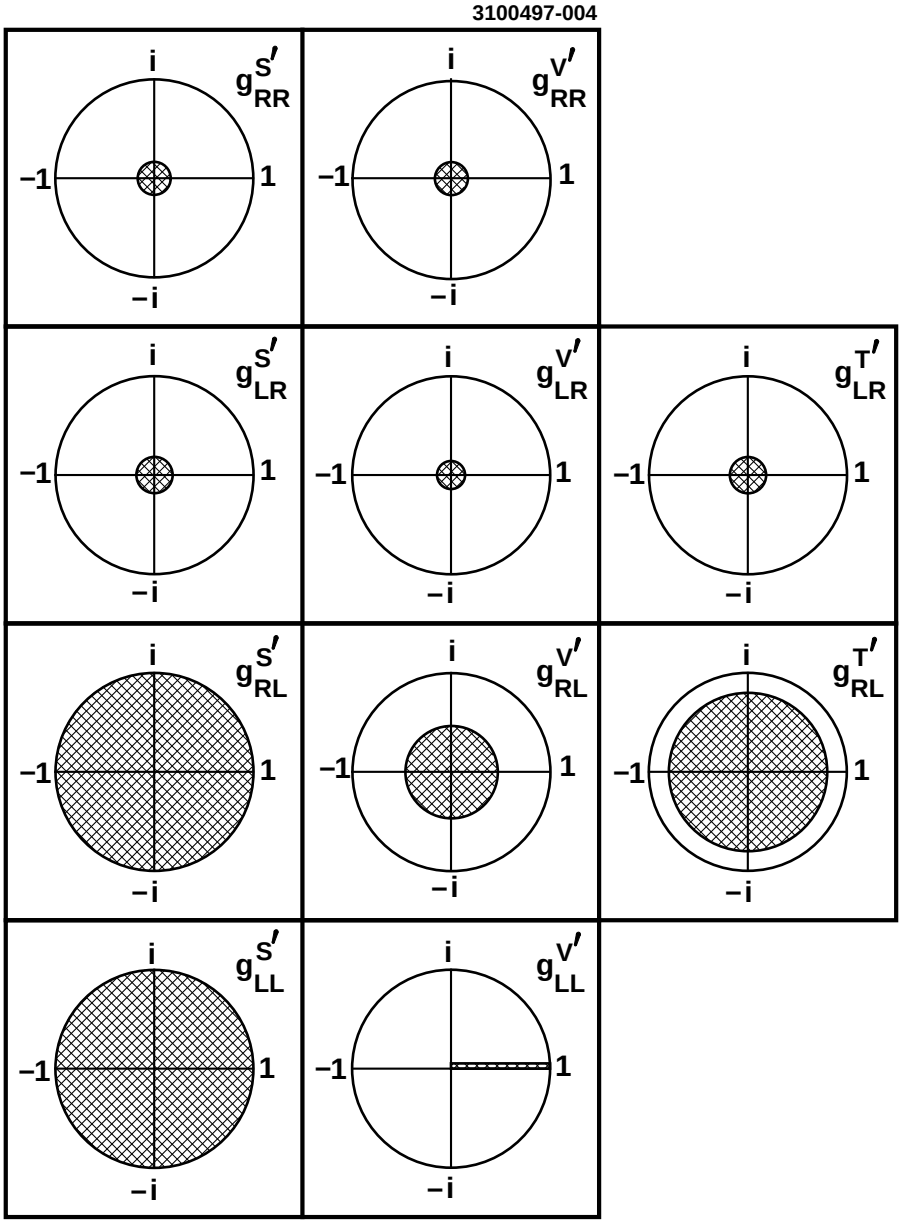

Fig. 7. 90% *C.L. limits for the reduced couplings* $g^{l\gamma}_{\lambda\mu}$ *in the decay* $\tau^- \to \nu_\tau l^- \overline{\nu}_l$ *(Ref. 8).*

1.5 Chirality of the Vector Current

Data on μ and τ decays have shown that scalar and tensor currents are below experimental sensitivity and that the weak charged transitions involve a dominant left-handed vector current. Assuming that only vector currents contribute, it is possible to investigate more directly the chirality structure of the interaction. The general vector current has the form

$$J^{\mu} = -i\frac{g_l}{\sqrt{2}}\,\overline{\nu}_l\gamma^{\mu}(\frac{v_l - a_l\gamma^5}{2})l. \tag{23}$$

The chirality information can be derived from the parameter

$$h_l = -\frac{2a_l v_l}{a_l^2 + v_l^2}, \tag{24}$$

already introduced in the previous section on τ decays. The parameter h_l is often referred to as the "ν_l helicity." In the Standard Model, one has: $v_l = a_l = 1$ and $h_l = -1$.

The Michel parameters can be expressed as functions of h_l given below for muon decay

$$\rho = \frac{3}{8}(1 + h_e h_\mu), \tag{25}$$

$$\xi = 2h_e - h_\mu, \tag{26}$$

$$\xi\delta = \frac{3}{8}(h_e + h_\mu). \tag{27}$$

Similar expressions hold for the two τ leptonic decays with the proper replacement of labels.

The experimental results on the Michel parameters can be summarized in the (h_e, h_μ), (h_e, h_τ), and (h_μ, h_τ) planes, as shown in Fig. 8, displaying very nicely the chiral nature of the weak current.

1.6 Placing Constraints on New Physics

The physics of the weak charged current may (and probably will) require an extension of the Standard Model (SM). In that case, some deviation will occur between a given observable and its SM prediction. Two possibilities are briefly examined here.

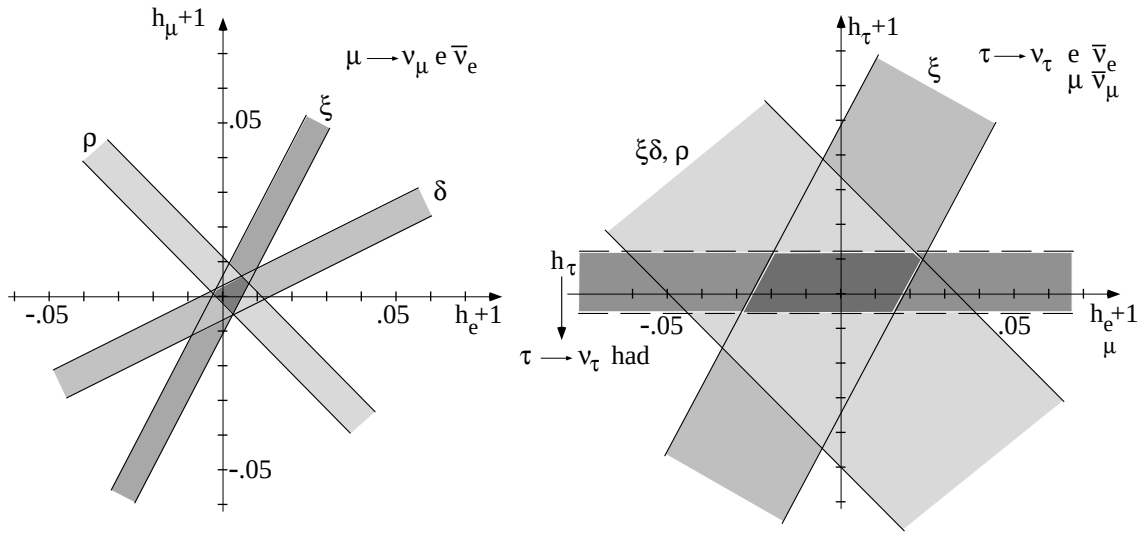

Fig. 8. *The experimental results on Michel parameters in μ and τ leptonic decays are consistent with a left-handed vector current. Also shown is the direct measurement of h_τ in hadronic τ decays. In the Standard Model, $h_e = h_\mu = h_\tau = -1$.*

1.6.1 New Vector Currents

The simplest and most natural extension of the maximally parity-violating theory based on the $SU(2)_L \times U(1)$ gauge group is provided by the group $SU(2)_L \times SU(2)_R \times U(1)$ where parity invariance is restored at some high mass scale.[11] The two $SU(2)$ groups generate W_L and W_R bosons which mix into the physical states W_1 (observed so far) and W_2 of higher mass.

Constraints on the mixing angle ζ and the W_2 mass expressed through the mass ratio $\alpha = \frac{M_1}{M_2}$ can be obtained from the measurements. The most significant limits come from CLEO[8] and are displayed in Fig. 9 in the $(\alpha, \tan\zeta)$ plane. Integrating over ζ the 90% C.L. limit reached is

$$M_2 > 260 \text{ GeV/c}^2. \tag{28}$$

The corresponding limit from muon decay[10] is

$$M_2 > 406 \text{ GeV/c}^2, \tag{29}$$

but it is valid only for a much less massive ν_{e_R} (less than 1 MeV/c^2).

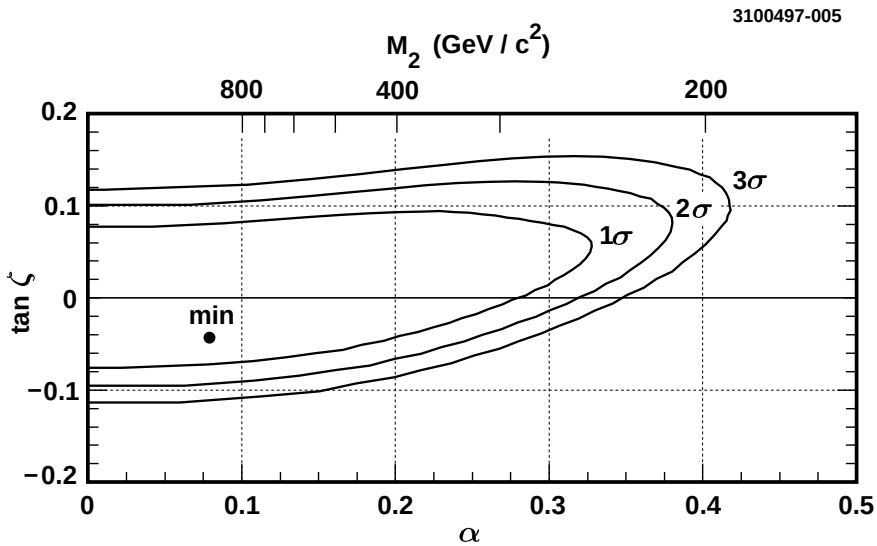

Fig. 9. *The limits obtained by CLEO*[8] *on the mass parameter* α *and the mixing angle* ζ *for* $SU(2)_L \times SU(2)_R \times U(1)$.

1.6.2 Scalar Currents

Charged Higgs bosons can contribute to weak scalar currents which could be detected through a nonzero value for the η parameter. From Eq. (10) to first order, one expects

$$\eta \sim \frac{1}{2} Re\, g^S_{RR}. \tag{30}$$

The experimental result from μ decay,[10]

$$\eta = -0.007 \pm 0.013, \tag{31}$$

is precise, but unfortunately not sensitive to a Higgs coupling (which is proportional to mass). The situation is just the reverse in τ decays: the direct measurement[7,12−14] from τ decays to muons [remember that in the decay rate (8) the η term is proportional to $\frac{m_l}{m_\tau}$],

$$\eta = -0.014 \pm 0.076, \tag{32}$$

does not allow a significant limit to be drawn on the Higgs contribution. However, assuming lepton universality for the dominant vector LL coupling, an indirect determination of η can be obtained by comparing the leptonic widths for $\tau \to$

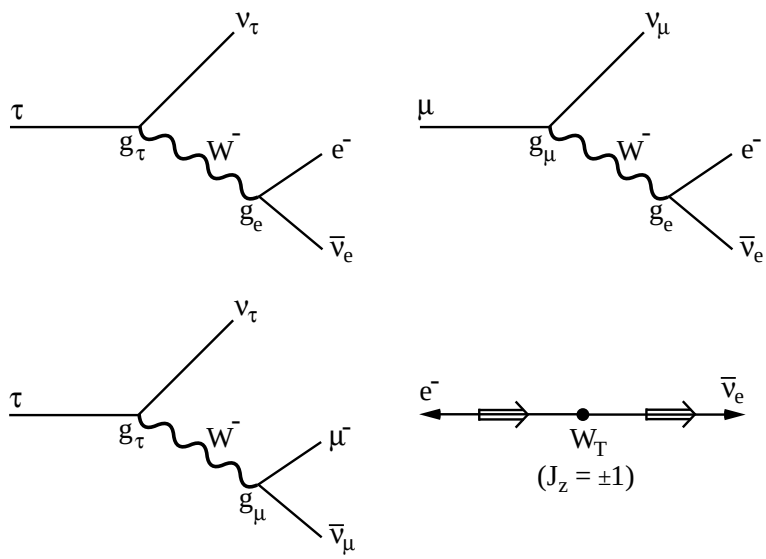

Fig. 10. *Transverse W's.*

$\nu_\tau e \overline{\nu}_e$ and $\tau \to \nu_\tau \mu \overline{\nu}_\mu$. The actual value, three times more precise than Eq. (32), will be discussed in Sec. 2.8.4.

1.7 Strength of the Left-Handed Vector Coupling

Having established the dominance of V–A currents, it remains to investigate the strength of the $Wl\nu_l$ coupling, $\frac{g_l}{\sqrt{2}}$. From μ decay the product $g_e g_\mu$ is related to the Fermi constant G in the local limit,

$$\frac{g_e g_\mu}{8M_W^2} = \frac{G}{\sqrt{2}}, \tag{33}$$

and G is experimentally determined from the muon lifetime τ_μ.

It is important to distinguish between couplings with W's of different helicities, as departures from the SM could affect them differently. The two cases—transverse ($\lambda_W = \pm 1$) and longitudinal ($\lambda_W = 0$)—are illustrated in Figs. 10 and 11. Transverse W's occur in leptonic decays, while only longitudinal W's are involved in decays with pseudoscalar mesons, such as $\pi^+ \to \mu^+ \nu_\mu$ or $\tau \to \nu_\tau \pi^-$. The total rate for leptonic decay can be obtained from Eq. (8) taking into account

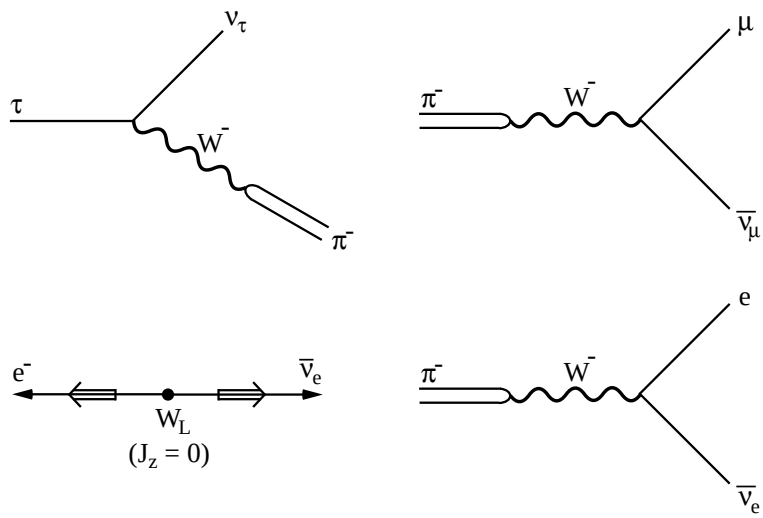

Fig. 11. *Longitudinal W's.*

QED radiative corrections and deviation from locality through the W propagator[15]:

$$\Gamma(\tau \to \nu_\tau l \overline{\nu}_l(\gamma)) = \frac{G_\tau G_l m_\tau^5}{192\pi^3} f_\tau(x_l)\delta_W \delta_\gamma, \tag{34}$$

where

$$G_l = \frac{g_l^2}{4\sqrt{2}M_W^2}, \tag{35}$$

$$\delta_W = 1 + \frac{3}{5}\frac{m_\tau^2}{M_W^2}, \tag{36}$$

$$\delta_\gamma = 1 + \frac{\alpha(m_\tau)}{2\pi}\left(\frac{25}{4} - \pi^2\right), \tag{37}$$

$$f_\tau = 1 - 8x + 8x^3 - x^4 - 12x^2 \ln x, \tag{38}$$

$$x_l = (\frac{m_l}{m_\tau})^2. \tag{39}$$

Similar expressions hold for μ decay with the proper label changes. The occurrence of the m_τ^5 factor in Eq. (34) on purely dimensional grounds bears an important consequence on the practical value for the τ lifetime.

Measurements of the leptonic widths provide a very direct test of universality of the g_l couplings. Through

$$\Gamma(\tau \to \nu_\tau e \overline{\nu}_e) = \frac{B_e}{\tau_\tau}, \tag{40}$$

$$\Gamma(\tau \to \nu_\tau \mu \overline{\nu}_\mu) = \frac{B_\mu}{\tau_\tau}, \tag{41}$$

$$\Gamma(\mu \to \nu_\mu e \overline{\nu}_e) = \frac{1}{\tau_\mu}, \tag{42}$$

where B_e and B_μ are the respective branching fractions for τ decay into the electron and muon final states, ratios of couplings can be obtained:

$$\left(\frac{g_\mu}{g_e}\right)^2_T = \frac{B_\mu}{B_e}\frac{f_\tau(x_e)}{f_\tau(x_\mu)}, \tag{43}$$

$$\left(\frac{g_\tau}{g_\mu}\right)^2_T = B_e \frac{\tau_\mu}{\tau_\tau}\frac{f_\mu(x_e)}{f_\tau(x_e)}\left(\frac{m_\mu}{m_\tau}\right)^5 \delta_{cor}. \tag{44}$$

The correction δ_{cor} can be derived from Eqs. (36) and (37). It is very close to one: $\delta_{cor} - 1 = -2.1 \times 10^{-4}$. All the phase space factors are practically equal to unity, except $f_\tau(x_\mu) = 0.9726$.

Longitudinal couplings are investigated in π decays and τ decay to $\nu_\tau \pi$. The rate for $\pi^+ \to e^+ \nu_e$ is suppressed by helicity compared to $\pi^+ \to \mu^+ \nu_\mu$ by a factor $(\frac{m_e}{m_\mu})^2$, giving

$$\left(\frac{g_e}{g_\mu}\right)^2_L = \frac{\Gamma(\pi \to e\nu_e)}{\Gamma(\pi \to \mu\nu_\mu)}\left(\frac{m_\mu}{m_e}\right)^2\left(\frac{m_\pi^2 - m_\mu^2}{m_\pi^2 - m_e^2}\right)^2 \delta_\pi. \tag{45}$$

Similarly, $\tau - \mu$ universality can be tested comparing the rates for $\tau \to \nu_\tau \pi^-$ and $\pi^- \to \mu \overline{\nu}_\mu$ through the relation

$$\left(\frac{g_\tau}{g_\mu}\right)^2_L = \frac{B_{\tau\to\nu_\tau\pi}}{B_{\pi\to\mu\nu_\mu}}\frac{\tau_\pi}{\tau_\tau}\frac{2m_\tau m_\mu^2}{m_\pi^3}\left(\frac{m_\pi^2 - m_\mu^2}{m_\tau^2 - m_\pi^2}\right)^2 \delta_{\tau,\pi}. \tag{46}$$

The radiative corrections included in the factors δ_π and $\delta_{\tau,\pi}$ have been computed.[16] They are rather involved, including not very well-known contributions depending on the pion structure. They yield $\delta_{\tau,\pi} - 1 = -(1.6\ ^{+0.9}_{-1.4})\ 10^{-3}$.

1.8 Testing Universality in μ, τ, and π Decays

1.8.1 The Measurement of m_τ

To test lepton universality through the relations given in the previous section, it is necessary to know precisely the τ mass. This is particularly true in Eq. (44) because of the fifth power involved. Fortunately, recent measurements of m_τ are

available from the BEPC storage ring in Beijing from a fine-step scan around the $\tau^+\tau^-$ threshold.

In 1992, a first determination was achieved using only 14 $e-\mu$ events yielding $m_\tau = (1776.9\ ^{+0.4}_{-0.5} \pm 0.2_{calib})$ MeV/c^2. More recently, in 1994, a more precise value was published[17] based on 64 events,

$$m_\tau = (1776.96\ ^{+0.18}_{-0.19}\ ^{+0.20}_{-0.16\,calib})\ \mathrm{MeV/c^2}. \tag{47}$$

The cross section measured is shown in Fig. 12. The non-τ background is very small and the threshold behavior is well reproduced after convolving the theoretical yield with the energy resolution of the beams ($\sigma_{\sqrt{s}} = 1.4$ MeV). The value (47) is a considerable improvement over the older result from DELCO[18] of $(1783\ ^{+3}_{-4})$ MeV/c^2. In the meantime, other determinations became available[19] from the study of hadronic τ decays, using the so-called pseudomass assuming $m_{\nu_\tau} = 0$; although they are much less precise than (47), they confirm a lower mass value as compared to the DELCO value.

1.8.2 Measurements of the τ Lifetime

LEP and SLC are the best places to measure τ_τ with precision. Produced τ's are nearly monoenergetic (small radiation loss) and $\tau^+\tau^-$ events can be reconstructed with high efficiency (~ 80 to 90%) and low background ($< 1\%$). Despite the large energy, the decay length is rather small, $\beta\gamma c\tau \simeq 2.2\ mm$, much smaller than the radius of the beampipe. To measure this length from outside the vacuum at a precision level of 1% or less appears to be a formidable task!

Fortunately, several factors play very favorably to reverse the trend:

(i) e^+e^- storage rings have small beam spots in the transverse plane (perpendicular to the beam axis), especially in the vertical direction y along the magnetic field. At LEP, $\sigma_y \sim 10\ \mu m$ and $\sigma_x \sim 150\ \mu m$. The situation is even better with the small emittance beams of SLC, with $\sigma_x \sim \sigma_y \sim 2.5\ \mu m$.

(ii) Experiments have installed very precise vertex detectors just around the beampipe. These solid-state devices are read out with strips (LEP) or pixels as for the CCD detector of SLD. The precision on the impact parameter δ depends on the intrinsic precision of the detector and the distance of extrapolation to the interaction point. Typical values are $\sigma_\delta \sim 10$–$25\ \mu m$.

(iii) Finally, the availability of large samples, $\sim 2 \times 10^5\ \tau\tau$ pairs for each LEP experiment, allows a large reduction of the statistical error. Even more

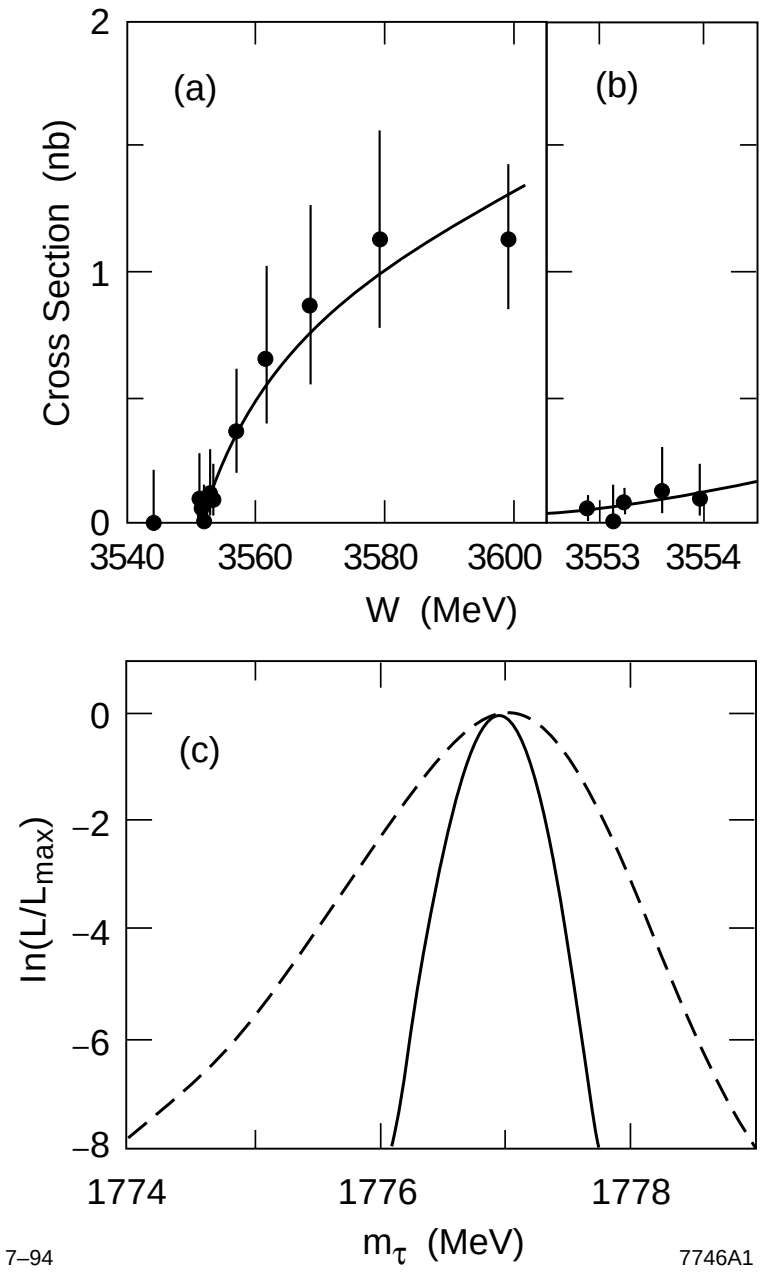

Fig. 12. *Cross section for* $e^-e^+ \to \tau^-\tau^+$ *close to threshold.*[17]

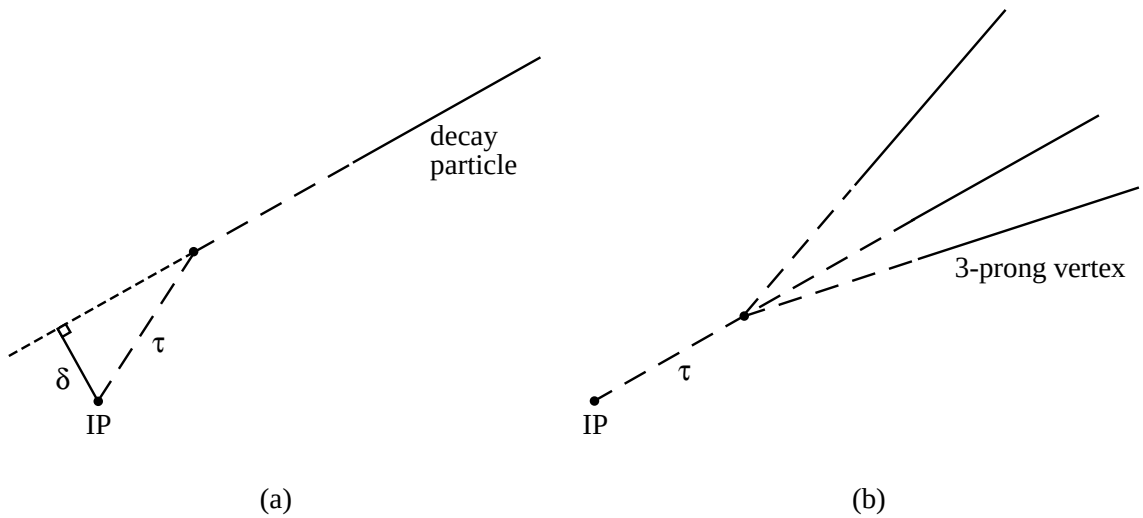

Fig. 13. *Measurement of the τ lifetime through the impact parameter (left) and the decay length (right) approaches.*

importantly, it enables detailed systematic studies to be performed in order to learn about possible biases in the measurement.

Many methods are available to measure the τ lifetime. Initially, only three-prong vertexing was used, with its direct access to the flight distance from the interaction point. Later, it became useful to consider the more numerous one-prong decays through the impact parameter approach (Fig. 13). Several schemes were then developed combining opposite one-prong decays in order to reduce the systematic uncertainties arising from the imperfect knowledge of the true event annihilation point and the true $\tau^+\tau^-$ line of flight usually approximated by the event thrust axis.

The impact parameter sum (IPS) method[20] for one-prong events was designed to be independent of the production point, which can only be known statistically from averaging many non-τ events. However, the method introduces some dependence on the τ direction with systematics for the Monte Carlo simulation. Conversely, the impact parameter difference (IPD) method[21] is sensitive to the beam spot position, but has no dependence on decay angles, nor on the resolution function. Finally, a new approach combining the advantages of both methods was introduced for events where both τ's decay hadronically. This three-dimensional impact parameter (3D-IP) method[22] takes advantage of double-sided vertex de-

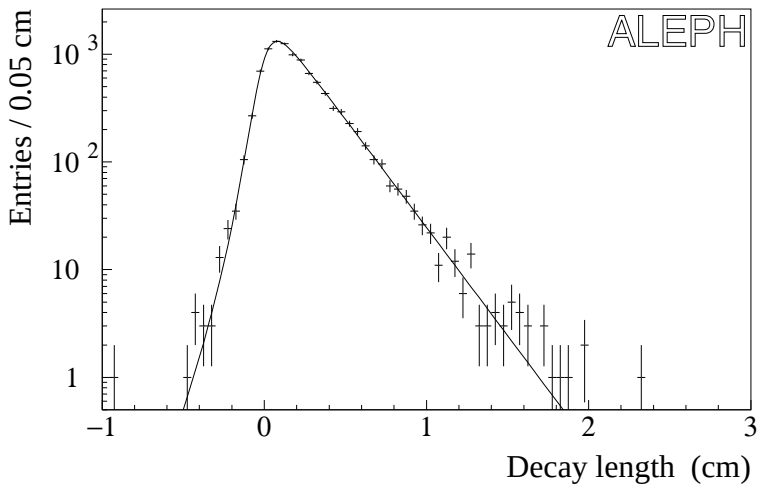

Fig. 14. *Decay length distribution for three-prong τ decays.*[24] *The curve represents the fit function, obtained by convolving the decay exponential shape with the detector resolution function. The effect of resolution is clearly seen for (unphysical) negative values of the decay length. The slope provides the measurement of τ_τ.*

tectors with readout of two orthogonal coordinates. In these events, where only two neutrinos are missing, it is possible to reconstruct the $\tau^+\tau^-$ direction up to a two-fold ambiguity.[23]

All these approaches involve a delicate trade-off between beam size uncertainty, approximation of the true τ line of flight, and sensitivity to detector resolution. The resulting compromise depends obviously on the detector design, but also on the accelerator properties. It may also be time-dependent; as with the increase in statistics, a given method may surpass its competitors because of smaller systematic uncertainties. *A priori*, the best conditions are met with the SLD detector at SLC. However, the data accumulated so far does not yet offset the advantage offered by the large statistics available to the LEP detectors.

Illustrative examples of some of the methods are given in Figs. 14 and 15.

The most recent τ_τ measurements are given in Table 3 (Ref. 25). The combined values of the different methods taking into account the correlations are shown in Fig. 16. Good agreement is observed between the different experiments, leading to a world-average value

$$\tau_\tau = (290.2 \pm 1.2)\ fs. \tag{48}$$

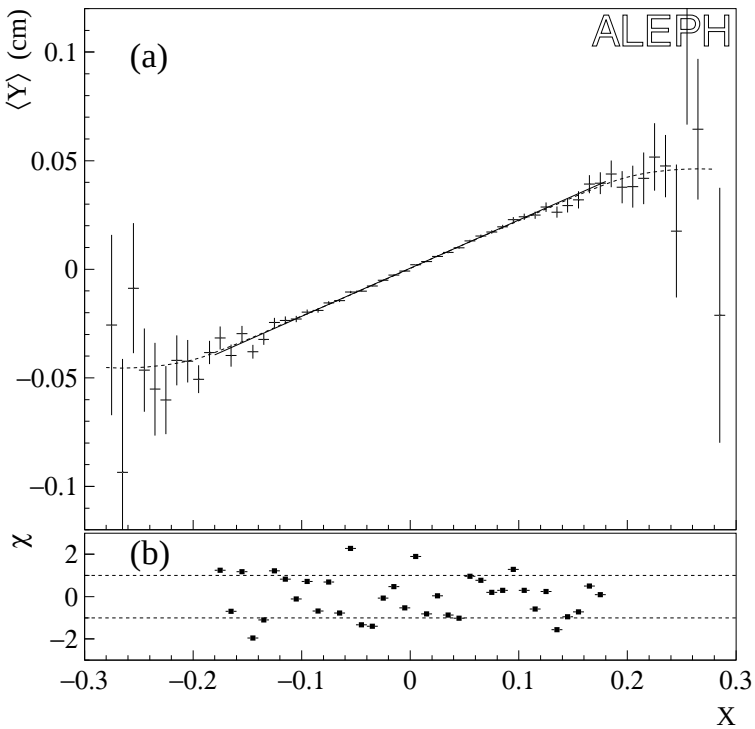

Fig. 15. *Distribution used to fit the τ lifetime in the IPD method.*[24] *The quantity Y is the impact parameter difference $\delta = \delta_+ - \delta_-$, while $X = \sin\theta\,\Delta\phi$, where $\Delta\phi$ is the acoplanarity between the two secondary tracks.*

experiment/data set	method	lifetime (fs)
SLD '94-'95	IP	$293.7 \pm 8.2 \pm 4.6$
	DL	$280 \pm 11 \pm 2$
	IPD	$287.8 \pm 7.7 \pm 3.5$
ALEPH '94	IPD	$290.4 \pm 3.2 \pm 1.7$
	DL	$288.5 \pm 3.1 \pm 2.6$
	MIPS	$290.2 \pm 1.8 \pm 3.9$
	3D-IP	$289.0 \pm 2.7 \pm 1.3$
DELPHI '92–'93	IPD	$293.9 \pm 4.8 \pm 1.5$
	IPS	$290.1 \pm 3.5 \pm 3.1$
	DL	$286.7 \pm 4.9 \pm 3.3$
L3 '94	IP	$287.5 \pm 3.8 \pm 3.9$
	DL	$293.0 \pm 5.3 \pm 2.5$
OPAL '94	IP	$290.4 \pm 3.5 \pm 2.2$
	DL	$289.0 \pm 3.6 \pm 1.8$
CLEO 2	DL 1-3	$287.6 \pm 2.9 \pm 4.0$
	DL 3-3	$309 \pm 11 \pm 9$

Table 3. *Measurements of the τ lifetime with different methods (described in the text).*[25]

1.8.3 Measurements of the τ Leptonic Branching Fractions

We now turn to the last input to universality tests, the leptonic branching ratios $B_e = B(\tau \to \nu_\tau e \overline{\nu}_e)$ and $B_\mu = B(\tau \to \nu_\tau \mu \overline{\nu}_\mu)$. A new generation of results appeared in the last few years[26] taking advantage of large statistics and small background.

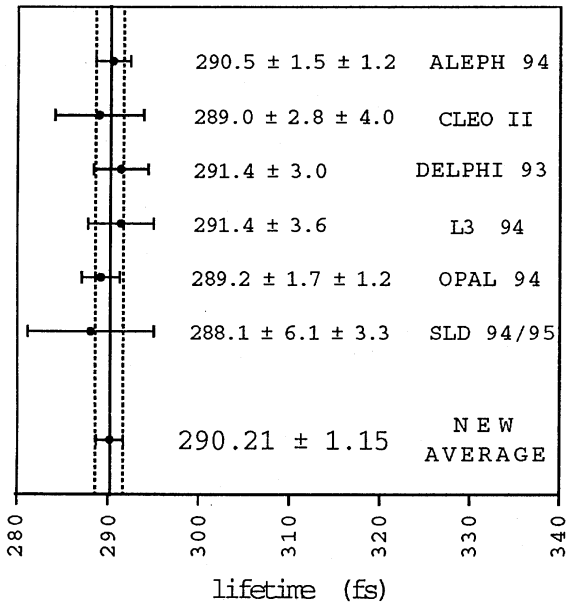

Fig. 16. *Measurements of the τ lifetime.*[25]

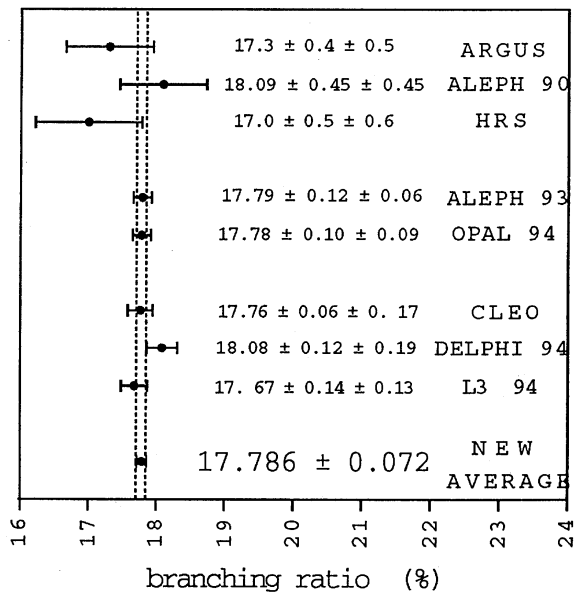

Fig. 17. *Measurements of the τ electronic branching fraction B_e (Ref. 25).*

An important experimental aspect is the control of the particle identification used in the analysis in order to separate the different τ decay channels. At the level of precision required, it is not realistic to rely on Monte Carlo simulation to compute the identification efficiencies and feedthrough backgrounds. The efficiency matrix for electrons, muons, and hadrons has to be measured with data. Fortunately, this is possible by selecting test samples of known particle types, using the processes $ee \to ee(\gamma)$, $ee \to \mu\mu(\gamma)$, $\gamma\gamma \to ee$, $\gamma\gamma \to \mu\mu$, and $\tau \to \nu_\tau h\pi^0$. The idea is to isolate such samples with negligible background, to tag one particle (a lepton or a π^0), and to study the identification of the recoil particle.

The recent results are given in Figs. 17 and 18. The progress achieved in the last two years is clearly seen. The combined world values are

$$B_e = (17.786 \pm 0.072)\%, \tag{49}$$

$$B_\mu = (17.317 \pm 0.078)\%. \tag{50}$$

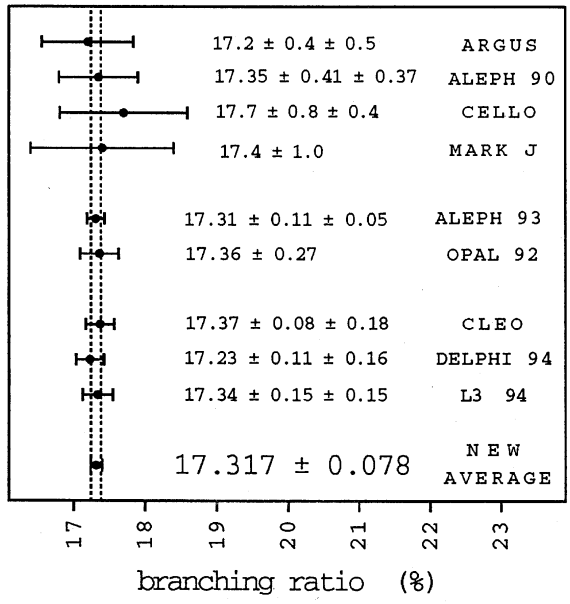

Fig. 18. *Measurements of the τ muonic branching fraction B_μ (Ref. 25).*

1.8.4 Results and Discussion

From the results of Eqs. (49) and (50), and relation (43), one obtains a test of $e-\mu$ universality:

$$\left(\frac{g_\mu}{g_e}\right)_T = 1.0008 \pm 0.0028. \tag{51}$$

This value can be compared to the corresponding result from π leptonic decays[27,28] using relation (45),

$$\left(\frac{g_\mu}{g_e}\right)_L = 1.0012 \pm 0.0015. \tag{52}$$

Testing universality of the τ and μ couplings involves the full set of measurements we have discussed. Relation (44) yields with the experimental input (47), (48), and (49)

$$\left(\frac{g_\tau}{g_\mu}\right)_T = 1.0003 \pm 0.0029, \tag{53}$$

where the total uncertainty receives contributions from τ_τ (0.0020), B_e (0.0020), and m_τ (0.004).

A test of $\tau-\mu$ universality for longitudinal W's is possible using relation (46) and the measured branching fraction for $\tau \to \nu_\tau(\pi, K)$ $B_h = (11.77 \pm 0.14)\%$

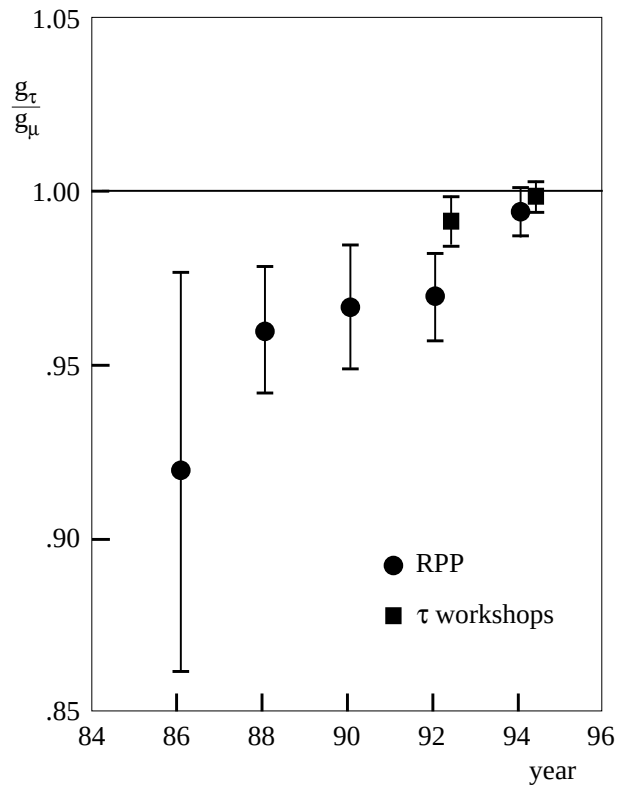

Fig. 19. *History of the test of $\tau - \mu$ universality.*

(Ref. 10) with the result

$$\left(\frac{g_\tau}{g_\mu}\right)_L = 1.0067 \pm 0.0064. \tag{54}$$

So all the tests for lepton universality in the charged current are positive at a precision level of 0.3%, except for $\tau - \mu$ for longitudinal W's where the precision reaches only 1.3%. This is the culmination of a ten-year-long story, in which a hint of a discrepancy was observed for $\tau - \mu$ universality, but was later cancelled by better lifetime measurements and the new determination of the τ mass (Fig. 19).

A relevant question at this point is the sensitivity of these tests to new physics beyond the SM. A popular candidate is supersymmetry with two Higgs doublets in the minimal scenario, generating three neutral and two charged Higgs bosons. The latter can contribute to leptonic τ decays giving[29]

$$B_l \sim B_{SM}(1 - \frac{2m_l^2}{M_{H^\pm}^2}\tan^2\beta), \tag{55}$$

where β is related to the vacuum expectation values of the two Higgs fields through $\tan\beta = \frac{v_2}{v_1}$. As expected, Eq. (55) introduces a correction for B_μ, leaving B_e practically unchanged. From the measurements (49) and (50), one obtains a limit for the $H^\pm$ mass

$$M_{H^\pm} > 1.5 \tan\beta \quad (\mathrm{GeV/c^2}), \tag{56}$$

which is only interesting for large $\tan\beta$ values, and is comparable to other limits given by studies of $B \to \tau\nu X$ decays, and from a recent investigation by CDF[30] in top decays through $t \to H^+ b$ and $H^+ \to \tau^+\nu_\tau$.

2 Leptonic Z Couplings

2.1 The Electroweak Standard Model

2.1.1 Phenomenology at Lowest Order

The electroweak Standard Model[31] is based on gauge invariance with respect to transformations of the symmetry group $SU(2)_L \times U(1)$. Each group generates an interaction, the intensity of which is determined by the couplings g and g', respectively, with exchanged bosons W^+, W^0, W^- for $SU(2)_L$ and B^0 for $U(1)$. Gauge symmetry is spontaneously broken through the Higgs mechanism in order to give masses to the originally massless gauge bosons. In this process the fields of the bosons W^0_μ and B^0_μ are mixed, giving rise to the electromagnetic field A_μ and to the Z boson field Z_μ as follows,

$$\begin{aligned} A_\mu &= B_\mu \cos\theta_W + W^3_\mu \sin\theta_W \\ Z_\mu &= -B_\mu \sin\theta_W + W^3_\mu \cos\theta_W, \end{aligned} \tag{57}$$

where θ_W is the electroweak mixing angle. Thus, the constants g, g', θ_W, and e are linked by the "unification" conditions:

$$g \sin\theta_W = g' \cos\theta_W = e. \tag{58}$$

The phenomenology of the weak interaction charged current, with maximal parity violation, requires placing left-handed fermions (f_L) in weak isospin doublets, while right-handed fermions (f_R) are not specified (as they do not participate in the charged current). From the point of view of $SU(2)_L$, simplicity and experimental results point to a structure with universal f_L families interacting with the same constants g and θ_W.

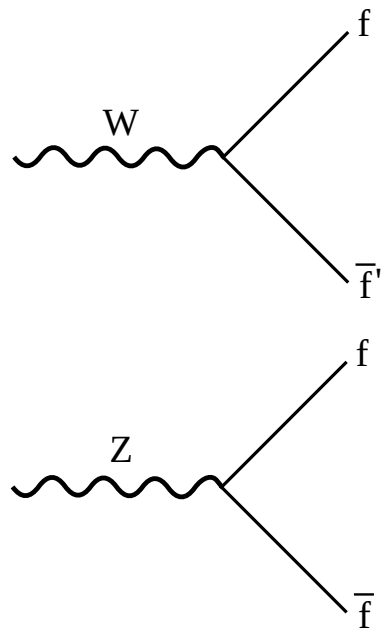

Fig. 20. *Couplings of W and Z bosons to fermions.*

The fundamental couplings between gauge bosons and fermions (Fig. 20) are expressed through the fermion currents in the charged sector

$$J^{\mu}_{CC} = -i\ \frac{g}{\sqrt{2}}\ \bar{f}'\gamma^{\mu}\left(\frac{1-\gamma^5}{2}\right) f, \tag{59}$$

and in the neutral sector

$$J^{\mu}_{NC} = -\frac{ig}{\cos\theta_W}\ \bar{f}\gamma^{\mu}\left(\frac{v_f - a_f\gamma^5}{2}\right) f, \tag{60}$$

with

$$\left\{\begin{array}{lcl} v_f & = & I_3(f_L) + I_3(f_R) - 2\ Q_f\ \sin^2\theta_W, \\ a_f & = & I_3(f_L) - I_3(f_R). \end{array}\right. \tag{61}$$

In the simplest case where right-handed fermions are isospin singlets, one has $I_3(f_R)\ =\ 0$.

After symmetry breaking, the masses of the W and Z bosons are completely specified at lowest order

$$M_W^2 = \frac{\pi\alpha}{\sqrt{2}\ G\ \sin^2\theta_W}, \tag{62}$$

$$\rho = \frac{M_W^2}{M_Z^2\ \cos^2\theta_W} = 1, \tag{63}$$

with the Fermi constant G defined in the local limit as

$$G = \frac{\sqrt{2}\, g^2}{8\, M_W^2}. \tag{64}$$

Relation (63) stems from the choice of a doublet of complex scalar Higgs fields for the symmetry breaking. It remains true for any number of doublets (for example, two doublets in the MSSM), but it would be different in the case of different Higgs multiplets.

The electroweak theory at lowest order is therefore set in a very constrained frame: Once one is given the constants e and G (the latter from the muon lifetime, for example), the knowledge of the only remaining parameter θ_W allows one to deduce the masses of the W and Z bosons, and all the couplings in the neutral sector as given in Table 4. Equation (63) provides $\sin^2\theta_W$ directly through the relation

$$\sin^2\theta_W = 1 - \frac{M_W^2}{M_Z^2} = \frac{e^2}{g^2}. \tag{65}$$

f	a_f	v_f	v_f for $s^2 = \sin^2\theta_W = 0.231$
ν_e	$\frac{1}{2}$	$\frac{1}{2}$	0.5
e	$-\frac{1}{2}$	$-\frac{1}{2} + 2s^2$	-0.038
u	$\frac{1}{2}$	$\frac{1}{2} - \frac{4}{3}\, s^2$	0.192
d	$-\frac{1}{2}$	$-\frac{1}{2} + \frac{2}{3}\, s^2$	-0.346

Table 4. *Fermionic couplings in universal neutral currents.*

2.1.2 The Need for Higher Orders

Already before LEP and SLC, the overall consistency between the fermionic couplings and the boson masses was not respected. On the one hand, from the measurement of M_W (Ref. 32), $M_W = (80.35 \pm 0.33 \pm 0.17)$ GeV/c^2, and Eq. (62), the value

$$(\sin^2\theta_W)_{masses} = 0.215 \pm 0.002 \tag{66}$$

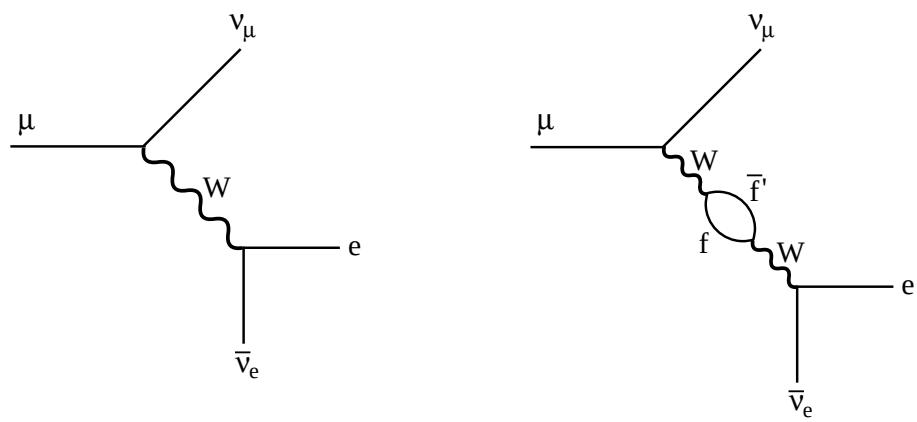

Fig. 21. *Muon decay at lowest order and in second order with a loop in the W propagator.*

was obtained. On the other hand, neutrino scattering on nucleons[33] allowed the measurement of the quark couplings, providing with the help of Table 4

$$(\sin^2\theta_W)_{couplages} = 0.233 \pm 0.003 \text{ (exp.)} \pm 0.005 \text{ (theo.)}. \tag{67}$$

Comparison of the results (66) and (67) shows a clear discrepancy

$$\Delta \sin^2\theta_W = 0.018 \pm 0.006. \tag{68}$$

However, it is important at this point to consider higher-order corrections to the theory. In particular, computing the second-order radiative corrections to the muon decay rate[34] (Fig. 21) leads to the modification Δr to relation (62)

$$G = \frac{\pi\alpha}{\sqrt{2}} \frac{1}{M_W^2 \ \sin^2\theta_W} \ (1 + \Delta r). \tag{69}$$

Some higher-order loop corrections can be resummed through

$$1 + \Delta r + (\Delta r)^2 + \ldots = \frac{1}{1 - \Delta r}. \tag{70}$$

The correction Δr can be split into two terms with quite different physics:

$$\Delta r = \Delta r_{EM} + \Delta r_{EW}. \tag{71}$$

- Δr_{EM} takes into account the evolution of α from $Q^2 = 0$ to $Q^2 = M_W^2$ from fermionic loops in the photon propagator.[35]

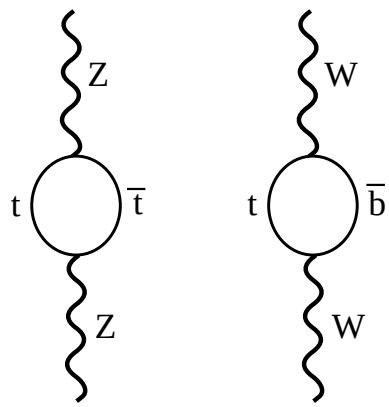

Fig. 22. *Top quark loop in the W and Z propagators.*

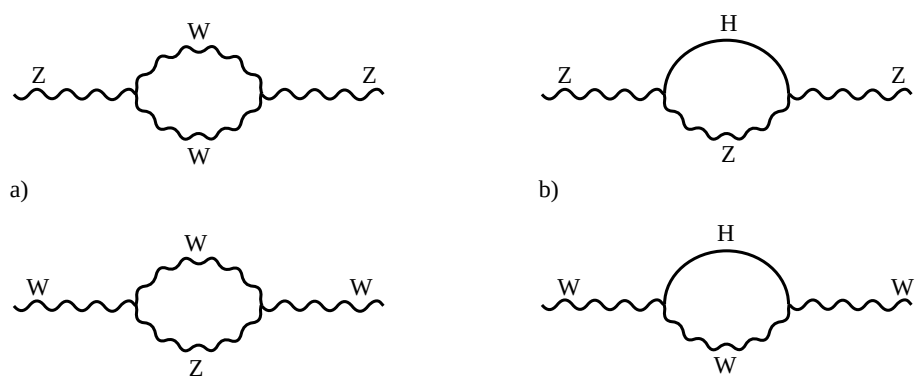

Fig. 23. *Bosonic loops in the W and Z propagators.*

- Δr_{EW} is given by the contribution of loops with heavy particles (t quark, Higgs boson) as shown in Figs. 22 and 23 with the following behavior[36,37]:

$$\begin{cases} \Delta r_{EW,t} & \sim & m_t^2, \\ \Delta r_{EW,H} & \sim & \ell n \frac{M_H}{M_W}. \end{cases} \tag{72}$$

Figure 24 shows the variation of Δr with m_t for different values of M_H; the effect is quite sizable, about 4% for $m_t \sim 150$ GeV/c^2.

Calculations of higher-order contributions allow us to re-write the expressions for the masses and the couplings in terms of renormalized quantities, as is usually done in QED. Among the parameters α, G, and $\sin^2\theta_W$, the first two are determined with precision from the quantum Hall effect and $(g-2)$ of the electron, and

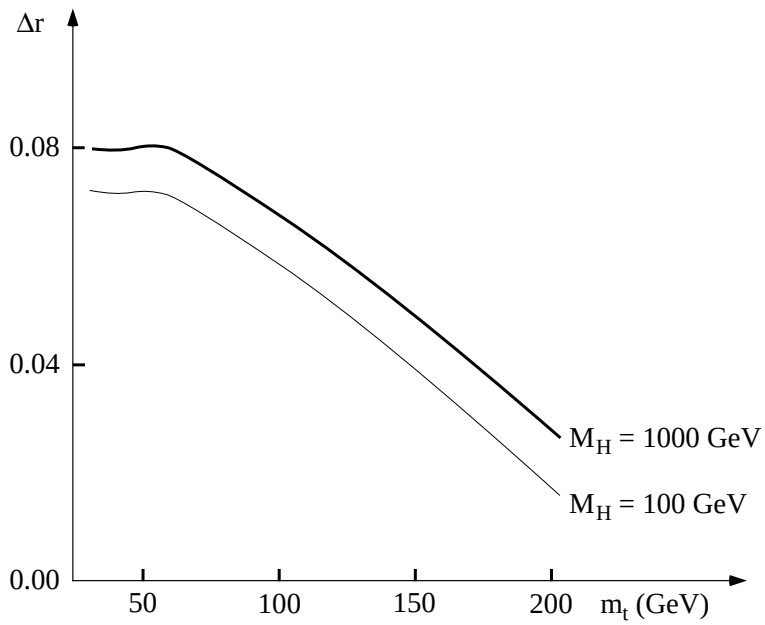

Fig. 24. *Correction Δr to the W mass as a function of m_t and M_H.*

the muon lifetime from Eq. (34), while the last one depends on the electroweak renormalization scheme. Several schemes have been proposed; here we will only consider an effective $\sin^2\theta_W$, noted $\overline{s}^2$, essentially defined through renormalized couplings at $s = M_Z^2$. To a very good approximation, higher-order corrections are effectively absorbed in a renormalization of the couplings, leaving the relations (61), (62), and (63) unchanged up to an overall factor:

$$\left\{ \begin{array}{rcl} \bar{v} & = & \sqrt{\bar{\rho}}\,(I_3 - 2Q\bar{s}^2), \\ \bar{a} & = & \sqrt{\bar{\rho}}\,I_3, \end{array} \right. \tag{73}$$

$$M_W^2 = \frac{\pi\,\bar{\alpha}}{\sqrt{2}\,G\,\bar{s}^2}, \tag{74}$$

$$M_Z^2 = \frac{M_W^2}{\bar{\rho}\,\bar{c}^2}. \tag{75}$$

The dominant correction term in $\overline{\rho}$ originates from loops involving the t quark, which introduce an $SU(2)$ violation because of the large mass splitting between the b and t quarks[36] (Fig. 22), yielding

$$\bar{\rho} = 1 + \frac{3\sqrt{2}\,G}{16\pi^2}\,m_t^2 + \ldots. \tag{76}$$

2.2 Observables in $e^-e^+ \to f\overline{f}$

Calculations of the transition amplitude can be done at lowest order according to the diagrams of Fig. 25, while renormalization is taken into account through the relations (73). Cross sections are expressed in the center-of-mass frame where θ is the angle of the outgoing fermion with respect to the incident electron (Fig. 26).

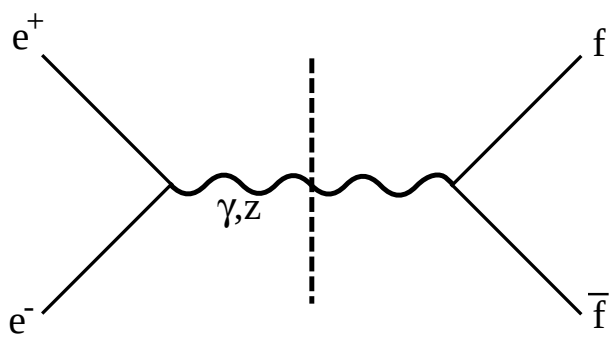

Fig. 25. *e^-e^+ annihilation into a fermion pair through γ and Z exchange.*

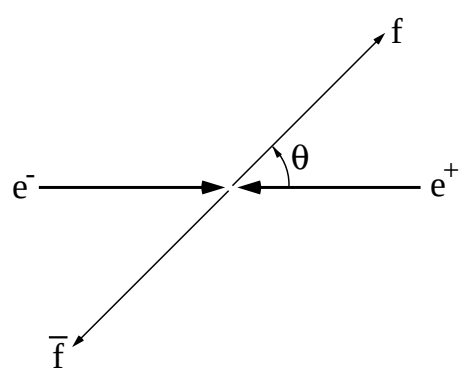

Fig. 26. *e^-e^+ annihilation in a fermion pair in the center-of-mass frame.*

2.2.1 $e^{\pm}$ Unpolarized and f Polarization Not Observed

Exchanges of γ and Z lead to

$$\begin{aligned}\frac{d\sigma_f}{d\cos\theta} = & \tfrac{3}{8}\, C_f\ \sigma_{pt} \Big\{ Q_f^2\ (1+\cos^2\theta) \\ & -8Q_f\ Re\chi\,[v_e\ v_f(1+\cos^2\theta) + 2a_e\ a_f\ \cos\theta] \\ & +16|\chi|^2 \left[(v_e^2+a_e^2)(v_f^2+a_f^2)(1+\cos^2\theta) + 8v_e\ v_f\ a_e\ a_f \cos\theta\right]\Big\}\end{aligned} \tag{77}$$

with

$$\chi = \frac{G}{8\ \pi\ \sqrt{2}\ \alpha}\ \frac{s\ M_Z^2}{s - M_Z^2 + i\ M_Z\ \Gamma_Z}. \tag{78}$$

Equation (77) displays the $|\gamma|^2$ term from QED alone, the $\gamma - Z$ interference proportional to the real part of the Z propagator which vanishes at $s = M_Z^2$, and the $|Z|^2$ term which dominates at the pole $s = M_Z^2$.

Near the pole ($s \sim M_Z^2$), Eq. (77) can be integrated over θ to yield

$$\sigma_f = \frac{G^2\ M_Z^6\ (v_e^2+a_e^2)(v_f^2+a_f^2)}{6\pi\ [(s-M_Z^2)^2 + M_Z^2\Gamma_Z^2],} \tag{79}$$

$$= \frac{12\pi\ \Gamma_{ee}\ \Gamma_{ff}}{(s-M_Z^2)^2 + M_Z^2\Gamma_Z^2,} \tag{80}$$

displaying the partial widths Γ_{ff} for the decay $Z \to f\overline{f}$ (consider the vertical cut in the Feynman diagram in Fig. 25) given by

$$\Gamma_{ff} = \frac{G\ M_Z^3}{6\ \sqrt{2}\pi}\ (v_f^2 + a_f^2). \tag{81}$$

Equation (77) induces a forward-backward asymmetry in the angular distribution. For $\cos\theta > 0$, one defines

$$A_{FB}^f\ (\cos\theta) = \frac{d\sigma_f(\cos\theta) - d\sigma_f(-\cos\theta)}{d\sigma_f(\cos\theta) + d\sigma_f(-\cos\theta)}. \tag{82}$$

Integrating over the hemispheres, the mean asymmetry is obtained,

$$A_{FB}^f = \frac{\int_0^1 d\sigma_f - \int_{-1}^0 d\sigma_f}{\int_{-1}^1 d\sigma_f} = \frac{F-B}{F+B}. \tag{83}$$

For $s = M_Z^2$,

$$A_{FB}^f(M_Z^2) = \frac{3}{4} A_e A_f, \tag{84}$$

where we have introduced the parity-violating observable A_f,

$$A_f = \frac{2v_f a_f}{v_f^2 + a_f^2}. \tag{85}$$

However, since it only involves the product $A_e A_f$, the observable A_{FB}^f does not violate parity.

2.2.2 $e^\pm$ Unpolarized and f Polarization Observed

Helicity is conserved at high energy for vector (γ^μ) or axial-vector ($\gamma^\mu\gamma^5$) interactions. It leads to the production of $J_z = \pm 1$ states, i.e., $f_L\overline{f_R}$ and $f_R\overline{f_L}$. The polarizations of the fermion and of the antifermion are thus opposite:

$$P_f = 2\langle\lambda_f\rangle = -P_{\overline{f}}. \tag{86}$$

The cross section for producing a fermion with helicity λ_f is given by

$$\left(\frac{d\sigma}{d\cos\theta}\right)_{\lambda_f} = F + 2\lambda_f G, \tag{87}$$

where F and G are functions of $\cos\theta$ and depend on the couplings v_e, v_f, a_e, a_f. Hence, the polarization can be calculated as a function of $\cos\theta$,

$$P_f(\cos\theta) = -\frac{A_f + A_e f(\cos\theta)}{1 + A_e A_f f(\cos\theta),} \tag{88}$$

with $f(x) = \dfrac{2x}{1+x^2}$. The polarization P_f is a parity-violating observable and its average over the angular distribution is proportional to A_f:

$$\langle P_f\rangle = -A_f. \tag{89}$$

2.2.3 $e^\pm$ Polarized

The annihilation cross section for an initial e^-e^+ state with respective helicities λ_- and λ_+ is given by

$$\begin{aligned} \sigma_{\lambda_-\lambda_+} &= \int \left(\frac{d\sigma}{d\cos\theta}\right)_{\lambda_-\lambda_+} d\cos\theta \\ &= (1 - 4\lambda_+\lambda_-)\sigma_1 + 2(\lambda_+ - \lambda_-)\sigma_2, \end{aligned} \tag{90}$$

where it can be readily verified that only $e_L^- e_R^+$ and $e_R^- e_L^+$ states contribute, i.e., $\lambda_+ = -\lambda_-$.

A very practical consequence follows: it is not necessary to polarize *both* electrons and positrons. Only electrons need to be polarized, as an e_L^- can only annihilate with an e_R^+, which constitutes on the average half of the unpolarized positrons (and similarly for an e_R^-).

A polarization asymmetry can be defined with the two nonvanishing cross sections,

$$A_{LR} = \frac{\sigma_{LR} - \sigma_{RL}}{\sigma_{LR} + \sigma_{RL}} = \frac{\sigma_2}{\sigma_1}. \tag{91}$$

It is a parity-violating observable and it is given simply by

$$A_{LR} = A_e. \tag{92}$$

2.3 Results on the Leptonic Widths

The measurement of the peak cross sections for the different leptons provides the values for the corresponding leptonic widths. Averaging over the four LEP experiments[38] gives

$$\Gamma_{ee} = (83.94 \pm 0.14) \text{ MeV/c}^2, \tag{93}$$

$$\Gamma_{\mu\mu} = (83.84 \pm 0.20) \text{ MeV/c}^2, \tag{94}$$

$$\Gamma_{\tau\tau} = (83.68 \pm 0.24) \text{ MeV/c}^2, \tag{95}$$

in good agreement with the universality hypothesis introduced in the standard theory. It should be remarked that in this test only the axial coupling is probed, because

$$\Gamma_{\ell\ell} \sim v_\ell^2 + a_\ell^2 \tag{96}$$

with $v_\ell \sim 0$, since $\sin^2\theta_W$ is close to $\frac{1}{4}$.

If universality is imposed, it is possible to compute the value of the universal leptonic width for a massless lepton ($m_l \ll M_Z$)

$$\Gamma_{\ell\ell} = (83.91 \pm 0.10) \text{ MeV/c}^2. \tag{97}$$

It is amusing to notice that, at the level of the experimental precision achieved, the mass of the τ lepton cannot be neglected against M_Z. On the one hand, the width for a vector coupling is

$$\Gamma_\tau^V = \frac{\beta(3-\beta^2)}{2}\Gamma_\tau^V(m_\tau = 0), \tag{98}$$

where the threshold factor (depending on the velocity β of the τ) is familiar from the process $e^+e^- \to \tau^+\tau^-$ with photon exchange only. On the other hand, the width for an axial coupling increases with energy much more slowly:

$$\Gamma_\tau^A = \beta^3\ \Gamma_\tau^A(m_\tau = 0). \tag{99}$$

The threshold factor differs from unity by 9×10^{-7} for the vector part and by 2.3×10^{-3} for the dominant axial part, a value comparable to the experimental accuracy.

2.4 Z Invisible Width and the Number of Neutrino Types

2.4.1 Standard Model with Universal Families and Situation before SLC/LEP

Since for each lepton family we have

$$\begin{cases} a_{\nu_\ell} &= v_{\nu_\ell} = \frac{1}{2} \\ a_\ell &= -\frac{1}{2}, \qquad v_\ell \sim 0, \end{cases} \tag{100}$$

the total rate for the Z to decay into neutrino pairs (an "invisible" width) can be predicted to be

$$\Gamma_{inv} = N_\nu \Gamma_{\nu\nu} \simeq 2N_\nu \Gamma_{\ell\ell}, \tag{101}$$

where N_ν is the number of neutrino types with masses $m_\nu \ll \frac{M_Z}{2}$.

Indeed, it is known that neutrinos have very small masses, less than 15 eV/c^2 for ν_e (Ref. 10), 170 keV/c^2 for ν_μ (Ref. 39), and 18 MeV/c^2 for ν_τ (Ref. 40). Moreover, cosmological considerations on the energy density of the universe lead to mass limits on the order of 100 eV (Ref. 41). The experimental investigation of the neutrino mass spectrum is therefore a very efficient way to explore the possibility of other higher-mass families of leptons and quarks.

Information on N_ν was scarce before SLC and LEP. From the ratio of W and Z production rates in hadronic collisions, a limit $N_\nu < 6.1$ (90% C.L.) was obtained.[42] The search for the process $e^+e^- \to \nu\bar{\nu}\gamma$ with PEP and PETRA[43] was a more direct method, yielding $N_\nu < 4.9$ (95% C.L.). A completely different

approach was based on the primordial synthesis of light elements in the cosmological model, giving the limit[44] $N_\nu \leq 4$. Even though no definite determination was available, the flexibility remained limited: since two neutrino types were already experimentally known,[45] the only possibilities left were $N_\nu = 3, 4$.

2.4.2 Measurement of the Invisible Z Width

Formally, the invisible width is obtained by comparing the total width (measured from the lineshape fit of the Z resonance) and the sum of all "visible" partial widths (obtained from the corresponding rates),

$$\Gamma_{inv} = \Gamma_Z - \sum_{f \text{ visible}} \Gamma_{ff} = N_\nu \Gamma_{\nu\nu}^{SM}, \tag{102}$$

where $\Gamma_{\nu\nu}^{SM}$ is the Standard Model prediction.

The total width is very precisely known (Fig. 27), and subtracting the measured leptonic and hadronic widths yields

$$\Gamma_{inv} = (500.1 \pm 1.8) \text{ MeV/c}^2. \tag{103}$$

Using the SM prediction

$$\left(\frac{\Gamma_{\ell\ell}}{\Gamma_{\nu\nu}}\right)_{SM} = 0.5022 \pm 0.0001, \tag{104}$$

the value $N_\nu = 2.99$ is obtained.

This is not the optimal method, however. It is preferable not to use directly the measurement of the total width, and rather involve only quantities measured precisely at the Z peak. Indeed, in the Standard Model, the peak cross section is directly linked to N_ν: If N_ν increases, Γ_Z increases too, and the peak cross section for visible channels decreases (Fig. 28). Concretely,

$$\begin{aligned} \frac{\Gamma_{inv}}{\Gamma_{\nu\nu}} &= \frac{\Gamma_{\ell\ell}}{\Gamma_{\nu\nu}} \frac{\Gamma_{inv}}{\Gamma_{\ell\ell}} \\ &= \left(\frac{\Gamma_{\ell\ell}}{\Gamma_{\nu\nu}}\right)_{SM} \left\{ \sqrt{\frac{12\pi R_Z}{M_Z^2 \sigma^\circ_{\text{had, peak}}}} - R_\ell - 3 \right\}, \end{aligned} \tag{105}$$

where

$$R_Z = \frac{\Gamma_{\text{had}}}{\Gamma_{\ell\ell}} = \frac{\sum_q \Gamma_{q\bar{q}}}{\Gamma_{\ell\ell}}. \tag{106}$$

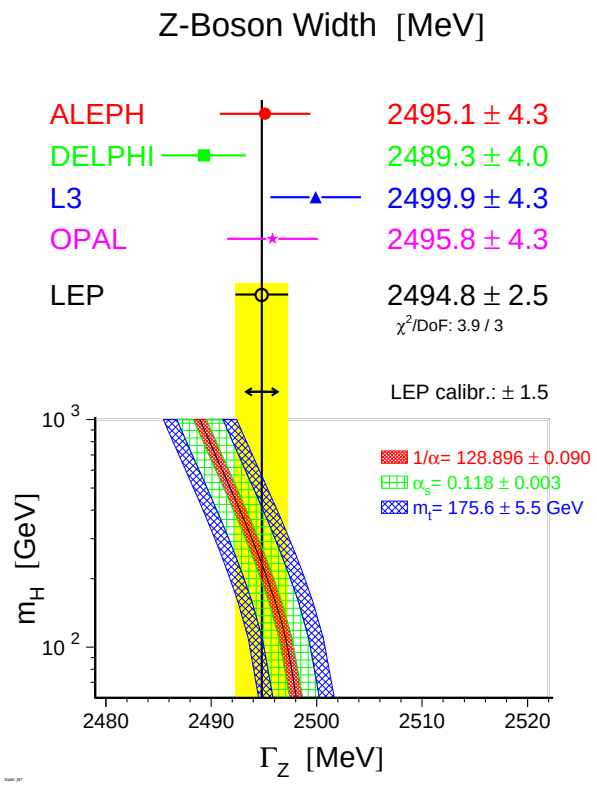

Fig. 27. *Measurements of* Γ_Z *at LEP.*

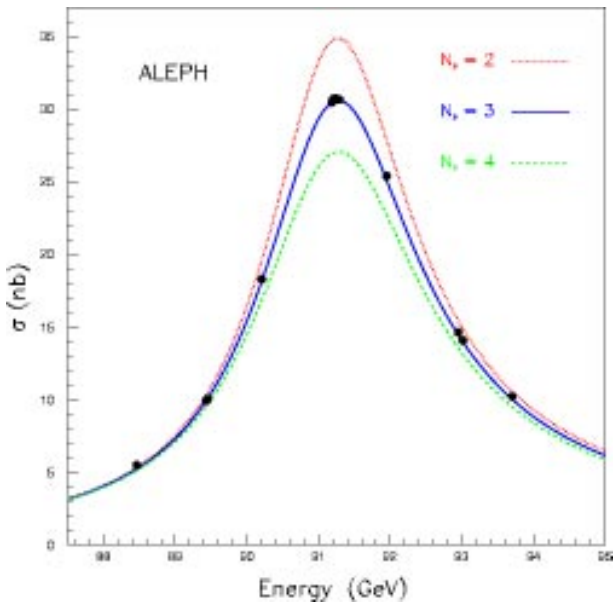

Fig. 28. *Cross section for $e^-e^+ \to Z \to$ hadrons and predictions for the Standard Model for different numbers of neutrino types N_ν.*

This method is advantageous since it only depends on the measurement of R_Z (involving only the separation of leptonic and hadronic channels) and of $\sigma^\circ_{\text{had, peak}}$ (depending on the luminosity determination and the radiative corrections).

The measured values of $\sigma^\circ_{\text{had, peak}}$ and R_Z are given in Figs. 29 and 30, respectively. The extracted value for N_ν is then:

$$N_\nu = 2.993 \pm 0.011. \tag{107}$$

2.4.3 Discussion

The result (107) is a very important milestone in particle physics. It is the achievement of more than ten years of research (Fig. 31). Let us now proceed to discuss the many consequences.

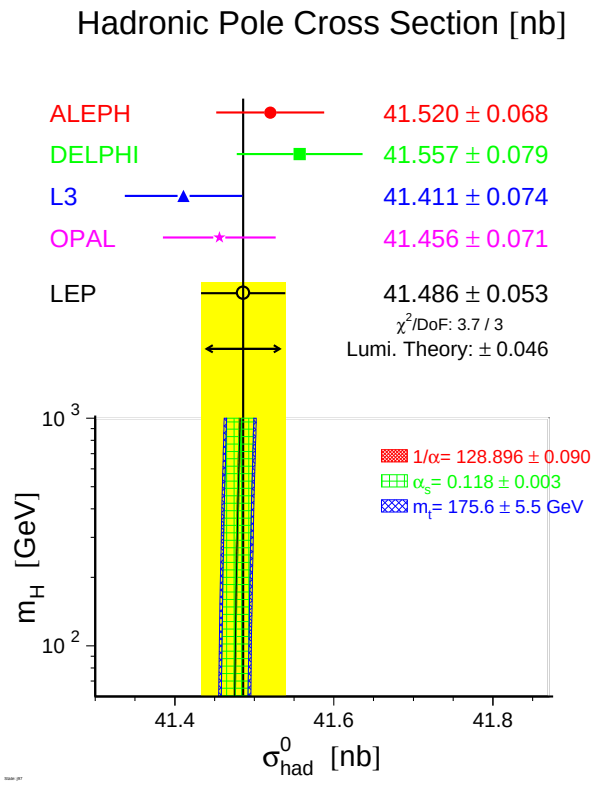

Fig. 29. *Measurements of the peak cross section at LEP for* $e^-e^+ \to Z \to$ *hadrons after correcting for radiation.*[38]

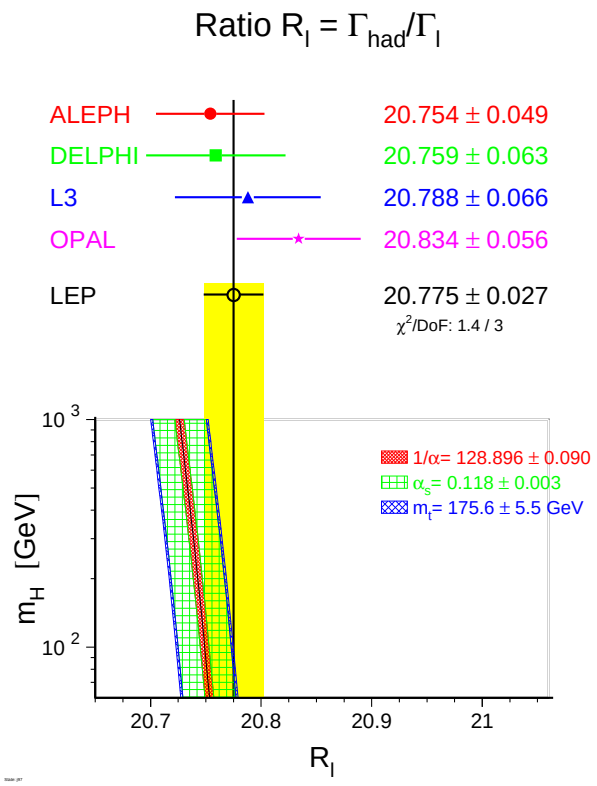

Fig. 30. *Measurements of R_Z at LEP.*[38]

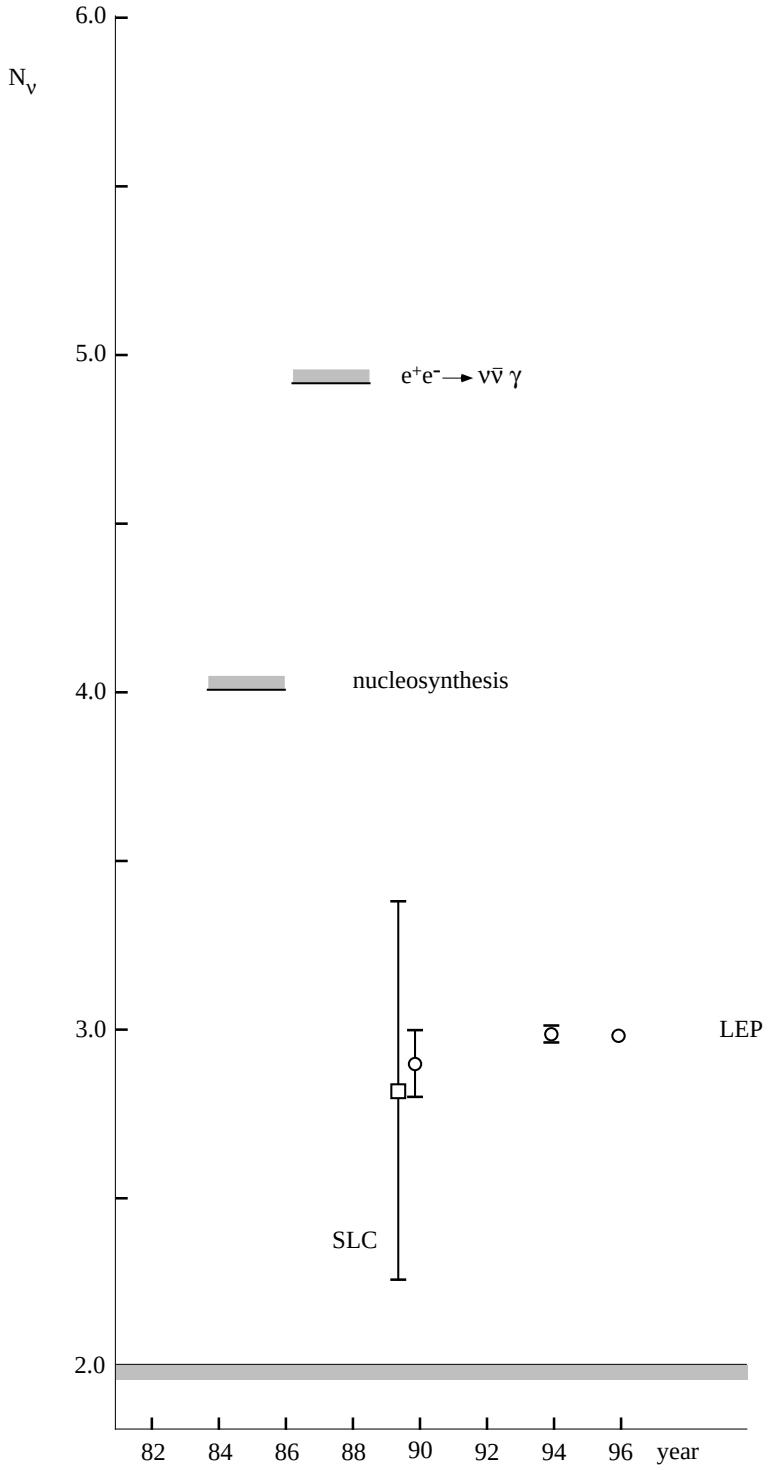

Fig. 31. *Progress in the knowledge of N_ν with SLC and LEP.*

(1) The measurement of N_ν is indeed consistent with an integer value! Furthermore, it is consistent with previous limits and the solution

$$N_\nu = 3 \tag{108}$$

is clearly chosen.

(2) Conversely, in the context of the standard scenario with three universal families of quarks and leptons, the measurement (107) can be reinterpreted as a determination of the width $\Gamma_{\nu\nu}$. The result

$$\frac{\Gamma_{\ell\ell}}{\Gamma_{\nu\nu}} = 0.5010 \pm 0.0020 \tag{109}$$

is consistent with the theoretical value (104) with a precision of 4×10^{-3}. This is a nice result for an undetectable final state!

(3) It is, of course, impossible to separate the three neutrino flavors.... However, the pre-LEP neutral current phenomenology was established with experiments using ν_μ and ν_e beams whose results can be formulated in terms of the widths $\Gamma_{\nu_e\nu_e}$ and $\Gamma_{\nu_\mu\nu_\mu}$ which are in agreement with the universal Standard Model. As a consequence, the third neutrino coupled to the Z is also standard and it is compatible with the ν_τ neutrino associated with the τ lepton. The ν_τ has not yet been detected experimentally, but its existence is attested to by the phenomenology of τ decays (see next lecture).

(4) The result (107) is only applicable to neutrinos with masses much smaller than $\frac{M_Z}{2}$. Nevertheless, the intrinsic accuracy of the measurement allows one to in fact exclude the production of a fourth neutrino up to a mass of 45 GeV/c^2. As an example, a 40 GeV/c^2 neutrino would have a width equal to 40% of the massless value, therefore well in excess of the experimental uncertainty in (107).

(5) The LEP measurement agrees with the estimates of the primordial nucleosynthesis of light elements. This can be turned around as a new powerful test of the standard Big Bang cosmology.

(6) The result $N_\nu = 3$ strongly suggests that the number N of quark-lepton families is also equal to three. This statement is strongly supported by the following three observations:

(a) The neutrino mass spectrum is experimentally confined to rather small masses, most probably smaller than 100 eV/c^2. It would be strange if the mass of the fourth (universal) neutrino were larger than 45 GeV/c^2, i.e., a factor larger than 10^9.

(b) No new charged lepton or new quark has been observed with LEP with a mass larger than 46 GeV/c^2.

(c) The experimental determination of the electroweak radiative corrections (76) shows that they are saturated by the known fermions, including of course the heavy top quark. Still higher-mass fermions would have a very large effect on these corrections if their masses violate the $SU(2)$ symmetry, as observed for the "chiral" fermions: $m_\ell \gg m_{\nu_\ell}$ and $m_t \gg m_b$. It is not possible to exclude in this way super-heavy mass-degenerate fermions.

(7) A last remark deals with the connection between the number of quark families and the observed CP violation in the weak interactions. The standard interpretation of this violation rests on the existence of at least three quark families. In this case, the weak mixing matrix for the charged current is complex, thus providing the necessary ingredient to describe CP violation. The determination $N_\nu = 3$ and its extension $N = 3$ represents therefore the minimal situation for this explanation.

2.5 Results on the Leptonic Asymmetries

2.5.1 Forward-Backward Asymmetries

The experiments determine the asymmetries at the Z pole ${A^\ell_{FB}}^{(0)}$, corrected for γ exchange, $\gamma - Z$ interference (for $s \neq M_Z^2$), and vacuum polarization for photon exchange. For $s \sim M_Z^2$ and since v_l is quite small (Table 4), the measured values[38] are tiny (Fig. 32):

$$ {A^e_{FB}}^{(0)} = 0.0160 \pm 0.0024, ^* \tag{110} $$

$$ {A^\mu_{FB}}^{(0)} = 0.0163 \pm 0.0014, \tag{111} $$

$$ {A^\tau_{FB}}^{(0)} = 0.0192 \pm 0.0018. \tag{112} $$

*The determination of ${A^e_{FB}}^{(0)}$ requires the subtraction of the t-channel γ-exchange contribution which is computed using QED. This explains the larger error.

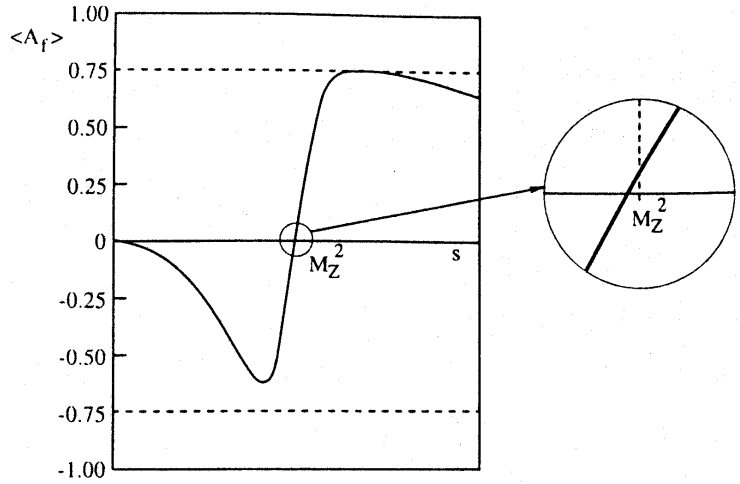

Fig. 32. *Forward-backward asymmetry in the process* $e^-e^+ \to f\overline{f}$. *The value at* $s = M_Z^2$ *is proportional to* $v_e v_f$.

These values are consistent with universality, where this time the vector couplings are mainly investigated, according to Eqs. (84) and (85). Assuming universality, the combined value is

$$A_{FB}^{\ell\ (0)} = 0.0171 \pm 0.0010. \tag{113}$$

It is used in conjunction with Eq. (97) for $\Gamma_{\ell\ell}$, in order to separate the couplings v_l and a_l up to some ambiguities. A different version of this is given in Fig. 33, where universality is shown to be satisfied.

2.5.2 τ Polarization

The principle of the measurement of τ polarization has been exposed in Sec. 1.4.2. At LEP the channels $\tau^- \to \nu_\tau X^-$ with $X^- \equiv e^-\ \overline{\nu}_e,\ \mu^-\ \overline{\nu}_\mu,\ \pi^-, \rho^-$, and a_1^- are used, where the secondary decays $\rho^- \to \pi^-\pi^0$ and $a_1^- \to \pi^-\pi^+\pi^-$ or $\pi^-\pi^0\pi^0$ have been measured.

The quantities A_e and A_τ are then separated from the $\cos\theta$ dependence of the τ polarization, according to Eq. (88), as outlined in Fig. (34). This provides a powerful way to test e–τ universality for the vector couplings.

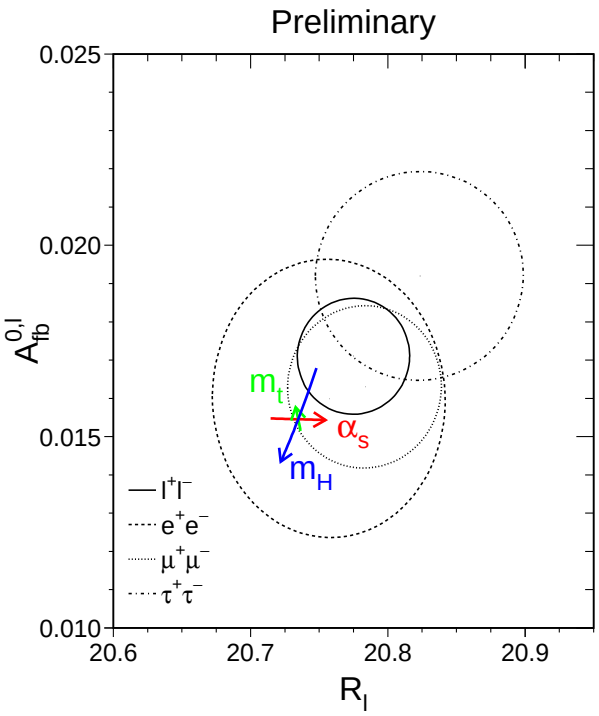

Fig. 33. *Determinations of* $A_{FB}^{(0)}$ *and* R_Z *at LEP for the three charged leptons. The dashed curves give the* 68% *C.L. contours and the solid curve corresponds to the combined measurement assuming lepton universality.*[38]

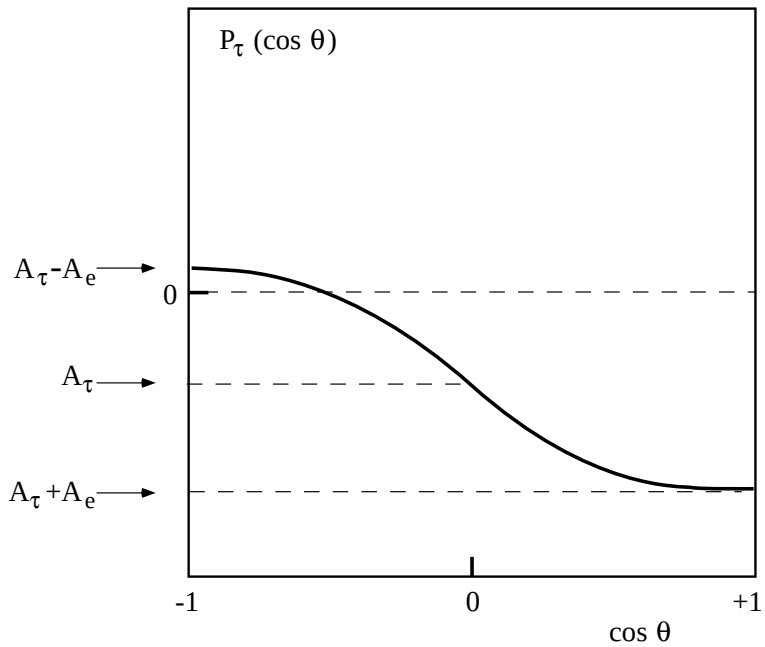

Fig. 34. *The expected dependence of $P_\tau(\cos\theta)$ not assuming e–τ universality.*

The current results (most experiments have not yet analyzed the full LEP1 statistics) from LEP,[38]

$$A_e = 0.1399 \pm 0.0073, \tag{114}$$

$$A_\tau = 0.1410 \pm 0.0064, \tag{115}$$

are in agreement with universality. The combined universal value is

$$A_\ell = 0.1406 \pm 0.0048. \tag{116}$$

2.5.3 LR Electron Asymmetry

The relative measurement at SLC of the cross sections $\sigma(e^-_L e^+)$ and $\sigma(e^-_R e^+)$ on the Z peak for any final state $f\bar{f}$ can be achieved with a small systematic uncertainty.[46] In particular, the electron polarization can be flipped from bunch to bunch in a random way, thus minimizing the effect of drifts in the performance of the detector and in the behavior of the beams. The statistical error is also minimal as all Z decays are used. The measured asymmetry A^{exp}_{LR} is given by

$$A_{LR}^{exp} = \frac{1}{P_e}\frac{N_L - N_R}{N_L + N_R}, \tag{117}$$

where P_e is the actual electron polarization at the collision point and $N_{L,R}$ are the numbers of events produced with the electron polarization L, R for the same integrated luminosity.

The data taken in 1992–95 correspond to about 1.5×10^5 produced Z's with a mean polarization P_e of 74%. After corrections taking into account γ exchange, off-pole effects including $\gamma - Z$ interference, and initial state radiation, the result obtained[47] is

$$A_{LR}{}^{(0)} = A_e = 0.1547 \pm 0.0032. \tag{118}$$

2.5.4 Discussion

The independent determinations of A_l from the FB lepton asymmetries at LEP, τ polarization at LEP, and LR electron asymmetry at SLC are not in very good agreement:

$$A_l \ \ (from\ A_{FB}) = 0.1510 \pm 0.0044, \tag{119}$$

$$A_l \ \ (from\ P_\tau) = 0.1406 \pm 0.0048, \tag{120}$$

$$A_l \ \ (from\ A_{LR}) = 0.1547 \pm 0.0032. \tag{121}$$

The average yields $A_l = 0.1505 \pm 0.0023$ with a χ^2 of 6.0 for 2 DF. The disagreement could be the result of bad luck or it could point to systematic effects not corrected for in some of the analyses. More data are welcome. On one hand, when all LEP1 results are available, the final accuracy on A_l from τ polarization should be around 0.0034. On the other hand, SLD continues to take data, as their method is statistically dominated: indeed, an updated value of $A_{LR}{}^{(0)} = 0.15245 \pm 0.00286$ was given[48] taking advantage of additional data in 1996–97. It will be interesting to watch the outcome of this critical test as its accuracy improves.

Another piece of information on A_l comes from the measurement of the FB asymmetry for $b\bar{b}$ pairs, obtained with good statistical accuracy at LEP. Since

$$A_{FB}^b(M_Z^2) = \frac{3}{4}A_e A_b, \tag{122}$$

and taking the expected value $A_b = 0.9355 \pm 0.0003$ in the Standard Model with $\sin^2\theta_W = 0.2315 \pm 0.0004$, the measurement[38] corrected to the pole, $A^b_{FB} = 0.0984 \pm 0.0024$, yields the result

$$A_e \;\; (from\ A^b_{FB}) = 0.1402 \pm 0.0034, \tag{123}$$

not in good agreement with the values from the purely leptonic asymmetries discussed above. The reasons for this discrepancy are not clear at this point: SM input for A_b, systematic effects in the measurements of A^b_{FB}? Here again, new analyses with more data are welcome. Indeed, a more recent analysis from ALEPH[49] yields a significantly larger value for A^b_{FB}, increasing the LEP average to 0.0997. Time will tell!

2.5.5 Determination of the Neutral-Current Leptonic Couplings

Summarizing the previous sections, the leptonic couplings a_l and v_l are determined from the following measurements:

$$\begin{array}{lcl} \Gamma_{\ell\ell} & \rightarrow & v_\ell^2 + a_\ell^2 \\ A^\ell_{FB} & \rightarrow & v_\ell a_\ell v_e a_e \\ A_e & \rightarrow & v_e a_e \\ A_\tau & \rightarrow & v_\tau a_\tau . \end{array} \tag{124}$$

The only solution retained satisfies $a_l < 0$, as imposed by pre-LEP results from neutrino-electron scattering. The values are given in Table 5 and in Fig. 35. Universality is satisfied with a precision of 0.2–0.3 % for a_l and 6–12 % for v_l. The fact that the latter value is poorer follows from the smallness of v_l, about 14 times smaller than a_l, itself a consequence of the particular value of $\sin^2\theta_W$. In fact, a better perception of the accuracy reached in the vector sector is given by the corresponding determinations of $\sin^2\theta_W$, given in Fig. 36 following the definition stemming from Eq. (73),

$$\bar{s}^2 = \frac{1}{4}\left(1 - \frac{\bar{v}_\ell}{\bar{a}_\ell}\right). \tag{125}$$

Finally, it is rewarding to look back at the recent progress achieved at LEP and SLC in the knowledge of the neutral current leptonic couplings. The previous situation, illustrated in Fig. 37, was dominated by ν_μ, $\bar{\nu}_\mu$, ν_e, $\bar{\nu}_e$ scattering on electrons, e^+e^- annihilation into lepton pairs at PETRA and PEP, and polarized

	couplings without universality
v_e	-0.03844 ± 0.00071
v_μ	-0.0358 ± 0.0032
v_τ	-0.0365 ± 0.0015
a_e	-0.50111 ± 0.00043
a_μ	-0.50098 ± 0.00065
a_τ	-0.50103 ± 0.00074
	ratios of couplings
v_μ/v_e	0.932 ± 0.087
v_τ/v_e	0.949 ± 0.044
a_μ/a_e	0.9997 ± 0.0016
a_τ/a_e	0.9998 ± 0.0018
	couplings with universality
v_l	-0.03793 ± 0.00058
a_l	-0.50103 ± 0.00031

Table 5. *Results for the effective vector and axial-vector couplings derived from LEP and SLC.*[38]

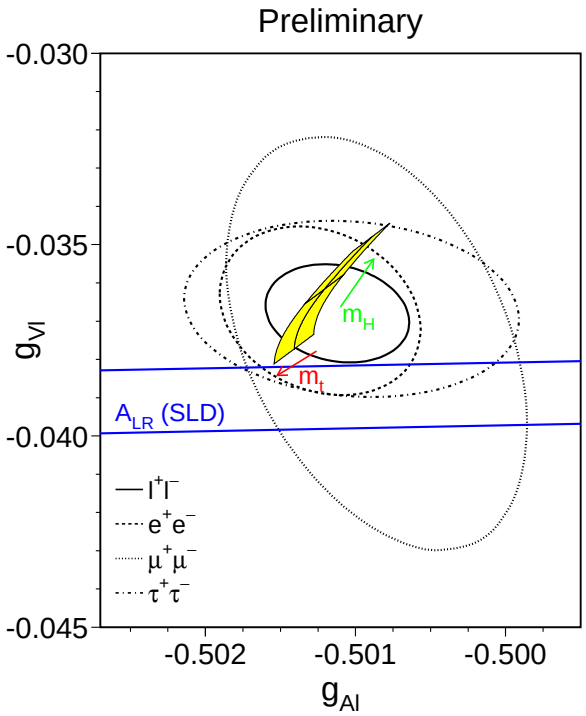

Fig. 35. *Universality test of the v_l and a_l couplings.*[38]

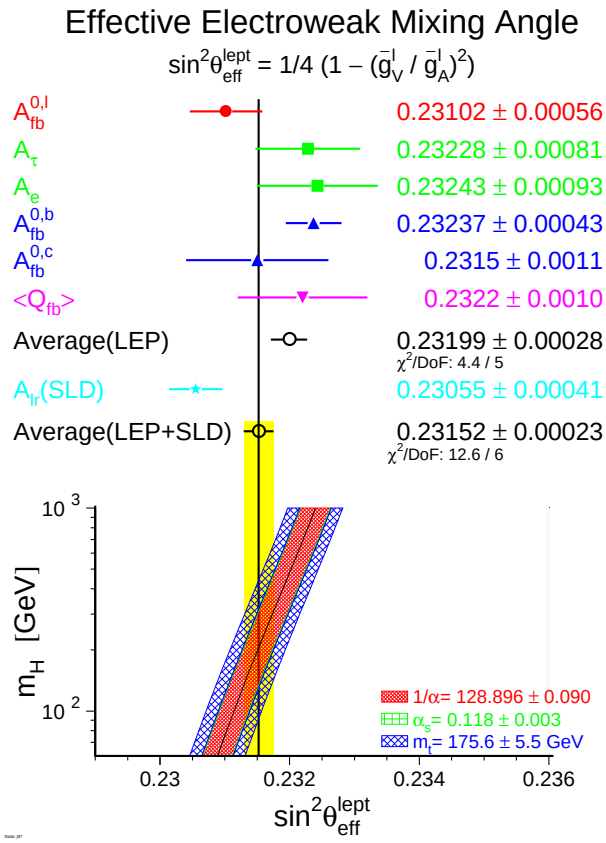

Fig. 36. *Measurements of* $\sin^2\theta_W$ *with asymmetries at LEP and SLC.*[38]

lepton scattering on nucleons. This is already a spectacular plot, pointing to a unique solution near $a_l \sim -0.5$ and $v_l \sim 0$. Zooming in twice on this spot with a magnification of ten each time, as pictured in Fig. 38, allows one to visualize the recent leap in precision which has been attained. This 100-fold increase in accuracy is the basis for precision tests of the Standard Theory, which we are going to discuss next.

2.6 Precision Tests of the Standard Model

2.6.1 Strategies

Calculations of observables in the Standard Model depend on the couplings e, g, and g'. It is, however, a more convenient choice to start with better known quantities, such as

$$\alpha^{-1}(0) = 137.0359895\ (61), \tag{126}$$

$$G = 1.166389\ (22)\ 10^{-5}\ \ \mathrm{GeV}^{-2}, \tag{127}$$

$$M_Z = 91186.7\ (2.0)\ \ \mathrm{MeV/c}^2. \tag{128}$$

QCD corrections depend on $\alpha_s(M_Z^2)$, which is precisely known from hadronic τ decays (see next lecture) or directly obtained through the global electroweak fit involving the Z width. The two determinations are in agreement and they are also well consistent with the other less precise values from lepton scattering and analyses of event shapes,[50] giving

$$\alpha_s(M_Z^2) = 0.1192 \pm 0.0020. \tag{129}$$

The basic test strategy is then to compare the measurement O_{exp} of an observable O for which the theoretical value depends on the input parameters $(\alpha, G, M_Z, \alpha_s)$ as well as on unknown quantities involved in the computation of radiative corrections (m_t, M_H):

$$O_{exp} = O_{th} = f(\alpha, G, M_Z, \alpha_s\ ;\ m_t, M_H). \tag{130}$$

The rule of the game is to find the range for m_t and M_H so that Eq. (130) is satisfied. This procedure should be repeated for all the electroweak observables in order to check the consistency.

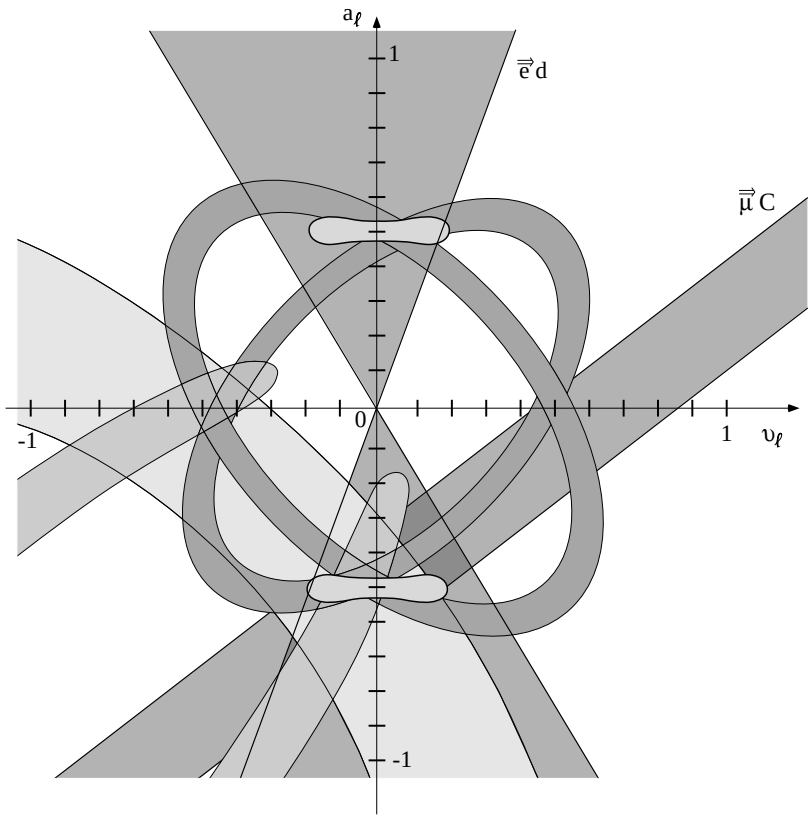

Fig. 37. *Allowed regions in the* (v_l, a_l) *plane from pre-LEP/SLC experiments (1986).*

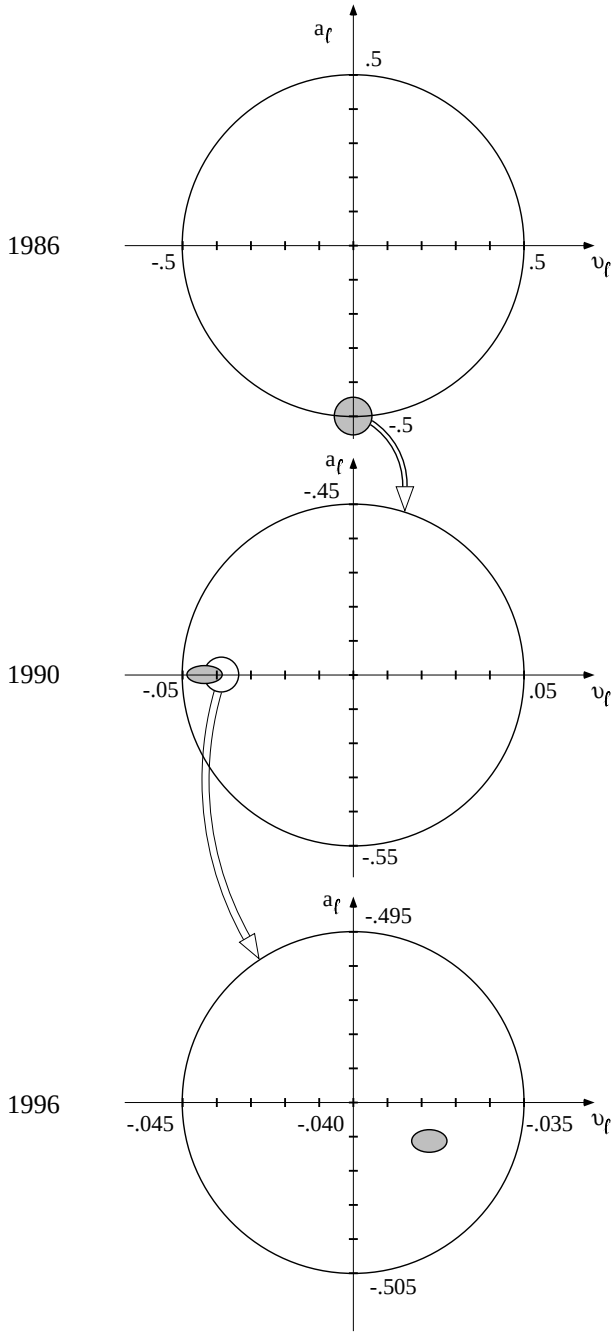

Fig. 38. *Progress in the determination of v_l, a_l with LEP and SLC.*[38] *Each zoom corresponds to a magnification of ten.*

2.6.2 The Mass of the Top Quark

The leading effect in the radiative corrections is proportional to m_t^2 [see Eqs. (72) and (76)]. Fixing the Higgs mass at 300 GeV/c^2 within a total range from 70 GeV/c^2 to 1 TeV/c^2, one derives

$$m_t = (177 \pm 7\ ^{+16}_{-19})\ \ \mathrm{GeV/c^2}, \tag{131}$$

where the second error accounts for the assumed Higgs range. This indirect determination of m_t is in very good agreement with the direct measurement at FNAL[51]:

$$m_t^{p\bar{p}} = (175.6 \pm 5.5)\ \ \mathrm{GeV/c^2}. \tag{132}$$

The consistency between the results (131) and (132) is another triumph of the Standard Model and the happy conclusion of more than a decade of top quark searches (Fig. 39).

2.6.3 The Mass of the Higgs Boson

With m_t now determined independently, the only unknown parameter remaining is M_H and it is clear from (131) and (132) that information can be extracted from the global electroweak fit. Before doing that, it is interesting to examine the most relevant observables in order to understand their respective sensitivities to M_H. They are M_W (or Δr), Γ_Z, Γ_l (or $\bar{\rho}$), and $\bar{s}^2$. Their present sensitivities are illustrated in Figs. 40, 41, 42, and 43.

At the present level of precision, the most significant constraint on M_H comes from asymmetries (providing $\bar{s}^2$). It is to be remarked that further progress here awaits improvements in the knowledge of $\alpha(M_Z^2)$, a point we shall return to in the next lecture. More experimental information is expected soon with the completion of the LEP1 analyses, the continuation of the A_{LR} measurement at SLAC, and the growing importance of the M_W determinations at FNAL and LEP2.

Figure 44 summarizes the results of the global electroweak fit: The allowed region for m_t and M_H shows a preference for a relatively light Higgs boson. When second-order EW corrections are taken into account[52] and new estimates of $\alpha(M_Z^2)$ are used,[50,53,54] the following determination is obtained[55]

$$M_H = (83\ ^{+61}_{-38})\ \ \mathrm{GeV/c^2}. \tag{133}$$

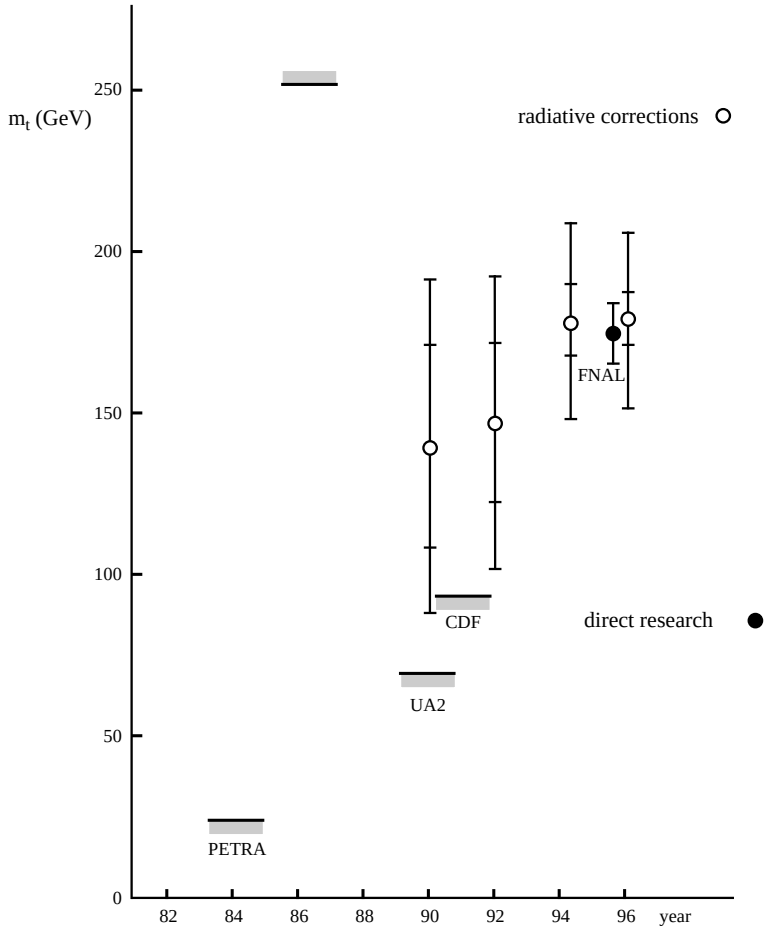

Fig. 39. *Progress in direct and indirect measurements of* m_t.

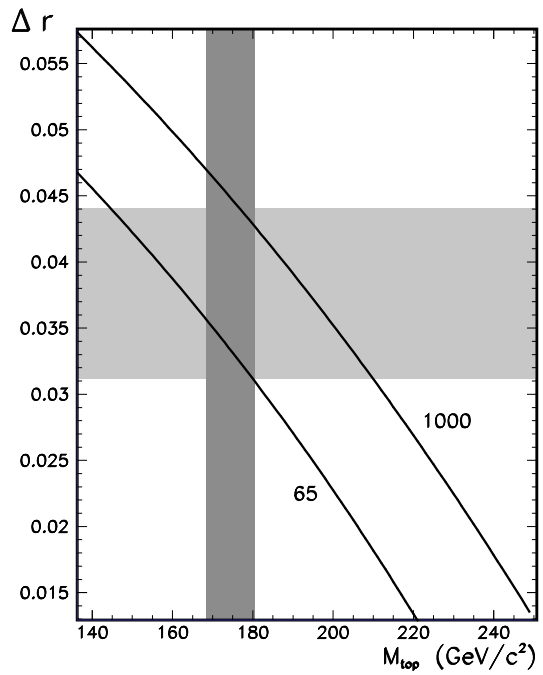

Fig. 40. *The sensitivity of* Δr *to* M_H*. The two curves are given for* $M_H = 65$ *and* $1000\ GeV/c^2$*. The vertical and horizontal bands correspond to the measurements, in particular* $M_W = (80.356 \pm 0.125)\ GeV/c^2$*.*

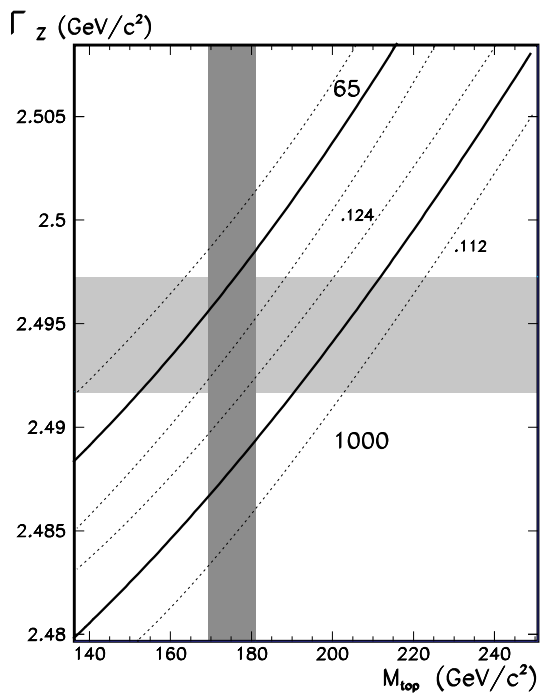

Fig. 41. *The sensitivity of* Γ_Z *to* M_H*. The dashed curves correspond to* $\alpha_s(M_Z^2) = 0.112$ *and* 0.124*.*

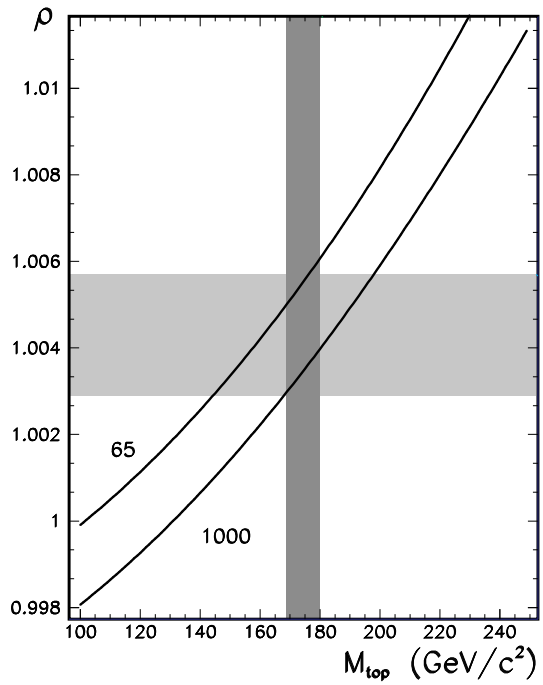

Fig. 42. *The sensitivity of* $\overline{\rho}$ *to* M_H.

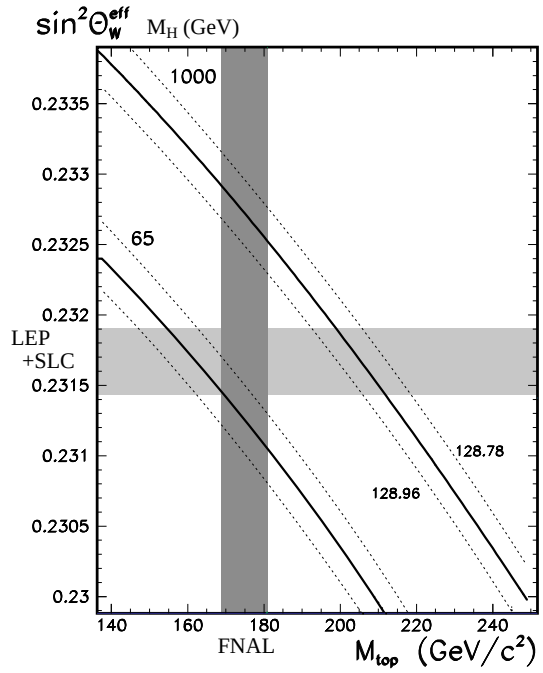

Fig. 43. *The sensitivity of* $\sin^2\theta_W$ *to* M_H. *The dashed curves correspond to* $\alpha^{-1} = 128.78$ *and* 128.96.

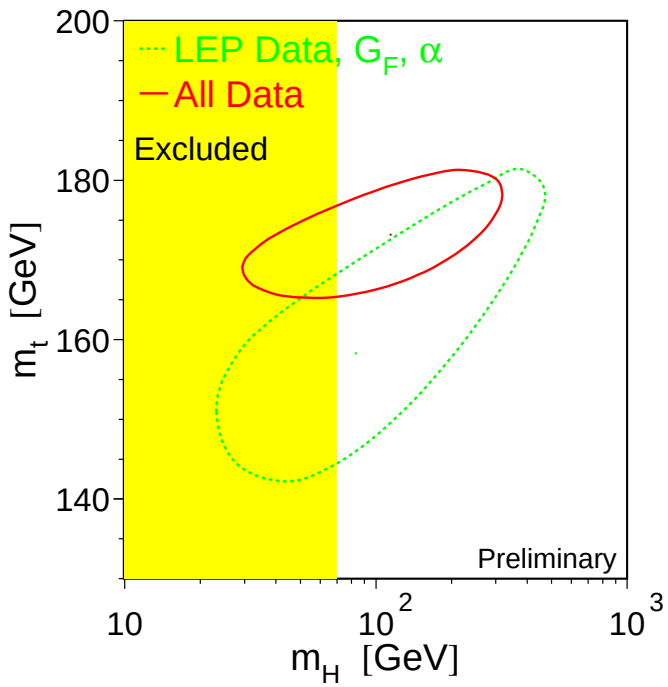

Fig. 44. *The allowed region in the* (m_t, M_H) *plane after the electroweak fit to LEP and SLC data.*[38]

The result (133) is an important product of the precision electroweak tests. This first experimental information about the Higgs mass complements the findings from the ρ parameter, which is in agreement with Higgs field doublets. Both results come from indirect methods, thus requiring confirmation through a direct Higgs boson(s) search. The result (133) is consistent with the 95% C.L. limit of 65 GeV/c^2 found at LEP1 and with the current limit of about 89 GeV/c^2 from LEP2. It makes the continuation of LEP2 running at the maximum energy particularly important. Masses up to about 105 GeV/c^2 will be explored with the foreseen LEP energies.

3 The τ, a Peculiar Standard Lepton

3.1 Introduction

In the first two lectures, we examined the weak leptonic couplings and concluded that they were universal to a precision of a few per mille. Thus, the Standard Electroweak Theory really involves three lepton (ν_l, l) doublets coupled universally to the gauge bosons. However, owing to their specific mass spectrum, the charged leptons show some quite distinct properties: The electron is stable, while the muon and the τ lepton are unstable. Moreover, the latter is heavy enough to decay into hadrons, hence opening a wide range of opportunities for studies which are not available with the lower-mass leptons. This peculiarity of the τ lepton is the subject of the last part of these lectures.

Hadronic decays of the τ are generated through the Feynman graph shown in Fig. 45(a). Since the involved exchange $(W^{\pm})$ is charged, the produced hadrons are in an $I = 1$ state. Because the weak transitions have $\Delta S = 1$, both $S = 0$ and $S = 1$ final states are present. Finally, since the current is $V - A$, both vector-like (V) and axial-vector-like (A) hadronic systems are produced, where V implies the spin-parities $J^P = 0^+, 1^-$ and $J^P = 0^-, 1^+$ for A.

It is instructive to compare hadronic τ decays to the process of e^+e^- annihilation into hadrons through the electromagnetic current, as depicted in Fig. 45(b). Here, only V (1^-) with $S = 0$ states are produced. However, both $I = 0$ and $I = 1$ final states are involved.

In the Standard Model, the "γ" and "W" vector currents with $S = 0$ are related through an isospin rotation. Thus, in the limit of massless u and d quarks (rather well satisfied in practice), the vector current is conserved (CVC) and the hadronic physics should factorize and be the same in the two processes.

3.2 Spectral Functions

In either τ decay or e^+e^- annihilation, hadrons can be seen as produced from the vacuum, as the initial state is purely leptonic. The corresponding transition is described by a *spectral function*.

In e^+e^- annihilation, it is essentially proportional to the cross section. For the $I = 1$ part, for example, one has

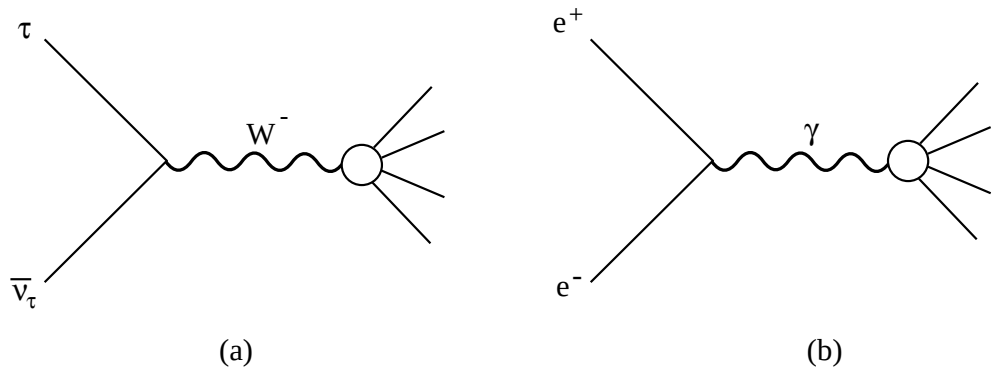

Fig. 45. *Hadronic production through weak and electromagnetic currents: (a) τ decay, and (b) e^+e^- annihilation.*

$$\sigma^{I=1}_{e^+e^-\to X^0}(s) \;=\; \frac{4\pi\alpha^2}{s}\, v_{1,\,X^-}(s), \tag{134}$$

where $v_1(s)$ is the nonstrange vector (isovector) spectral function.

In τ decay, the spectral functions are directly related to the invariant mass spectra of the hadronic final states, normalized to their respective branching ratios and corrected for the τ decay kinematics. The spectral function v_1 (a_1, a_0), where the subscript refers to the spin J of the hadronic system, is here defined for a nonstrange vector (axial-vector) hadronic τ decay channel $V^-\,\nu_\tau$ ($A^-\,\nu_\tau$). The spectral function is obtained by dividing the normalized invariant mass-squared distribution $(1/N_{V/A})(dN_{V/A}/ds)$ for a given hadronic mass $\sqrt{s}$ by the appropriate kinematic factor,

$$\begin{aligned} v_1(s) \;&\equiv\; \frac{M_\tau^2}{6\,|V_{ud}|^2\,S_{\rm EW}}\,\frac{B(\tau^-\to V^-\,\nu_\tau)}{B(\tau^-\to e^-\,\bar\nu_e\nu_\tau)} \\ &\qquad\times\frac{dN_V}{N_V\,ds}\left[\left(1-\frac{s}{m_\tau^2}\right)^2\left(1+\frac{2s}{M_\tau^2}\right)\right]^{-1}, \end{aligned} \tag{135}$$

$$\begin{aligned} a_1(s) \;&\equiv\; \frac{M_\tau^2}{6\,|V_{ud}|^2\,S_{\rm EW}}\,\frac{B(\tau^-\to A^-\,\nu_\tau)}{B(\tau^-\to e^-\,\bar\nu_e\nu_\tau)} \\ &\qquad\times\frac{dN_A}{N_A\,ds}\left[\left(1-\frac{s}{M_\tau^2}\right)^2\left(1+\frac{2s}{M_\tau^2}\right)\right]^{-1}, \end{aligned} \tag{136}$$

$$a_0(s) \;\equiv\; \frac{M_\tau^2}{6\,|V_{ud}|^2\,S_{\rm EW}}\,\frac{B(\tau^-\to \pi^-\,\nu_\tau)}{B(\tau^-\to e^-\,\bar\nu_e\nu_\tau)}\,\frac{dN_A}{N_A\,ds}\left(1-\frac{s}{M_\tau^2}\right)^{-2}, \tag{137}$$

where $|V_{ud}| = 0.9752 \pm 0.0007$ (Ref. 10) denotes the CKM weak mixing matrix element and $S_{\rm EW} = 1.0194 \pm 0.0040$ accounts for electroweak radiative corrections[15] (see also the discussion in Ref. 56). Due to the conserved vector current, there is no $J = 0$ contribution to the vector spectral function, while the only contribution to a_0 is assumed to be from the pion pole. It is connected via PCAC to the pion decay constant, $a_{0,\pi}(s) = 4\pi^2 f_\pi^2\, \delta(s - m_\pi^2)$. The spectral functions are normalized by the ratio of the vector/axial-vector branching fraction $B(\tau^- \to V^-/A^-\, \nu_\tau)$ to the branching fraction of the massless leptonic, i.e., electron, channel

$$B(\tau^- \to e^-\, \bar{\nu}_e \nu_\tau) = (17.794 \pm 0.045)\%, \tag{138}$$

where the value includes the improvement in accuracy provided by the universality assumption of leptonic currents together with the measurements of $B(\tau^- \to e^-\, \bar{\nu}_e \nu_\tau)$, $B(\tau^- \to \mu^-\, \bar{\nu}_\mu \nu_\tau)$, and the τ lifetime.

Using unitarity and analyticity, the spectral functions of hadronic τ decays are connected to the imaginary part of the two-point correlation (or hadronic vacuum polarization) functions[57,58] $\Pi^{\mu\nu}_{ij,U}(q) \equiv i \int d^4x\, e^{iqx} \langle 0|T(U^\mu_{ij}(x) U^\nu_{ij}(0)^\dagger)|0\rangle = (-g^{\mu\nu} q^2 + q^\mu q^\nu)\, \Pi^{(1)}_{ij,U}(q^2) + q^\mu q^\nu\, \Pi^{(0)}_{ij,U}(q^2)$ of vector ($U^\mu_{ij} \equiv V^\mu_{ij} = \bar{q}_j \gamma^\mu q_i$) or axial-vector ($U^\mu_{ij} \equiv A^\mu_{ij} = \bar{q}_j \gamma^\mu \gamma_5 q_i$) color-singlet quark currents in corresponding quantum states and for time-like momenta-squared $q^2 > 0$. A Lorentz decomposition is used to separate the correlation function into its $J = 1$ and $J = 0$ parts. Thus, using the definitions (135)–(137), one identifies for nonstrange quark currents

$$\mathrm{Im}\, \Pi^{(1)}_{\bar{u}d,V/A}(s) = \frac{1}{2\pi} v_1/a_1(s), \qquad \mathrm{Im}\, \Pi^{(0)}_{\bar{u}d,A}(s) = \frac{1}{2\pi} a_0(s), \tag{139}$$

which provide the basis for comparing theory with data.

3.3 Determination of the Spectral Functions in τ Decays

The V/A separation is in principle easy because it only involves pion counting in every event. This is a consequence of isospin invariance, expressed through the G parity. For an eigenstate of particle-antiparticle symmetry, one has $G = (-1)^n = C(-1)^I$, where n is the number of pions (charged or neutral). In e^+e^- annihilation, $C = -1$ and n is even (odd) for $I = 1$ ($I = 0$) states, respectively. The same applies to τ decays because of CVC and therefore n is even (odd) for V (A) states. Since a $K\bar{K}$ pair is not an eigenstate of G parity, some additional

information must be used for final states involving such pairs. Fortunately, they do not occur frequently in τ decays.

The measurement of the τ spectral functions defined in Eq. (135) requires the determination of the physical invariant mass-squared distribution. To extract it from the measured one, it needs to be unfolded from the effects of measurement distortion. A complete determination of the V and A spectral functions has been published by the ALEPH Collaboration.[59,60] We now proceed to discuss these results and extract the relevant hadron physics.

The exclusive vector and axial-vector τ decay channels are listed in Table 6. Unless otherwise specified, their branching ratios are taken from ALEPH publications,[61,62] applying small corrections taking into account new ALEPH results on branching fractions of τ decay modes involving kaons.[63] In some cases, additional information is taken from the Particle Data Group[10] as described in Ref. 59. The individual fractions have been refitted so that the sum of all hadronic and leptonic branching ratios adds up to 100%, where the latter are derived from Eq. (138) assuming universality of the lepton couplings. This normalization slightly modifies the values given in the above references. The branching ratios of the subsequent meson decays are taken from Ref. 10. The two-, four-, and, in part, the six-pion modes are exclusively reconstructed. Special care is taken with isospin-violating ω and η decays, and with kaon pair production.

The spectral functions of the dominant two- and four-pion vector modes are shown in the first three plots of Fig. 46. The errors shown are the diagonal elements of the covariance matrix (some systematic effects and the unfolding procedure do correlate the uncertainties in different bins). They include both statistical and systematic uncertainties. The $2\pi^-\pi^+\pi^0\,\nu_\tau$ decay mode is compared to data of the ARGUS Collaboration.[64]

Among many tests of the unfolding, including the method itself and the understanding of the detector performance, Fig. 47 shows the unfolded $2\pi^-\pi^+\,\nu_\tau$ and $\pi^-2\pi^0\,\nu_\tau$ mass spectra with reasonable agreement in shape and normalization.

The complete inclusive τ vector spectral function and its contributions are shown in Fig. 48. The dashed line depicts the naive parton model prediction while the massless QCD prediction[65] using $\alpha_s(M_Z^2) = 0.120$ (solid line) lies roughly 14% higher at m_τ^2. One observes that at $s \sim m_\tau^2$ the inclusive τ vector spectral function is larger than the QCD prediction, i.e., it is not yet in the asymptotic region.

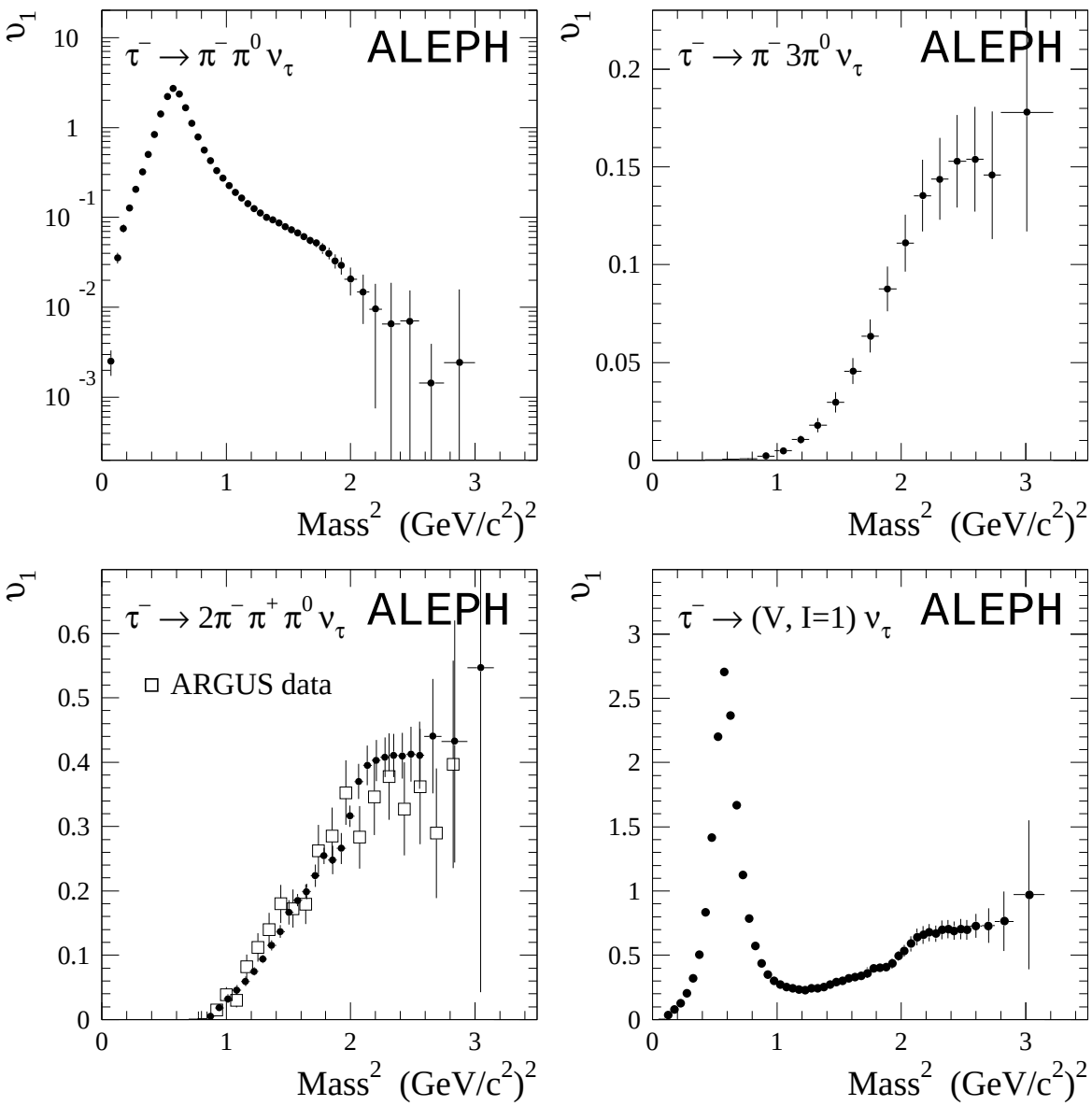

Fig. 46. *Spectral functions of the τ decay channels $\pi^-\pi^0\,\nu_\tau$, $\pi^-3\pi^0\,\nu_\tau$, $2\pi^-\pi^+\pi^0\,\nu_\tau$, and the total τ vector spectral function. The error bars are the diagonal elements of the covariance matrices. They contain both statistical and systematic contributions. The ARGUS data*[64] *in the $\tau^- \to 2\pi^-\pi^+\pi^0\,\nu_\tau$ channels contain statistical errors only.*

Vector	BR (in %)	Axial-Vector	BR (in %)
$\pi^-\pi^0\,\nu_\tau$	25.34 ± 0.19	$\pi^-\,\nu_\tau$	11.23 ± 0.16
$\pi^-3\pi^0\,\nu_\tau$	1.18 ± 0.14	$\pi^-2\pi^0\,\nu_\tau$	9.23 ± 0.17
$2\pi^-\pi^+\pi^0\,\nu_\tau$	2.42 ± 0.09	$2\pi^-\pi^+\,\nu_\tau$	9.15 ± 0.15
$\pi^-5\pi^0\,\nu_\tau$	0.04 ± 0.02	$\pi^-4\pi^0\,\nu_\tau$	0.03 ± 0.03
$2\pi^-\pi^+3\pi^0\,\nu_\tau$		$2\pi^-\pi^+2\pi^0\,\nu_\tau$	0.10 ± 0.02
$3\pi^-2\pi^+\pi^0\,\nu_\tau$		$3\pi^-2\pi^+\,\nu_\tau$	0.07 ± 0.01
$\omega\,\pi^-\,\nu_\tau$	1.93 ± 0.10	$\omega\,\pi^-\pi^0\,\nu_\tau$	0.39 ± 0.11
$\eta\,\pi^-\pi^0\,\nu_\tau$	0.17 ± 0.03	$\eta\,2\pi^-\pi^+\,\nu_\tau$	0.04 ± 0.01
–	–	$\eta\,\pi^-2\pi^0\,\nu_\tau$	0.02 ± 0.01
$K^-K^0\,\nu_\tau$	0.19 ± 0.04	–	–
$K^-K^+\pi^-\,\nu_\tau$	0.08 ± 0.08	$K^-K^+\pi^-\,\nu_\tau$	0.08 ± 0.08
$K^0\bar{K}^0\pi^-\,\nu_\tau$	0.08 ± 0.08	$K^0\bar{K}^0\pi^-\,\nu_\tau$	0.08 ± 0.08
$K^-K^0\pi^0\,\nu_\tau$	0.05 ± 0.05	$KK^0\pi^0\,\nu_\tau$	0.05 ± 0.05
$K\bar{K}\pi\pi\,\nu_\tau$	0.08 ± 0.08	$K\bar{K}\pi\pi\,\nu_\tau$	0.08 ± 0.08
Total Vector	31.58 ± 0.29	Total Axial-Vector	30.56 ± 0.30

Table 6. *Vector and axial-vector hadronic τ decay modes with their contributing branching fractions. The branching ratios shown are refitted so that the compilation of all τ decay channels sums up to one.*

The total inclusive axial-vector spectral function and its contributions are plotted in Fig. 49 together with the naive parton model and the massless, perturbative QCD prediction. One again notices that the asymptotic regime has apparently not been reached at the τ mass scale.

3.4 Comparison to e^+e^-

3.4.1 Tests of CVC

The most precise spectral function measurements of the τ vector current final states $\pi^-\pi^0$, $\pi^-3\pi^0$, and $2\pi^-\pi^+\pi^0$ can be compared to the cross sections of the corresponding e^+e^- annihilation isovector states $\pi^+\pi^-$, $\pi^+\pi^-\pi^+\pi^-$, and $\pi^+\pi^-\pi^0\pi^0$.

If for the $\pi^-\pi^0$ state the comparison is straightforward, some care should be exercised for the four-pion modes. In the classification developed by Pais,[66] pion

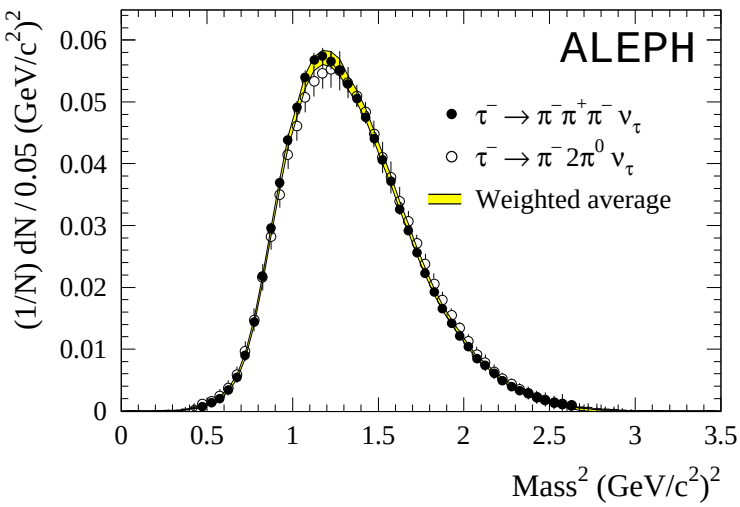

Fig. 47. *Unfolded (physical) invariant mass-squared spectra of the τ final states $2\pi^-\pi^+\,\nu_\tau$ and $\pi^-2\pi^0\,\nu_\tau$, and their weighted average.*

isospin states are organized in symmetry classes with orthogonal wave functions. To each isospin class $\{ijk\}$ corresponds a partial width Γ_{ijk} in τ decays and a cross section σ_{ijk} in e^+e^- annihilation. In these terms, the four-pion isovector states are linear combinations of the classes $\{310\}$ and $\{211\}$:

$$\begin{aligned}
\Gamma_{\pi^\pm 3\pi^0} &= \frac{2}{5}\Gamma_{310}, \\
\Gamma_{3\pi^\pm\pi^0} &= \Gamma_{211} + \frac{3}{5}\Gamma_{310}, \\
\sigma_{\pi^+\pi^-\pi^+\pi^-} &= \frac{4}{5}\sigma_{310}, \\
\sigma_{\pi^+\pi^-\pi^0\pi^0} &= \sigma_{211} + \frac{1}{5}\sigma_{310}.
\end{aligned}$$

Using Eq. (135) and isospin rotation, the following relations hold:

$$\sigma^{I=1,0}_{e^+e^-\to\pi^+\pi^-} - \Delta I_{\rho\omega} = \frac{4\pi\alpha^2}{s}\, v_{1,\,\pi^-\pi^0\,\nu_\tau}, \tag{140}$$

$$\sigma^{I=1}_{e^+e^-\to\pi^+\pi^-\pi^+\pi^-} = 2\cdot\frac{4\pi\alpha^2}{s}\, v_{1,\,\pi^-\,3\pi^0\,\nu_\tau}, \tag{141}$$

$$\sigma^{I=1}_{e^+e^-\to\pi^+\pi^-\pi^0\pi^0} = \frac{4\pi\alpha^2}{s}\left[v_{1,\,2\pi^-\pi^+\pi^0\,\nu_\tau} - v_{1,\,\pi^-\,3\pi^0\,\nu_\tau}\right]. \tag{142}$$

In Eq. (140) the small isospin-violating, isoscalar, electromagnetic contribution $\omega(782) \to \pi^+\pi^-$ is taken into account through its interference with the main

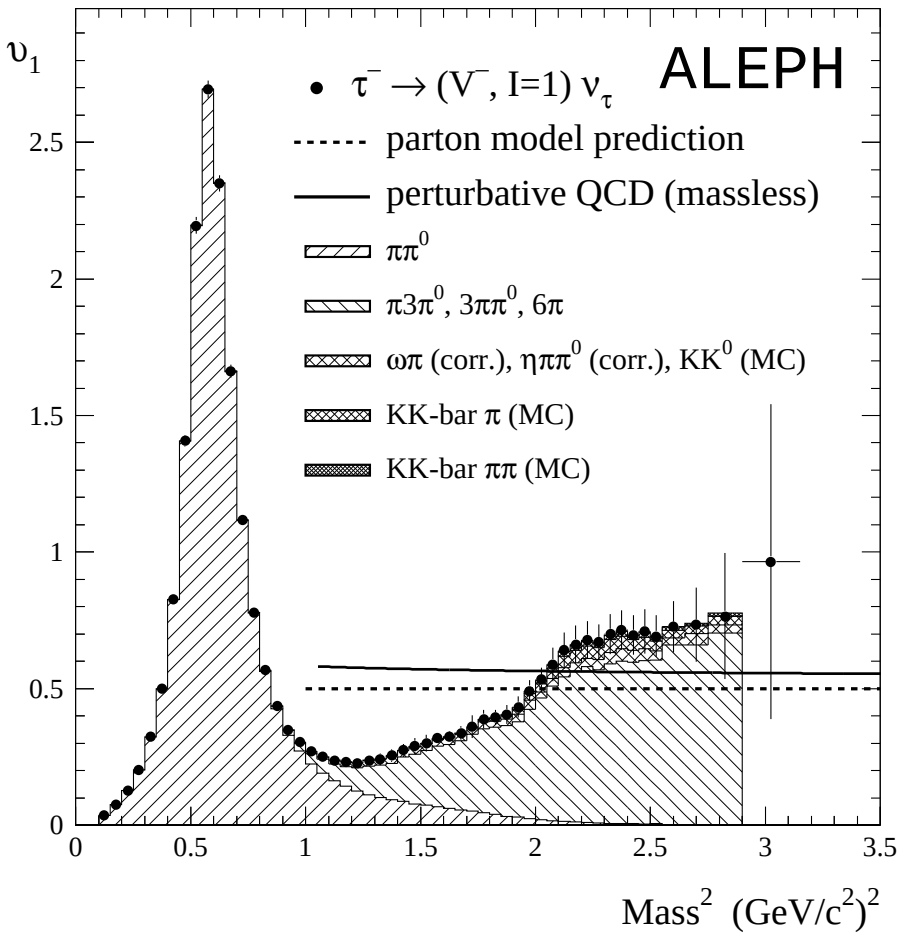

Fig. 48. *Total vector spectral function. The shaded areas indicate the contributions from the exclusive τ vector channels, where the shapes of the contributions labeled* "MC" *are taken from the Monte Carlo simulation. The lines show the predictions from the naive parton model and from massless perturbative QCD using $\alpha_s(M_Z^2) =$* 0.120.

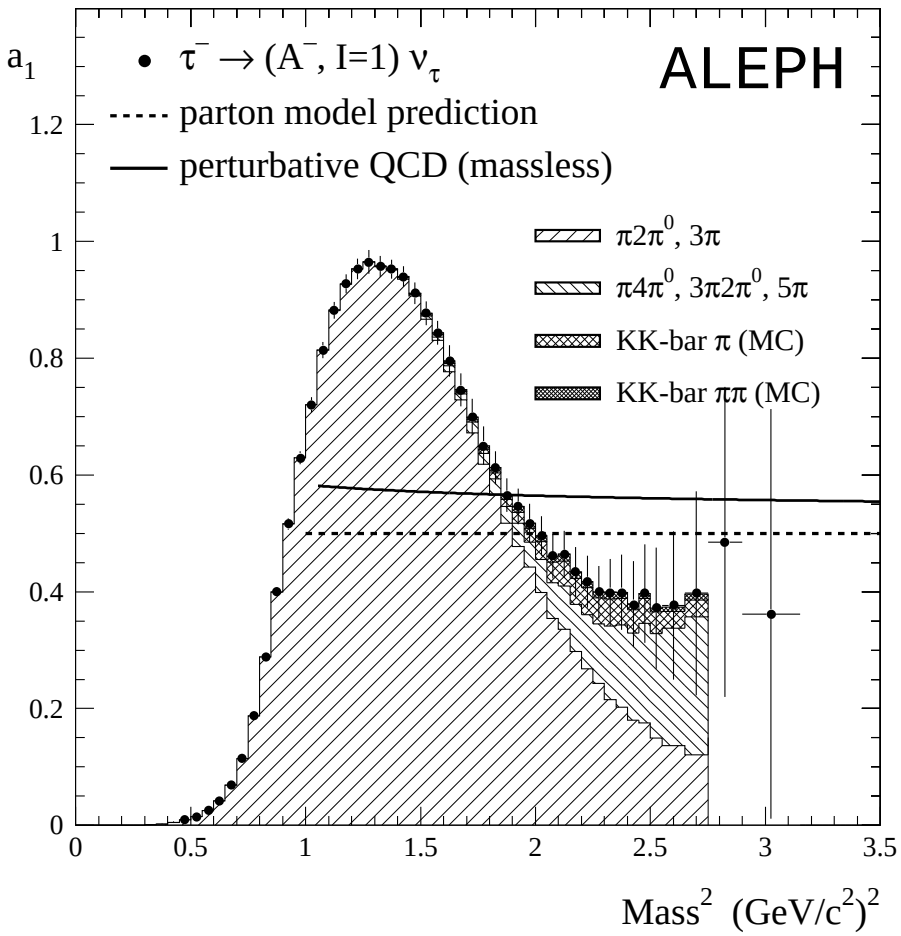

Fig. 49. *Total inclusive τ axial-vector current spectral function (without the pion pole). The lines show the prediction from the naive parton model and from massless perturbative QCD using $\alpha_s(M_Z^2) = 0.120$.*

isovector contribution yielding the (s-dependent) correction $\Delta I_{\rho\omega}$ obtained from a fit of the total $e^+e^- \to \pi^+\pi^-$ cross section.[67]

The comparison is shown in Fig. 50 for the two-pion channel and in Fig. 51 for the four-pion modes. Satisfactory agreement is found in both cases, although the quality of the $e^+e^- \to \pi^+\pi^-\pi^0\pi^0$ data is poor.

Finally, the total e^+e^- isovector cross section is compared to the τ vector current spectral function in Fig. 52. This comparison provides a good global test of CVC.

3.4.2 Fit of the Pion Form Factor

The two-pion spectral function is closely related to the pion form factor:

$$|\tilde{F}_\pi^{I=1}(s)|^2 \;=\; \frac{12}{\beta_\pi^3(s)}\, v_{1,\,\pi^-\pi^0}(s), \tag{143}$$

where $\beta_\pi(s) = (1 - 4m_\pi^2/s)^{1/2}$ is the pion velocity in the hadronic center of mass. The weak pion form factor can be identified with the isovector electromagnetic form factor, given by

$$|F_\pi^{I=1}(s)|^2 \;=\; \frac{3}{\pi}\,\frac{s}{\alpha^2\,\beta_\pi^3(s)}\,\sigma^{I=1}_{e^+e^-\to\pi^+\pi^-}, \tag{144}$$

using isospin invariance (CVC).

In the time-like region, the pion form factor is given by contributions from the known isovector meson resonances $\rho(770)$, $\rho(1450)$, and $\rho(1700)$, taking into account $\rho-\omega$ interference[67]:

$$F_\pi^{I=1,0}(s) \;=\; \frac{\mathrm{BW}_{\rho(770)}(s)\,\frac{1+\delta\,\mathrm{BW}_{\omega(783)}(s)}{1+\delta} \;+\; \beta\,\mathrm{BW}_{\rho(1450)}(s) \;+\; \gamma\,\mathrm{BW}_{\rho(1700)}(s)}{1 \;+\; \beta \;+\; \gamma}, \tag{145}$$

with the Breit-Wigner propagators

$$\mathrm{BW}^{\mathrm{KS}}_{\rho(M_\rho)}(s) \;=\; \frac{M_\rho^2}{M_\rho^2 \;-\; s \;-\; i\sqrt{s}\,\Gamma_\rho(s)} \tag{146}$$

and the energy-dependent width

$$\Gamma_\rho(s) \;=\; \Gamma_\rho(M_\rho^2)\,\left(\frac{M_\rho^2}{s}\right)\left(\frac{k(s)}{k(M_\rho^2)}\right)^3, \tag{147}$$

where $k(s) = \frac{1}{2}\sqrt{s}\,\beta_\pi(s)$ and $k(M_\rho^2)$ is the pion momentum in the ρ rest frame.

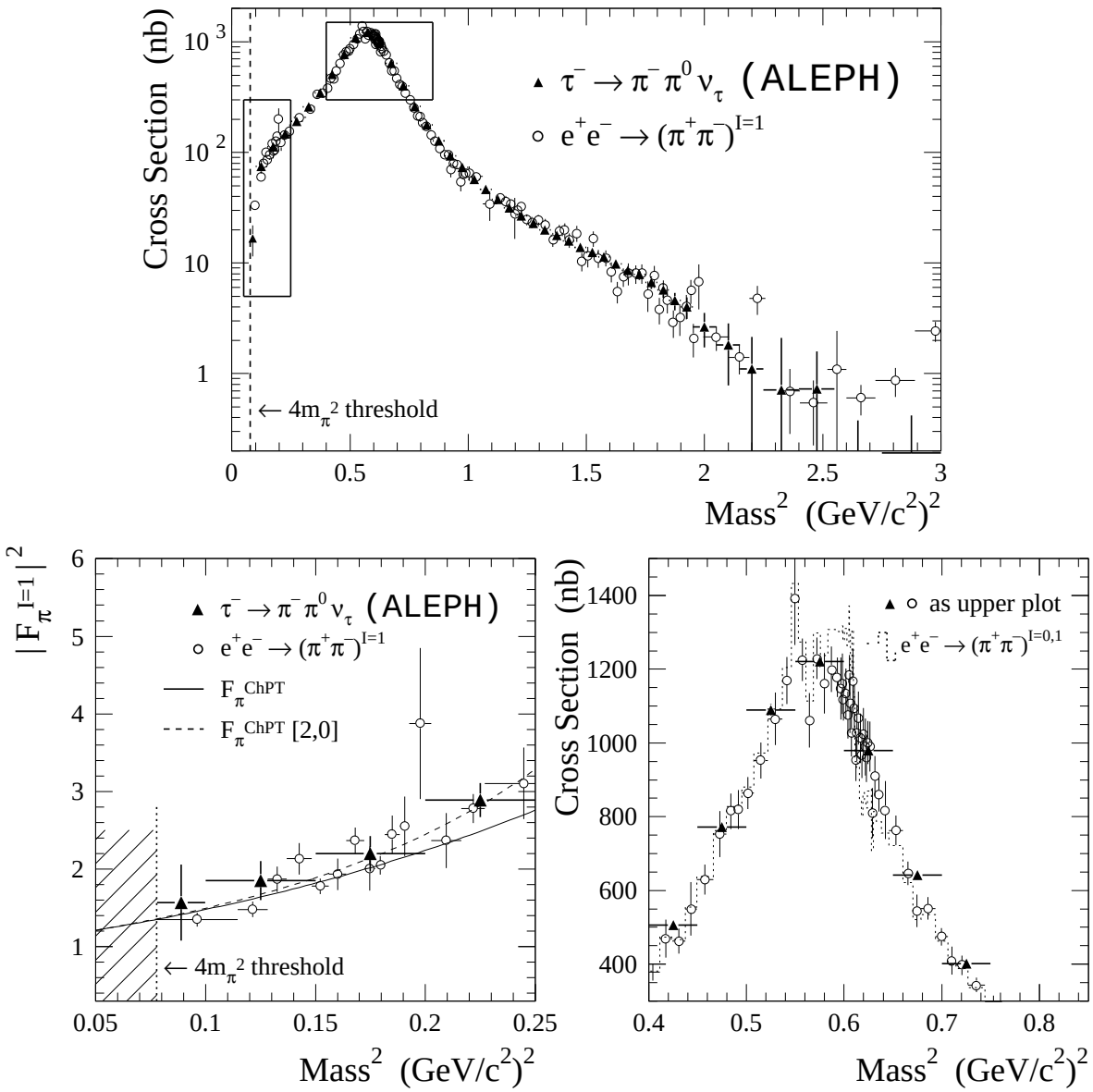

Fig. 50. *The two-pion data from τ decays compared to the corresponding* <u>*isovector*</u> *e^+e^- cross section (data points from different e^+e^- experiments, measured at the same mass have been averaged). Both distributions are shown with statistical and systematic errors. The two rectangles indicate the regions that are expanded in (b) and (c); (b) shows the pion form factor near threshold. The additional function labeled "$[2,0]$" (indistinguishable from "$[1,1]$" in the plotted energy region) denotes different parametrizations (Padé approximants*[68]*) deduced from Chiral Perturbation Theory as discussed in Refs. 70 and 71. The dotted line in (c) represents the total (uncorrected) isoscalar and isovector e^+e^- cross section.*

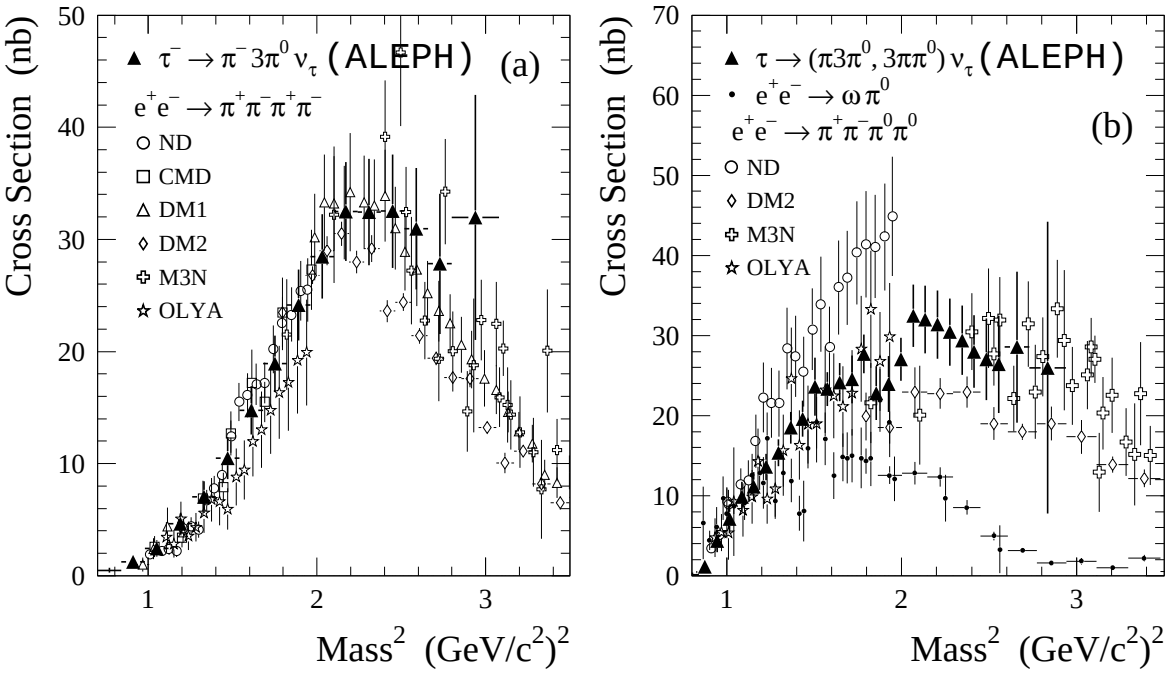

Fig. 51. *Comparison of the isospin-rotated four-pion τ data with the corresponding e^+e^- cross sections, for the final states (a) $\pi^+\pi^-\pi^+\pi^-$ and (b) $\pi^+\pi^-\pi^0\pi^0$. The error bars shown contain both statistical and systematic errors. An enhancement in the low mass part of the $\pi^+\pi^-\pi^0\pi^0$ channel in (b) is expected from the resonant $\omega\pi$ contribution (small dots).*

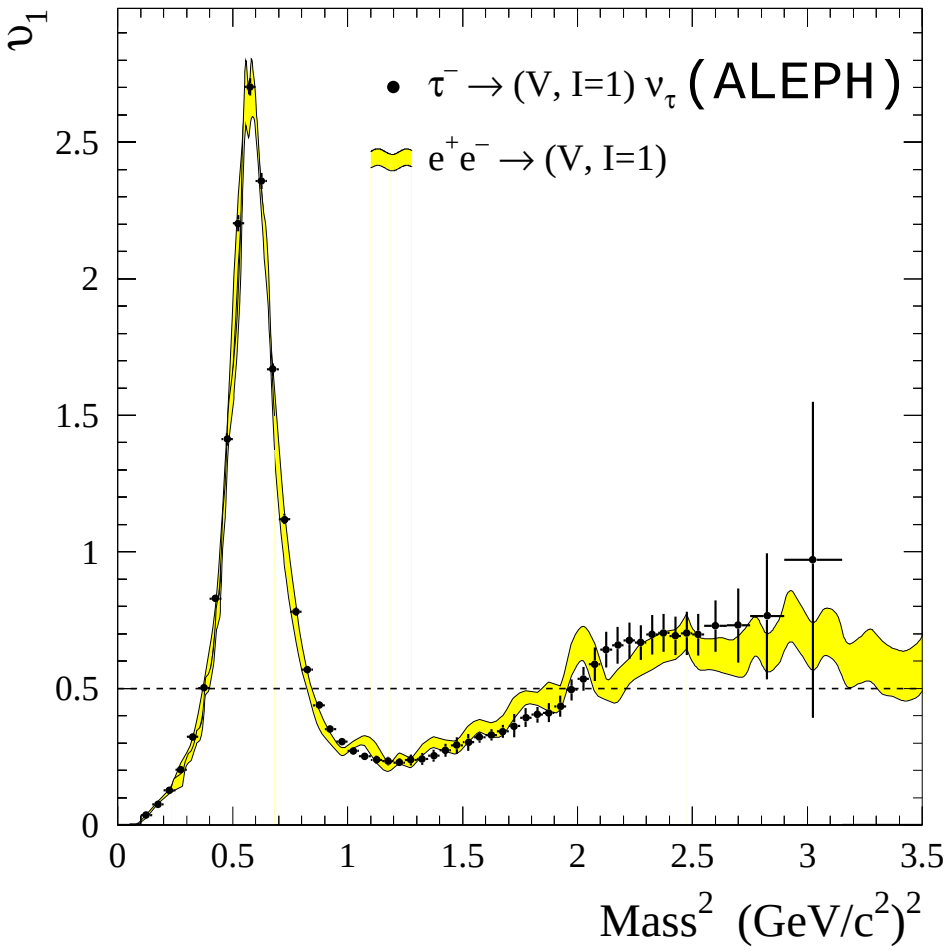

Fig. 52. *Total hadronic vector current spectral function from τ decays (data points), and the corresponding distribution calculated from e^+e^- isovector states using isospin symmetry. The shaded band includes statistical and systematic errors. The dashed line corresponds to the naive isovector quark-parton prediction.*

A more refined description of the broad ρ resonance line shape is provided by the Gounaris-Sakurai parametrization[69] which satisfies analyticity, contrary to the previous one.

The fits to the ALEPH τ data establish the need for the $\rho(1450)$ contribution to the weak pion form factor in the KS and GS parametrizations ($\beta = -0.087 \pm 0.012$) with a fitted mass $M_{\rho(1450)} = (1380 \pm 24)$ MeV/c^2 when fixing the width at $\Gamma_{\rho(1450)} = 310$ MeV/c^2 (Ref. 10). No significant evidence of a $\rho(1700)$ contribution is found ($\gamma = -0.008 \pm 0.008$). The previous values are the weighted averages between the results of both fit types. Their errors account for statistical and systematic uncertainties coming from model dependence. Figure 53 shows the fits using one and three Breit-Wigner amplitudes.

It is interesting to perform a combined fit of the pion form factor using both e^+e^- and τ data in order to explore *with the same resonance parametrization* isospin invariance for the dominant ρ contribution (the statistics of the data at larger masses does not allow us to check this for the other resonances, which are assumed to be isospin invariant).

Although the absolute values of the $\rho(770)$ masses and widths depend significantly on the resonance parametrization, their respective differences, i.e., $\Delta M_{\rho(770)} = M_{\rho^\pm(770)} - M_{\rho^0(770)}$ and $\Delta\Gamma_{\rho(770)} = \Gamma_{\rho^\pm(770)} - \Gamma_{\rho^0(770)}$ are stable. Averaging the two types of fit, the following results are obtained:

$$\begin{aligned} \Delta M_{\rho(770)} &= (0.0 \pm 1.0 \pm 0.1) \ \text{MeV/c}^2, \\ \Delta\Gamma_{\rho(770)} &= (0.1 \pm 1.8 \pm 0.5) \ \text{MeV/c}^2. \end{aligned}$$

The first errors are due to statistical and systematic uncertainties (including correlations between the fit parameters), while the second ones account for differences from the resonance parametrizations. Figure 54 shows the results with its 39% C.L. error ellipse taking into account correlations.

A difference between $\Gamma_{\rho^\pm}$ and Γ_{ρ^0} could occur on one hand through electromagnetic isospin-violating decay modes such as $\rho \to \pi\pi\gamma$, which is observed at the 1% level for the ρ^0 (Ref. 10). On the other hand, the dominant $\rho \to \pi\pi$ channel could also manifest some isospin violation. An obvious contribution comes from the observed $\pi^\pm - \pi^0$ and potential $\rho^\pm - \rho^0$ mass differences which are reflected in different values for the width according to Eq. (147). The ρ mass dependence is

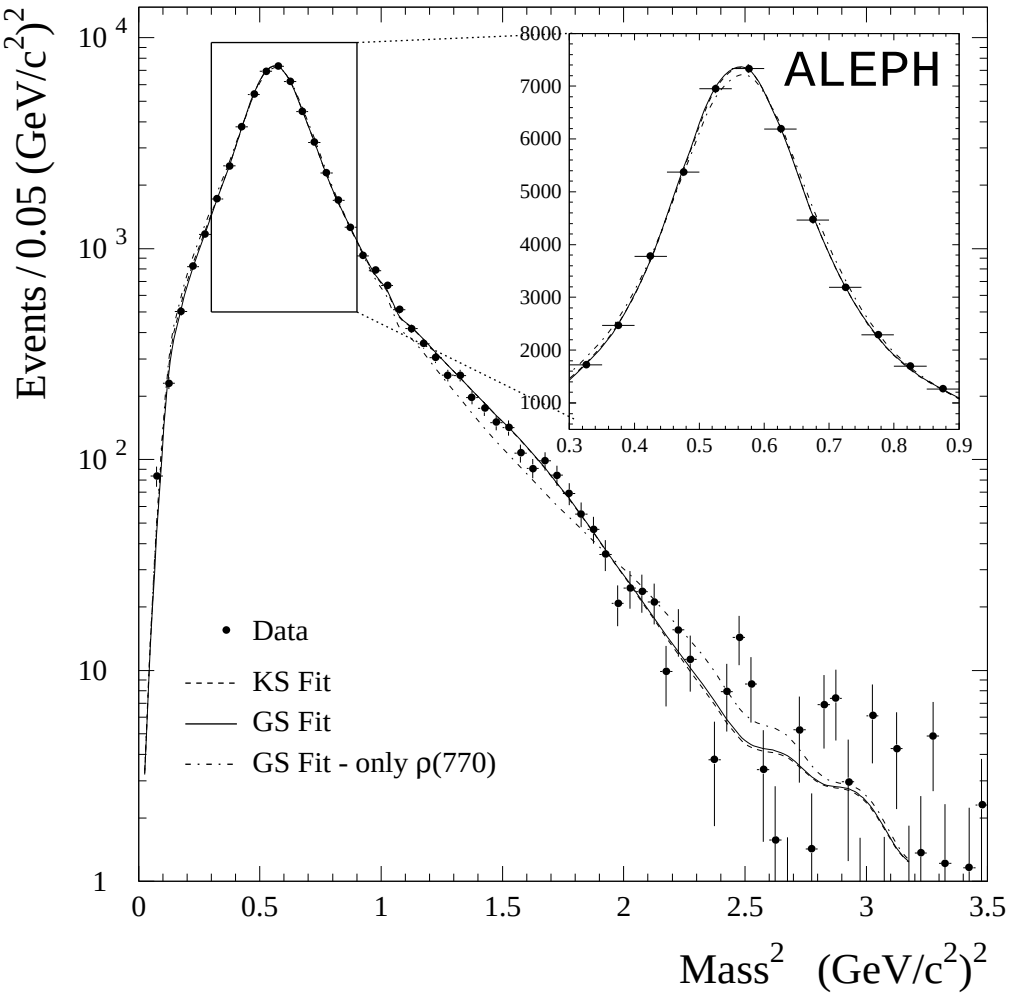

Fig. 53. *Fit of the* $\tau^- \to \pi^-\pi^0\,\nu_\tau$ *invariant mass spectrum using the Kühn-Santamaria (KS) and the Gounaris-Sakurai (GS) parametrizations. The solid and dashed curves are the functions corresponding to the KS/GS-type form factor fits. They have been convolved with the detector resolution and the* τ *phase space. Due to statistical fluctuations in the detector response matrix, the functions are not smooth after convolution. The dashed-dotted line corresponds to a GS-type fit in which only the* $\rho(770)$ *contribution is taken into account.*

not completely clear: one could consider a variation given by

$$\Gamma_\rho \sim k^3(M_\rho^2)/M_\rho^2, \tag{148}$$

or, as argued in Chiral Perturbation Theory,[72]

$$\Gamma_\rho \sim k^3(M_\rho^2). \tag{149}$$

According to the charge of the ρ, the pion momentum in the ρ rest system is given by $2k(M_{\rho^0}^2) = (M_{\rho^0}^2 - 4m_{\pi^\pm}^2)^{1/2}$ for the neutral ρ^0 and $2k(M_{\rho^\pm}^2) = [M_{\rho^\pm}^2 - 2(m_{\pi^\pm}^2 + m_{\pi^0}^2) + (m_{\pi^\pm}^2 - m_{\pi^0}^2)^2/M_{\rho^\pm}^2]^{1/2}$ for the charged $\rho^\pm$. The dashed and solid lines in Fig. 54 give the functional dependence of the width difference $\Delta\Gamma_\rho$ on ΔM_ρ in the approximations of Eqs. (148) and (149), respectively, normalized to the fitted value of Γ_ρ.

It is interesting to observe that the measured ΔM_ρ is significantly smaller than the mass difference between charged and neutral pions $\Delta M_\pi = M_{\pi^\pm} - M_{\pi^0}$ = (4.5936 ± 0.0007) MeV/c^2 (Ref. 10), where the dominant effect is understood to be of electromagnetic origin ($\Delta M_\pi^{\rm em} \simeq 4.5$ MeV/c^2, Ref. 73). The ΔM_ρ measurement can be compared, however, to the (model dependent) result of $\Delta M_\rho = (-0.3 \pm 2.2)$ MeV/c^2 (Ref. 10) obtained in hadronic production, and is in good agreement with this determination. The Mark III Collaboration exploited data on $J/\psi \to \pi^+\pi^-\pi^0$ decays, dominated by $J/\psi \to \rho\pi$, to measure the mass difference of the charged and neutral ρ's (Ref. 74). Their preliminary result is found to be in good agreement with the result presented here. Note that the value deduced from the difference in the mean values taken from Ref. 10, $\langle M_{\rho^\pm}\rangle - \langle M_{\rho^0}\rangle = (-1.8 \pm 1.4)$ MeV/c^2, is potentially unreliable as they both represent the weighted mean of independent measurements which did not necessarily use the same parametrizations. A theoretical electromagnetic ρ mass difference of -0.7 MeV/c^2 $< \Delta M_\rho < 0.4$ MeV/c^2, in agreement with the measurement, has recently been evaluated in Ref. 75. The measured difference $\Delta\Gamma_\rho$ is found to be consistent with the expected isospin violation from the $\pi^\pm$–π^0 and $\rho^\pm$–ρ^0 mass differences.

3.5 $V - A$ Spectral Functions and Chiral Sum Rules

The application of chiral symmetry leads to low-energy sum rules involving the difference of vector and axial-vector spectral functions by virtue of the optical

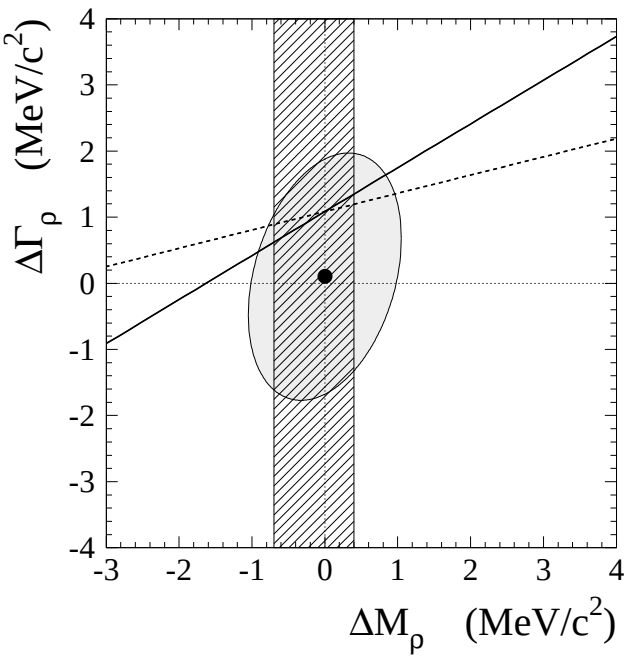

Fig. 54. *Width difference* $\Delta\Gamma_{\rho(770)} = \Gamma_{\rho^\pm(770)} - \Gamma_{\rho^0(770)}$ *as a function of the difference in the* $\rho(770)$ *mass* $\Delta M_{\rho(770)} = M_{\rho^\pm(770)} - M_{\rho^0(770)}$. *The point is the measurement with its correlated one-sigma error ellipse. The dashed and solid lines show the expected dependences from Eqs.* (148) *and* (149), *respectively. The hatched area depicts the electromagnetic* ρ *mass difference predicted in Ref.* 75.

theorem. These sum rules are dispersion relations between real and absorptive parts of a two-point correlation function that transforms symmetrically under $SU(2)_L \times SU(2)_R$ in the case of nonstrange currents. The corresponding integrals are:

$$\frac{1}{4\pi^2}\int_0^{s_0\to\infty} ds\,\frac{1}{s}\,[v_1(s)-a_1(s)] = f_\pi^2\frac{\langle r_\pi^2\rangle}{3} - F_A, \tag{150}$$

$$\frac{1}{4\pi^2}\int_0^{s_0\to\infty} ds\,[v_1(s)-a_1(s)] = f_\pi^2, \tag{151}$$

$$\frac{1}{4\pi^2}\int_0^{s_0\to\infty} ds\,s\,[v_1(s)-a_1(s)] = 0, \tag{152}$$

$$\frac{1}{4\pi^2}\int_0^{s_0\to\infty} ds\,s\ln\frac{s}{\lambda^2}\,[v_1(s)-a_1(s)] = -\frac{4\pi f_\pi^2}{3\alpha}\,(m_{\pi^\pm}^2 - m_{\pi^0}^2). \tag{153}$$

Equation (150) is known as the Das-Mathur-Okubo (DMO) sum rule.[76] It relates the given integral to the square of the pion decay constant $f_\pi = (92.4 \pm 0.3)$ MeV (Ref. 10) obtained from the decays $\pi^- \to \mu^-\bar{\nu}_\mu$ and $\pi^- \to \mu^-\bar{\nu}_\mu\gamma$, to the pion axial-vector form factor F_A for radiative decays $\pi^- \to \ell^-\bar{\nu}_\ell\gamma$, and to the pion charge radius-squared $\langle r_\pi^2\rangle = (0.439 \pm 0.008)$ fm^2 obtained from a one-parameter fit to space-like data.[77] Equations (151) and (152) are the first and the second Weinberg sum rules (WSR).[78] When switching quark masses on, only the first WSR remains valid while the second WSR breaks down due to contributions from the difference of nonconserved vector and axial-vector currents of order m_q^2/s, leading to a quadratic divergence of the integral. Equation (153) represents the electromagnetic splitting of the pion masses.[79] Although apparently containing an arbitrary renormalization scale λ, the sum rule is actually independent of λ by virtue of the second WSR (152). Only for s_0 values for which Eq. (152) has not reached convergence does Eq. (153) maintains its λ dependence.

The $(v_1 - a_1)$ spectral function is shown in Fig. 55. The oscillating behavior of the respective v_1 and a_1 spectral functions is emphasized and the asymptotic behavior is clearly not attained at m_τ^2.

The above integrals are calculated with variable upper integration bounds $s_0 \leq m_\tau^2$ using the spectral functions and their respective covariance matrices in order to provide a straightforward Gaussian error propagation taking into account the strong bin-to-bin correlations of the spectral functions. Also considered are

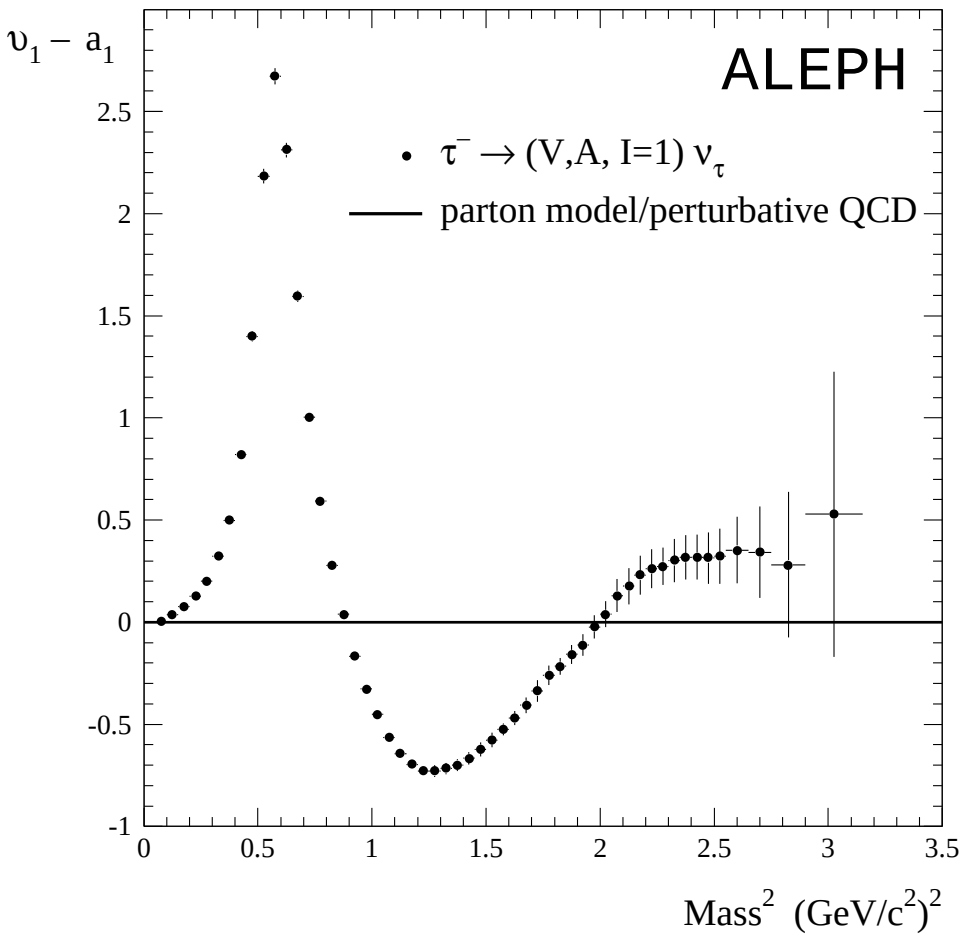

Fig. 55. *Inclusively measured vector minus axial-vector ($v_1 - a_1$) spectral function. In the parton model as well as in perturbative QCD, the vector and axial-vector contributions are degenerate.*

the anticorrelations between v_1 and $a_{1,0}$ due to the estimates of the vector/axial-vector parts of the final states $K\bar{K}\pi$ and $K\bar{K}\pi\pi$, and the τ hadronic branching ratios.

The sum rules (150)–(153) are plotted versus the upper integration bound $s_0 \leq m_\tau^2$ in Figs. 56(a)–(d). The horizontal band depicts the corresponding chiral predictions of the integrals taken from Ref. 80. One observes that only for the DMO sum rule [Fig. 56(a)], for which contributions from higher mass-squared values are suppressed, does the saturation within the one sigma error seem to occur at the τ mass scale. The other sum rules [Figs. 56(b)–(c)] are apparently not saturated at m_τ^2 (nonzero slope) as indicated by the nonvanishing $(v_1 - a_1)$ spectral function at the end of the τ phase space (Fig. 55) and its oscillatory behavior.

3.6 QCD Analysis of Hadronic τ Decays

3.6.1 Motivation

The total hadronic τ width, properly normalized to the known leptonic width,

$$R_\tau = \frac{\Gamma(\tau^- \to \text{hadrons}^- \, \nu_\tau)}{\Gamma(\tau^- \to e^- \, \bar{\nu}_e \nu_\tau)}, \tag{154}$$

should be well predicted by QCD as it is an inclusive observable. Compared to the similar quantity defined in e^+e^- annihilation, it is even doubly inclusive: not only are all produced hadronic states at a given mass summed over, but an integration is performed over all the possible masses from m_π to m_τ.

This favorable situation could be spoiled by the fact that the Q^2 scale is rather small, so that questions about the validity of a perturbative approach can be raised. At least two levels are to be considered: the convergence of the perturbative expansion and the control of the nonperturbative contributions. Happy circumstances discussed below make these contributions indeed very small.[81,82]

3.6.2 Theoretical Prediction for R_τ

According to Eq. (139), the imaginary parts of the vector and axial-vector two-point correlation functions $\Pi^{(J)}_{\bar{u}d,V/A}(s)$, with the spin J of the hadronic system, are proportional to the τ hadronic spectral functions with corresponding quantum numbers. The nonstrange ratio R_τ can be written as an integral of these spectral

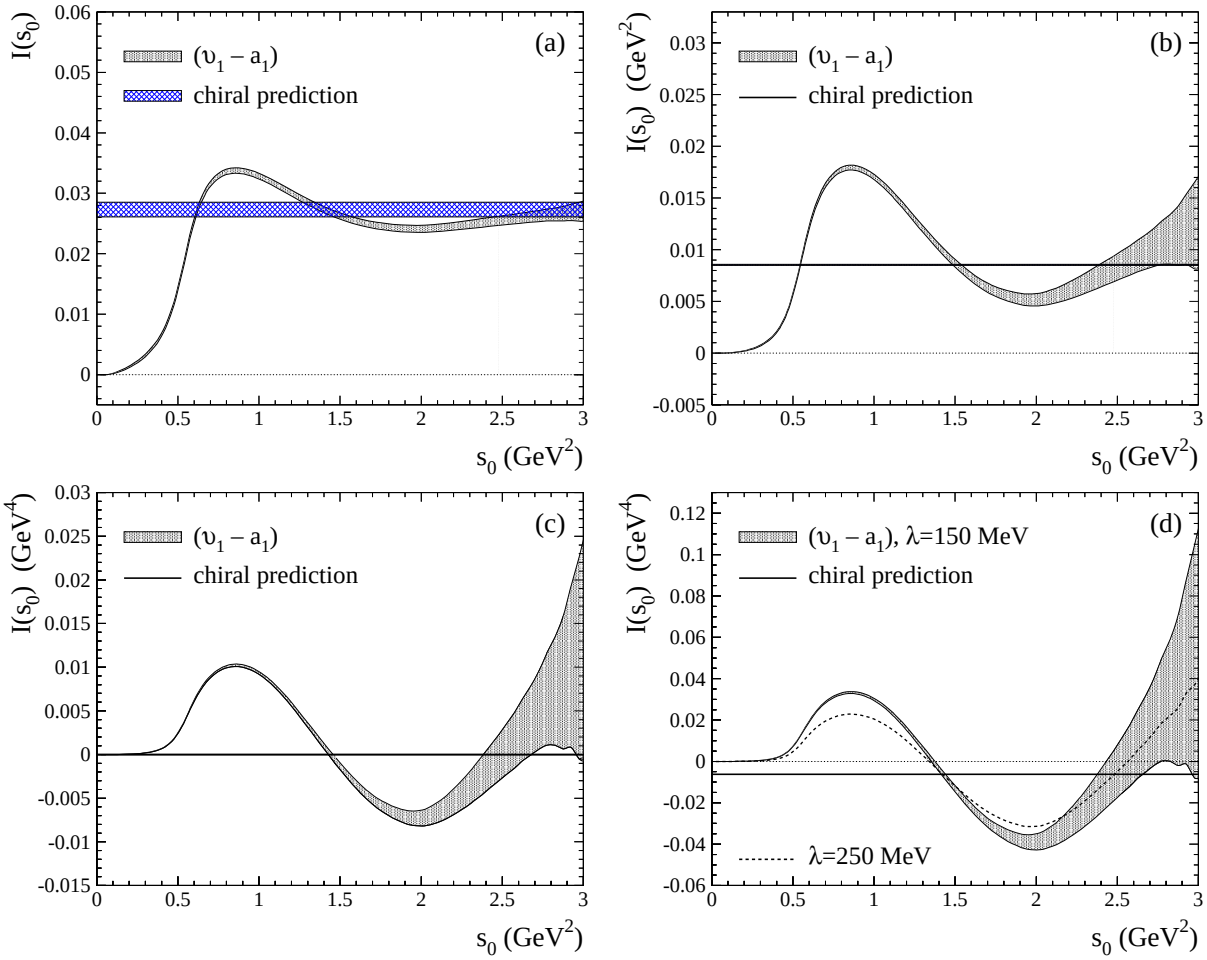

Fig. 56. *Sum rules corresponding to Eqs.* (150)–(153) *vs the upper integration bound* s_0.

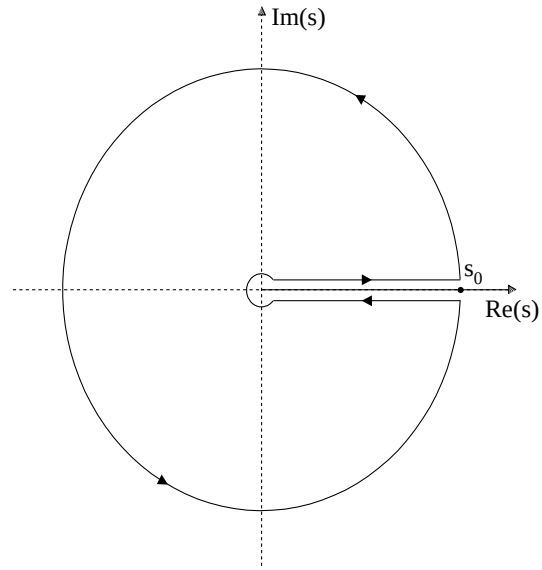

Fig. 57. *Integration contour in the complex s plane for* $R_\tau(s_0)$.

functions over the invariant mass-squared s of the final state hadrons[57]:

$$R_\tau(s_0) \;=\; 12\pi S_{\rm EW} \int\limits_0^{s_0} \frac{ds}{s_0}\left(1-\frac{s}{s_0}\right)^2 \left[\left(1+2\frac{s}{s_0}\right) {\rm Im}\Pi^{(1)}(s+i\epsilon) \;+\; {\rm Im}\Pi^{(0)}(s+i\epsilon)\right], \tag{155}$$

where $\Pi^{(J)}$ can be decomposed as $\Pi^{(J)} = |V_{ud}|^2 \left(\Pi^{(J)}_{ud,V} + \Pi^{(J)}_{ud,A}\right)$. The correlation function $\Pi^{(J)}$ is analytic in the complex s plane everywhere except on the positive real axis where singularities exist. Hence by Cauchy's theorem, the imaginary part of $\Pi^{(J)}$ is proportional to the discontinuity across the positive real axis (Fig. 57).

The energy scale s_0 for $s_0 = m_\tau^2$ is large enough that contributions from nonperturbative effects are small. It is therefore assumed that one can use the *Operator Product Expansion* (OPE) to organize perturbative and nonperturbative contributions to $R_\tau(s_0)$. The factor $(1 - s/s_0)^2$ suppresses the contribution from the region near the positive real axis where $\Pi^{(J)}(s)$ has a branch cut and OPE validity is restricted.[81]

The theoretical prediction for the vector and axial-vector ratio $R_{\tau,V/A}$ can thus be written as:

$$R_{\tau,V/A} = \frac{3}{2}|V_{ud}|^2 S_{\rm EW}\left(1+\delta^{(0)}+\delta'_{\rm EW}+\delta^{(2-{\rm mass})}_{ud,V/A}+\sum_{D=4,6,\ldots}\delta^{(D)}_{ud,V/A}\right), \qquad (156)$$

with the residual nonlogarithmic electroweak correction $\delta'_{\rm EW} = 0.0010$ (Ref. 83), neglected in the following, and the dimension $D = 2$ contribution $\delta^{(2-{\rm mass})}_{ud,V/A}$ from quark masses which is lower than 0.1% for u, d quarks. The term $\delta^{(0)}$ is the purely perturbative contribution, while the $\delta^{(D)}$ are the OPE terms in powers of $s_0^{-D/2}$:

$$\delta^{(D)}_{ud,V/A} = \sum_{{\rm dim}\mathcal{O}=D} C_{ud,V/A}(S_0\mu)\frac{\langle\mathcal{O}_{ud}(\mu)\rangle_{V/A}}{(-s_0)^{D/2}}, \qquad (157)$$

where the parameter μ separates the long-distance nonperturbative effects, absorbed into the vacuum expectation elements $\langle\mathcal{O}_{ud}(\mu)\rangle$, from the short-distance effects which are included in the Wilson coefficients $C_{ud,V/A}(s,\mu)$ (Ref. 84).

3.6.3 Perturbative Prediction

The perturbative prediction adopted in this analysis follows in detail Ref. 85. The perturbative contribution is given in the chiral limit. Effects from quark masses have been calculated in Ref. 86 and are found to be well below 1% for the light quarks. Thus, the contributions from vector and axial-vector currents coincide to any given order of perturbation theory and the results are flavor independent.

The perturbative contribution in Eq. (156) is then given by Ref. 85,

$$1+\delta^{(0)} = \sum_{n=0}^{3} K_n A^{(n)}(\alpha_s), \qquad (158)$$

with $K_0 = K_1 = 1$, $K_2 = 1.63982$, and $K_3 = 6.37101$ for three active flavors in the $\overline{\rm MS}$ scheme.[65] The coefficients K_n are known up to three-loop order (α_s^3) and for $n \geq 2$ they depend on the renormalization scheme employed. The functions $A^{(n)}(\alpha_s)$ in Eq. (158) are the contour integrals †

$$A^{(n)}(\alpha_s) = \frac{1}{2\pi i}\oint_{|s|=s_0}\frac{ds}{s}\left[1-2\frac{s}{s_0}+2\left(\frac{s}{s_0}\right)^3-\left(\frac{s}{s_0}\right)^4\right]\left(\frac{\alpha_s(-s)}{\pi}\right)^n, \qquad (159)$$

† The negative energy-squared in $\alpha_s(-s)$ is introduced when going from the spacelike Euclidean space, where the correlators are defined, to the timelike Minkowski space by virtue of analyticity.

where the contour runs counter-clockwise around the circle from $s_0 + i\epsilon$ to $s_0 - i\epsilon$ (Fig. 57). The strong coupling constant in the vicinity of s_0 can be expanded in powers of $\alpha_s(s_0)$, with coefficients that are polynomials in $\ln(s/s_0)$ (Ref. 57). The perturbative prediction then becomes a function of the K_n coefficients and elementary integrals. Up to fourth order the fixed-order perturbation theory (FOPT) expansion reads

$$\begin{aligned} 1 + \delta_{\rm E}^{(0)} &= 1 + \frac{\alpha_s(s_0)}{\pi} + 5.2023 \left(\frac{\alpha_s(s_0)}{\pi}\right)^2 + 26.366 \left(\frac{\alpha_s(s_0)}{\pi}\right)^3 \\ &\quad + (K_4 + 78.00) \left(\frac{\alpha_s(s_0)}{\pi}\right)^4 \end{aligned} \tag{160}$$

with the unknown K_4 coefficient.

Another approach to the solution of the contour integral (159) is to perform a direct numerical evaluation using the solution of the renormalization group equation (RGE) to four loops[87] as input for the running $\alpha_s(-s)$ (Refs. 85 and 88). It provides a resummation of all known higher-order logarithmic integrals and improves the convergence of the perturbative series. While, for instance, the third-order term in the expansion (160) contributes with 17% to the total (truncated) perturbative prediction, the corresponding term of the numerical solution amounts only to 6.6% [assuming $\alpha_s(m_\tau^2) = 0.35$]. This numerical solution of Eq. (158) will be referred to as *contour-improved* fixed-order perturbation theory ($\mathrm{FOPT_{CI}}$) in the following.

Despite a number of arguments expressed in Ref. 85, the intrinsic ambiguity between FOPT and $\mathrm{FOPT_{CI}}$ is unresolvable at present. This is due to the truncation of the perturbative approximation of $\delta^{(0)}$ at finite order in α_s. A conservative measure of this ambiguity is obtained from the deviation in R_τ found when cutting all additional orders in α_s (which is FOPT) and keeping them ($\mathrm{FOPT_{CI}}$), respectively. Both methods are likewise considered in this analysis.

3.6.4 Nonperturbative Contributions

Following SVZ,[89] the first contribution to $R_\tau(s_0)$ beyond the $D = 0$ perturbative expansion is the nondynamical quark mass correction of dimension $D = 2$, i.e., corrections in powers of $1/s_0$. They have been calculated up to next-to-leading order α_s (Ref. 90).

The dimension $D = 4$ operators have dynamical contributions from the gluon condensate $\langle(\alpha_s/\pi)GG\rangle$ and quark condensates $m_u\langle 0|\bar{u}u|0\rangle$, $m_d\langle 0|\bar{d}d|0\rangle$ of the light u, d quarks. The remaining $D = 4$ operators are the running quark masses to the fourth power. The contribution of the gluon condensate to $R_{\tau,V/A}$ vanishes in first order, $\alpha_s(s_0)$. However, there appear second-order terms in the Wilson coefficients due to the logarithmic s dependence of $\alpha_s(s)$, which after performing the integral (155) becomes $\alpha_s^2(s_0)$.

The contributions from dimension $D = 6$ operators are rather complex. The large number of independent operators of the four-quark type occurring can be reduced by means of the vacuum saturation approximation[57,89] to leading order (α_s). The operators are then expressed as products of scale-dependent two-quark condensates of the type $\alpha_s(\mu)\langle\bar{q}_i q_i(\mu)\rangle\langle\bar{q}_j q_j(\mu)\rangle$. Since the vacuum saturation approximation is a simplifying assumption, possible deviations are accounted for by introducing an effective scale-independent operator of the form $\rho\alpha_s\langle\bar{q}q\rangle^2$ that is fit to the data.

The dimension $D = 8$ contribution has a structure of nontrivial quark-quark, quark-gluon, and four-gluon condensates, the explicit form of which is given for the vector case in Ref. 91. For the theoretical prediction of $R_\tau(s_0)$ used here, the complete long- and short-distance part is absorbed into the scale invariant phenomenological $D = 8$ operator $\langle\mathcal{O}_8\rangle$.

Higher order contributions from $D \geq 10$ operators are expected to be small because, as with the gluon condensate, constant terms and terms in leading order (α_s) vanish in Eq. (155) after integration.

3.6.5 Spectral Moments

It was shown in Ref. 92 that it is possible to benefit from the information provided by the explicit shape of the spectral functions in order to obtain additional constraints on $\alpha_s(s_0)$ and—more importantly—on the nonperturbative condensates. The spectral moments at m_τ^2 are defined as:

$$R^{kl}_{\tau,V/A} \equiv \int_0^{m_\tau^2} ds \left(1 - \frac{s}{m_\tau^2}\right)^k \left(\frac{s}{m_\tau^2}\right)^l \frac{dR_{\tau,V/A}}{ds} \tag{161}$$

with $R^{00}_{\tau,V/A} = R_{\tau,V/A}$. The factor $(1 - s/m_\tau^2)^k$ suppresses the integrand at the crossing of the positive real axis where the validity of the OPE is less certain

and the experimental accuracy is statistically limited. Its counterpart $(s/m_\tau^2)^l$ projects out higher energies. The new spectral information is used to fit simultaneously $\alpha_s(m_\tau^2)$ and the phenomenological operators $\langle(\alpha_s/\pi)GG_{D=4}\rangle$, $\langle\mathcal{O}_{D=6}\rangle$, and $\langle\mathcal{O}_{D=8}\rangle$. Due to the intrinsic strong correlations, only five moments are used as input to the fits.

In analogy to R_τ the contributions to the moments originating from perturbative and nonperturbative QCD are separated via the OPE. The prediction of the perturbative contribution takes then the form

$$\delta^{(0,kl)} = \sum_{n=1}^{3} K_n A^{(n,kl)}(\alpha_s), \tag{162}$$

where the contour integrals $A^{(n,kl)}(\alpha_s)$ (Ref. 92) are expanded up to $\alpha_s^3(s)$ (FOPT) or are numerically evaluated for the running $\alpha_s(-s)$ obtained from the RGE ($\mathrm{FOPT_{CI}}$).

In the chiral limit and neglecting the logarithmic s dependence of the Wilson coefficients, the dimension $D = 2, 4, 6, 8$ nonperturbative contributions to the moments read

$$\delta^{(D,kl)}_{ud,V/A} = 8\pi^2 \begin{pmatrix} (D=2) & (D=4) & (D=6) & (D=8) & (k,l) \\ 1 & 0 & -3 & -2 & (0,0) \\ 1 & 1 & -3 & -5 & (1,0) \\ 0 & -1 & -1 & 3 & (1,1) \\ 0 & 0 & 1 & 1 & (1,2) \\ 0 & 0 & 0 & -1 & (1,3) \end{pmatrix} \sum_{\dim\mathcal{O}=D} C(\mu)\frac{\langle\mathcal{O}(\mu)\rangle}{m_\tau^D}, \tag{163}$$

where the matrix is defined by the choice of the coefficients for the moments $k = 1$, $l = 0, 1, 2, 3$. It can be seen that with increasing weight l, the low dimension operators give no contributions.

For practical purposes, it is more convenient to define moments that are normalized to the corresponding $R_{\tau,V/A}$ in order to decouple the normalization from the shape of the τ spectral functions:

$$D^{kl}_{\tau,V/A} \equiv \frac{R^{kl}_{\tau,V/A}}{R_{\tau,V/A}} = \int_0^{m_\tau^2} ds \left(1 - \frac{s}{m_\tau^2}\right)^k \left(\frac{s}{m_\tau^2}\right)^l \frac{1}{N_{V/A}} \frac{dN_{V/A}}{ds}. \tag{164}$$

There now exist two sets of experimentally almost uncorrelated observables—$R_{\tau,V/A}$ and spectral moments—which provide independent constraints on $\alpha_s(m_\tau^2)$ and thus an important test of consistency.

3.6.6 Measurement of R_τ and the Moments

The ratio of the nonstrange hadronic width to the electronic branching fraction is calculated from the difference of the total hadronic width ratio,

$$\begin{aligned} R_\tau &= \frac{1 - B(\tau^- \to e^- \bar{\nu}_e \nu_\tau) - B(\tau^- \to \mu^- \bar{\nu}_\mu \nu_\tau)}{B(\tau^- \to e^- \bar{\nu}_e \nu_\tau)} = \frac{1}{B(\tau^- \to e^- \bar{\nu}_e \nu_\tau)} - 1.9726, \\ &= 3.647 \pm 0.014 \end{aligned} \tag{165}$$

obtained from the world average value (138), and the strange width ratio,

$$R_{\tau,S} = 0.155 \pm 0.008, \tag{166}$$

taken from Ref. 93, yielding the result

$$R_{\tau,V+A} = 3.492 \pm 0.016. \tag{167}$$

There is no advantage in including $R_{\tau,S}$ (or equivalently using R_τ) in this analysis, because the strange quark sector introduces another parameter, the strange quark mass, which the additional data is used to fit.[94] Computing the ratio of the inclusive vector and axial-vector branching fractions taken from Table 6, to the electronic branching fraction yields

$$R_{\tau,V} = 1.775 \pm 0.017 \tag{168}$$

$$R_{\tau,A} = 1.717 \pm 0.018. \tag{169}$$

The moments are determined from the V, A, and $V+A$ spectral functions. For the latter, many systematic effects cancel as V/A separation is no longer required. The $V + A$ spectral function is shown in Fig. 58. The improvement in precision in comparison to an exclusive sum of Fig. 48 and Fig. 49 is obvious at higher mass-squared. One clearly sees the oscillating behavior of the spectral function, but unlike the vector/axial-vector spectral functions, it does approximately reach the asymptotic limit predicted by perturbative QCD as $s \to m_\tau^2$.

3.6.7 The Fits to the Data and the Theoretical Uncertainties

The combined fits to the measured V, A, and $(V + A)$ ratios, R_τ, and moments adjust the parameters $\alpha_s(m_\tau^2)$, $\langle(\alpha_s/\pi)GG\rangle$, $\langle\mathcal{O}_6\rangle_{V/A}$, and $\langle\mathcal{O}_8\rangle_{V/A}$ of the OPE in the theoretical predictions (156) and (161) of the above quantities.

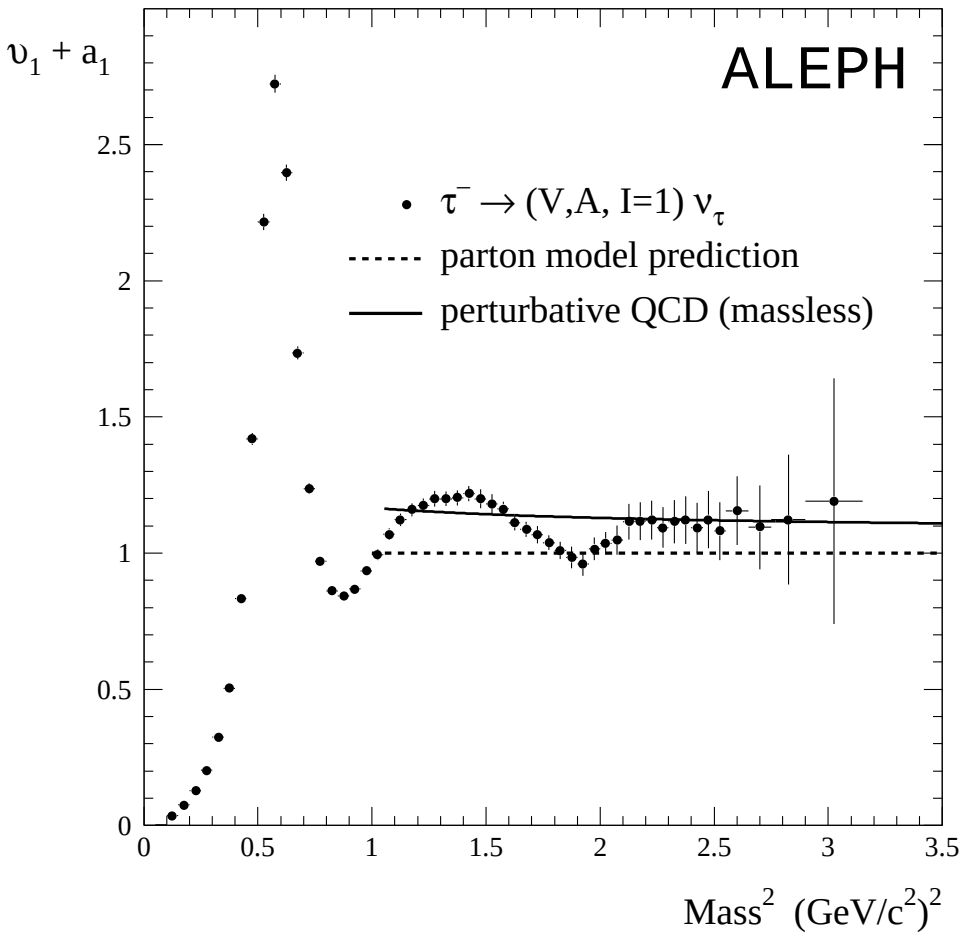

Fig. 58. *Inclusively measured vector plus axial-vector ($v_1 + a_1$) spectral function and predictions from the parton model and from massless perturbative QCD using* $\alpha_s(M_Z^2) = 0.120$.

The uncertainties entering the theoretical predictions are now estimated. Errors from the light quark masses are negligible while the others, in particular $\Delta S_{\rm EW}$, must be taken into account. For the quark condensates which contribute to dimension $D = 4$, the PCAC relation

$$(m_u + m_d)\langle 0|\bar{u}u + \bar{d}d|0\rangle \simeq -2f_\pi^2 m_\pi^2 \tag{170}$$

is used.

The errors in the truncated perturbative expansion originate mainly from the unknown higher order expansion coefficient K_4. The authors of Ref. 95 advocate the principle of minimal sensitivity (PMS),[96] which allows the computation of a renormalization scheme (RS) with optimal convergence, i.e., with minimal dependence on higher order corrections. The difference between an observable calculated using the PMS and the $\overline{\rm MS}$ schemes can be used to provide an estimate of the missing terms accumulated in K_4. The procedure results in $K_4 \simeq 36$. In Ref. 97, an experimental estimate of K_4 is performed using the *a priori* freedom of the choice of the renormalization scale μ to increase the sensitivity of the perturbative series on K_4. This yields $K_4 = 27 \pm 5$. Motivated by the above and the expectation that the perturbative series for $\delta^{(0)}$ should have a constant sign behavior with increasing coefficients,[98] K_4 is chosen to be 50 ± 50.

Another important point is the renormalization scale (μ) dependence of the prediction expressed in the RGE which governs the running of α_s. Formally, the integrals (159) in Eq. (158) also obey the RGE.[85] In a truncated series, the renormalization scale dependence remains and is therefore an intrinsic uncertainty of the theoretical prediction. In order to estimate its size, μ is varied from m_τ to $\mu = 1.1$ GeV and $\mu = 2.5$ GeV (Ref. 85). When changing the μ scale, the coefficients K_n of the perturbative expansion, as well as α_s, are reexpressed according to the RGE.

In addition to the renormalization scale dependence, the arbitrariness of the choice of the renormalization scheme leaves an ambiguity. Again, an estimate of its associated uncertainty is obtained by changing the RS from $\overline{\rm MS}$ to the PMS scheme. This transformation induces a reduction of $\alpha_s(m_\tau^2)$ of approximately 0.010 (Ref. 99), which is taken as the corresponding uncertainty.

The OPE power terms of dimensions $D = 4, 6, 8$ have no theoretical errors since they are freely varying parameters of the fits and are therefore determined experimentally. Contributions from higher orders have not been calcu-

lated yet. However, they can only contribute indirectly via a logarithmic dependence on s to R_τ. The operators of dimension $D = 10$ are then suppressed by $(\alpha_s/\pi)^2/m_\tau^{10} \sim 4 \times 10^{-5}$, and are thus neglected in this analysis. Also neglected is any nonstandard dimension $D = 2$ term (except for the quark masses). Such terms are not generated by a dynamical QCD action and are therefore absent in the SVZ approach. However, they are not ruled out experimentally and are still controversial theoretically.[100] No additional theoretical error is introduced to cover the possible existence of a $\delta^{(0)} \sim (\Lambda^2/s)$ term from the first ultraviolet singularity (renormalon) of the Borel resummed large-β_0 approximation of the perturbative series.[101] Any such uncertainty is assumed to be taken into account by the error ascribed to K_4.

In Refs. 102–104, R_τ has been calculated employing a renormalon resummation of $\delta^{(0)}$ in the large-β_0 limit. The resummation is performed by evaluating the integral of the Borel transform in the large-β_0 limit, where infrared (IR) and ultraviolet (UV) singularities appear in the Borel plane. The UV renormalons, situated outside the integration range, have alternating signs and can be resummed. However, the IR renormalons lie inside the integration range on the positive axis and give rise to nonperturbative power contributions which are absorbed in the OPE. The authors of Ref. 105 developed an RS-invariant all-orders renormalon resummation.

Figure 59 shows the results for $\delta^{(0)}$ using different methods to evaluate the perturbative series. The fixed-order PT corresponds to the Taylor expansion Eq. (160) and the contour-improved prediction is Eq. (158) with a numerical evaluation of the $A^{(n)}$ integrals. These procedures are applied here. The large-β_0 limit resummed perturbative prediction is taken from Ref. 103, and for the theoretical prediction of the RS-invariant large-β_0 resummed $\delta^{(0)}$, the formulae given in Ref. 105 are used. Both resummed predictions are corrected for the first three exactly known fixed-order coefficients. Also shown is the fit result of this analysis with its estimated theoretical uncertainty. It covers the whole range of perturbative approaches presented above within one standard deviation.

3.6.8 Results of the Fits

The results of the fits are given in Table 7. The limited number of observables and the strong correlations between the spectral moments introduce large correlations,

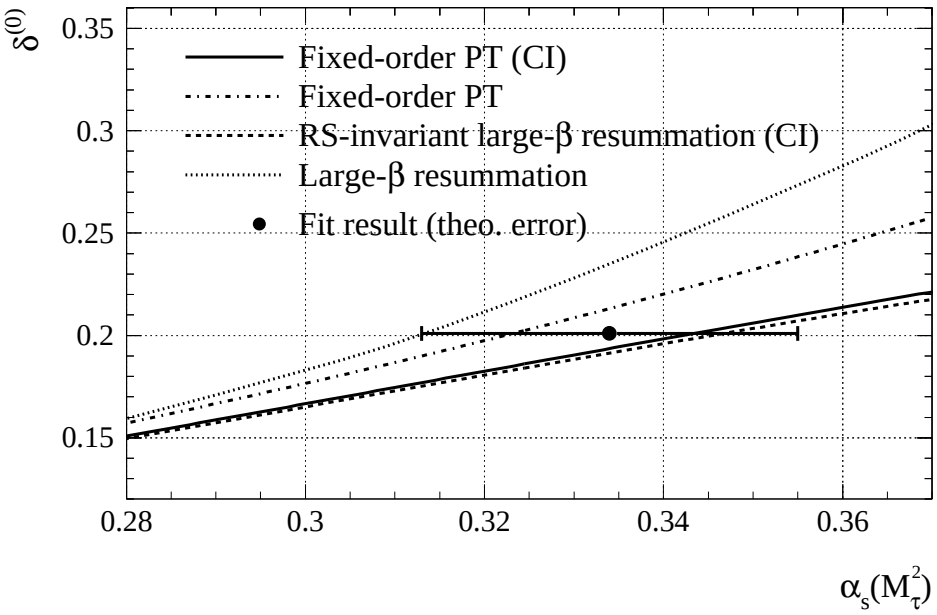

Fig. 59. *Perturbative contribution* $\delta^{(0)}$ *to* $R_{\tau,V/A}$ *with different approaches. "CI" means contour-improved. The fixed-order PT curves are given for* $K_4 = 50$. *Both large-*β_0 *resummations are corrected for the first three exactly known fixed-order coefficients. Also shown is the result Eq.* (171) *of this analysis within its estimated theoretical uncertainty.*

especially between the fitted nonperturbative operators. The precision of $\alpha_s(m_\tau^2)$ obtained with the two perturbative methods employed is comparable; however, their central values differ by about 0.02 as seen in Fig. 59. The differences between $\mathrm{FOPT_{CI}}$ and FOPT for the nonperturbative parameters are negligible compared to their errors so that only the $\mathrm{FOPT_{CI}}$ values are given. The $\delta^{(2)}$ term is the pure theoretical contribution from the known masses of the light u, d quarks. No anomalous dimension $D = 2$ operator has been fitted since empirically it is found to be degenerate to α_s. The $\delta^{(4)}$ term receives contributions from the quark and gluon condensates and the quartic light quark masses. While the quark condensates and the quark masses are rather well-known and are fixed theoretically by Eq. (170), the gluon condensate is adjusted in the fit.

One notices a remarkable agreement within statistical errors between the $\alpha_s(m_\tau^2)$ values using vector and axial-vector data. The results can be compared to the one obtained in the previous ALEPH analysis[106] where, applying $\mathrm{FOPT_{CI}}$,

ALEPH	Vector (V)	Axial-Vector (A)	$V + A$
$\alpha_s(m_\tau^2)$ (FOPT$_{\rm CI}$)	$0.340 \pm 0.016 \pm 0.017$	$0.349 \pm 0.015 \pm 0.017$	$0.345 \pm 0.007 \pm 0.017$
$\alpha_s(m_\tau^2)$ (FOPT)	$0.320 \pm 0.012 \pm 0.019$	$0.328 \pm 0.011 \pm 0.019$	$0.322 \pm 0.005 \pm 0.019$
$\delta^{(0)}$ (FOPT$_{\rm CI}$)	0.198 ± 0.017	0.206 ± 0.018	0.202 ± 0.013
$\delta^{(0)}$ (FOPT)	0.197 ± 0.025	0.206 ± 0.026	0.200 ± 0.022
$\delta^{(2)}$	$-(0.3 \pm 0.3)\times 10^{-3}$	$-(0.6 \pm 0.3)\times 10^{-3}$	$-(0.4 \pm 0.2)\times 10^{-3}$
$\delta^{(4)}$	$(0.6 \pm 0.8)\times 10^{-3}$	$(-5.7 \pm 0.9)\times 10^{-3}$	$-(2.5 \pm 0.8)\times 10^{-3}$
$\delta^{(6)}$	0.029 ± 0.004	-0.029 ± 0.004	0.001 ± 0.004
$\delta^{(8)}$	-0.009 ± 0.001	0.008 ± 0.001	-0.001 ± 0.001
Total $\delta_{\rm NP}$	0.020 ± 0.004	-0.027 ± 0.004	-0.003 ± 0.004
χ^2/d.o.f.	0.1/1	0.1/1	0.2/1

Table 7. *Fit results of $\alpha_s(m_\tau^2)$ and the OPE nonperturbative contributions from vector, axial-vector, and $(V + A)$ combined fits using the corresponding ratios R_τ and the spectral moments as input parameters. Where two errors are given, they denote experimental (first number) and theoretical uncertainties (second number). The differences between* FOPT$_{\rm CI}$ *and* FOPT *for the nonperturbative parameters are negligible compared to their errors. The $\delta^{(2)}$ term is the pure theoretical prediction. The quark condensates in the $\delta^{(4)}$ term are fixed to their theoretical values, Eq.* (170)*, and only the gluon condensate is varied as a free parameter. The total nonperturbative contribution is the sum $\delta_{\rm NP} = \delta^{(4)} + \ldots + \delta^{(8)}$.*

the strong coupling was measured to be $\alpha_s(m_\tau^2) = 0.330 \pm 0.046$ using the much smaller data set of 8500 τ decays.

The total nonperturbative contribution to $R_{\tau,V+A}$ is compatible with zero within an uncertainty of 0.4% that is much smaller than the error arising from the perturbative term. The advantage of separating the vector and axial-vector channels and comparing to the inclusive $(V + A)$ fit becomes obvious in the adjustment of the leading nonperturbative contributions of dimension $D = 6$ and $D = 8$, which cancel in the inclusive sum. This cancellation of the nonperturbative terms increases the confidence on the $\alpha_s(m_\tau^2)$ determination from the inclusive $(V + A)$ observables. The gluon condensate is fixed by the first $l = 0, 1$ moments which receive lowest order contributions while it is suppressed in R_τ by $(\alpha_s/\pi)^2$.

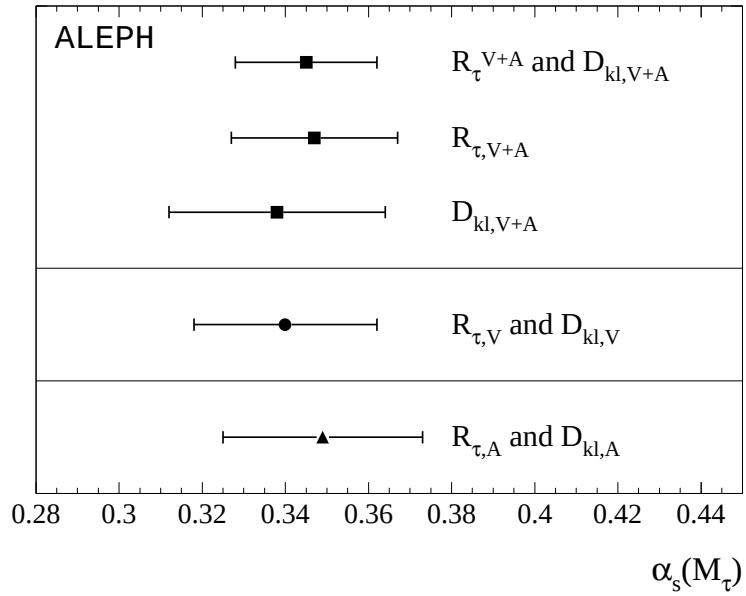

Fig. 60. *Results for $\alpha_s(m_\tau^2)$ using $R_{\tau,V+A}$ only, the moments D^{kl}_{V+A} only, and the combined information from vector and axial-vector τ decays using* $\mathrm{FOPT_{CI}}$. *The measurements are strongly correlated due to the dominant theoretical errors.*

Taking the value obtained in the $(V+A)$ inclusive fit and adding as systematic uncertainties half of the difference between the vector and axial-vector fits as well as the $\mathrm{FOPT_{CI}}$ and FOPT results, the gluon condensate is found to be $\langle(\alpha_s/\pi)GG\rangle = (0.001 \pm 0.015)\ \mathrm{GeV}^4$. An interesting observation is the alternating sign in both vector and axial-vector cases between the $\delta^{(6)}$ and $\delta^{(8)}$ terms. This is connected with the special form of the shape of $R_{\tau,V}(s_0)$ ($R_{\tau,A}(s_0)$) as a function of a varying "τ mass" $s_0 \leq m_\tau^2$, as will be discussed in the following section.

In order to check the consistency of the different approaches, one can use either the normalization, i.e., the ratio R_τ obtained from the hadronic branching ratios, or the intrinsic shape of the spectral functions, i.e., the spectral moments. The value of $\alpha_s(m_\tau^2)$ can then be determined using variables coming from only one of these inputs. This is done for the $(V+A)$ case for which contributions from nonperturbative terms are small, so that the effect of additional theoretical assumptions are minimized. The results of these fits using $\mathrm{FOPT_{CI}}$ are shown in Fig. 60.

As mentioned above, there exists no constraining prescription which allows a resolution of the ambiguity between $\mathrm{FOPT_{CI}}$ and FOPT. The final result on

$\alpha_s(m_\tau^2)$ is thus the average of the two values given in Table 7, with half of their difference added as theoretical error:

$$\alpha_s(m_\tau^2) = 0.334 \pm 0.007_{(\text{exp.})} \pm 0.021_{(\text{theo.})}. \tag{171}$$

The first error accounts for the experimental uncertainty; the second number gives the uncertainty of the theoretical prediction of R_τ and the spectral moments as well as the ambiguity of the theoretical approaches employed.

One can express the value of $\alpha_s(m_\tau^2)$ in terms of the $\overline{\text{MS}}$ renormalization scale $\Lambda_{\overline{\text{MS}}}$ at four-loop level. For the result (171) with three active flavors, one has

$$\Lambda_{\overline{\text{MS}}}^{(3)} = (370 \pm 13_{(\text{exp.})} \pm 38_{(\text{theo.})})\ \text{MeV}. \tag{172}$$

3.6.9 Test of the Running of $\alpha_s(s)$ at Low Energies

The analysis presented in the preceeding section indicates that the framework of the perturbative expansion and the OPE approach, used for the theoretical prediction of the measured quantities, describes the data phenomenologically. The exclusive measurement of the vector and axial-vector spectral functions allows further investigations of QCD phenomena at low energies up to the τ mass.

Using the spectral functions, one can simulate the physics of a hypothetical τ lepton with a mass $\sqrt{s_0}$ smaller than m_τ through Eq. (155). Assuming quark-hadron duality, the evolution of $R_\tau(s_0)$ provides a direct test of the running of $\alpha_s(s_0)$, governed by the RGE β-function. On the other hand, it is a test of the validity of the OPE approach in τ decays. The studies performed in this section employ only FOPT_{CI}. Results obtained with FOPT are similar and differ only in the central $\alpha_s(m_\tau^2)$ value.

The functional dependence of $R_{\tau,V+A}(s_0)$ is plotted in Fig. 61 together with the theoretical prediction, using the results of Table 7. The spread due to uncertainties are shown as bands. In the $(V+A)$ case, the experimental errors are diminished by normalizing $R_{\tau,V+A}(s_0 = m_\tau^2)$ to Eq. (167). The correlations between two adjacent bins $s_1 < s_2$ are large as the only new information is provided by the small mass difference between the two bins and the slightly different weight function. They are reinforced by the original experimental and theoretical correlations. Below 1 GeV^2, the error of the theoretical prediction of $R_{\tau,V+A}(s_0)$ starts to blow up due to the increasing uncertainty from the unknown K_4 perturbative term; errors of

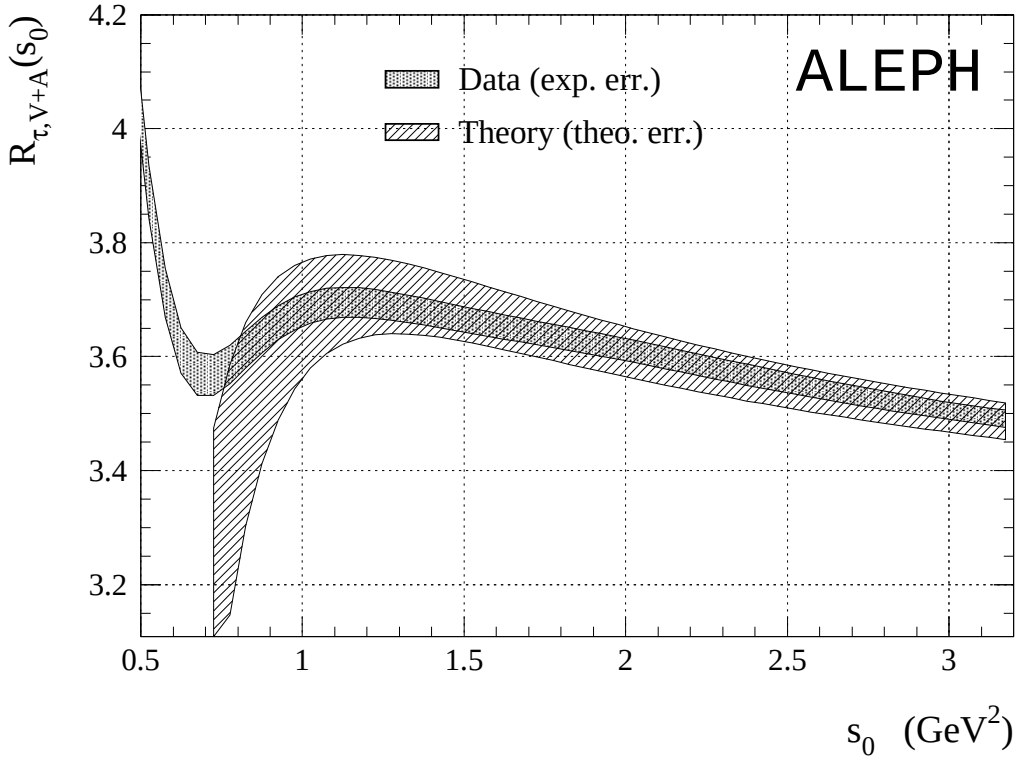

Fig. 61. *The ratio $R_{\tau,V+A}$ versus the squared "τ mass" s_0. The curves are plotted as error bands to emphasize their strong point-to-point correlations in s_0. Also shown is the theoretical prediction using* $\mathrm{FOPT_{CI}}$ *and the results for $R_{\tau,V+A}$ and the nonperturbative terms from Table* 7.

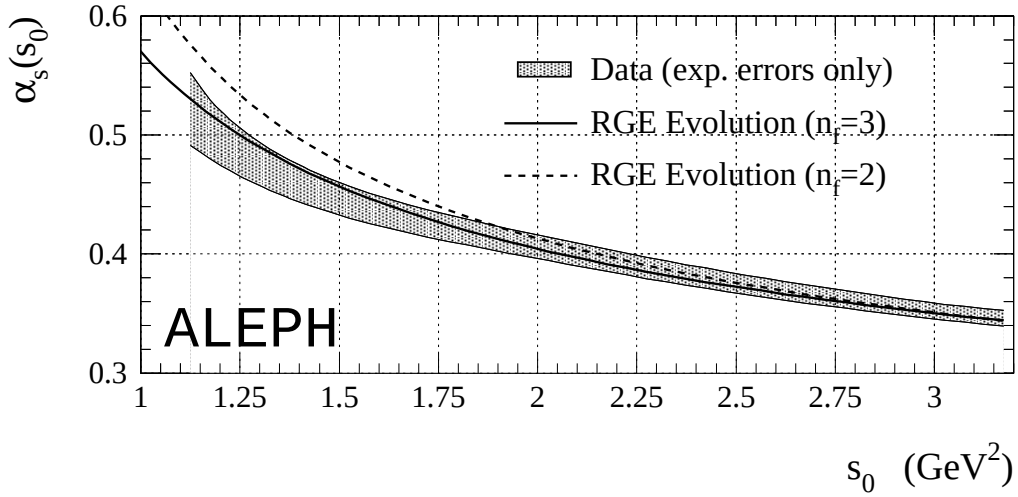

Fig. 62. *The running of $\alpha_s(s_0)$ obtained from the fit of the theoretical prediction to $R_{\tau,V+A}(s_0)$. The shaded band shows the data including experimental errors. The curves give the four-loop RGE evolution for two and three flavors.*

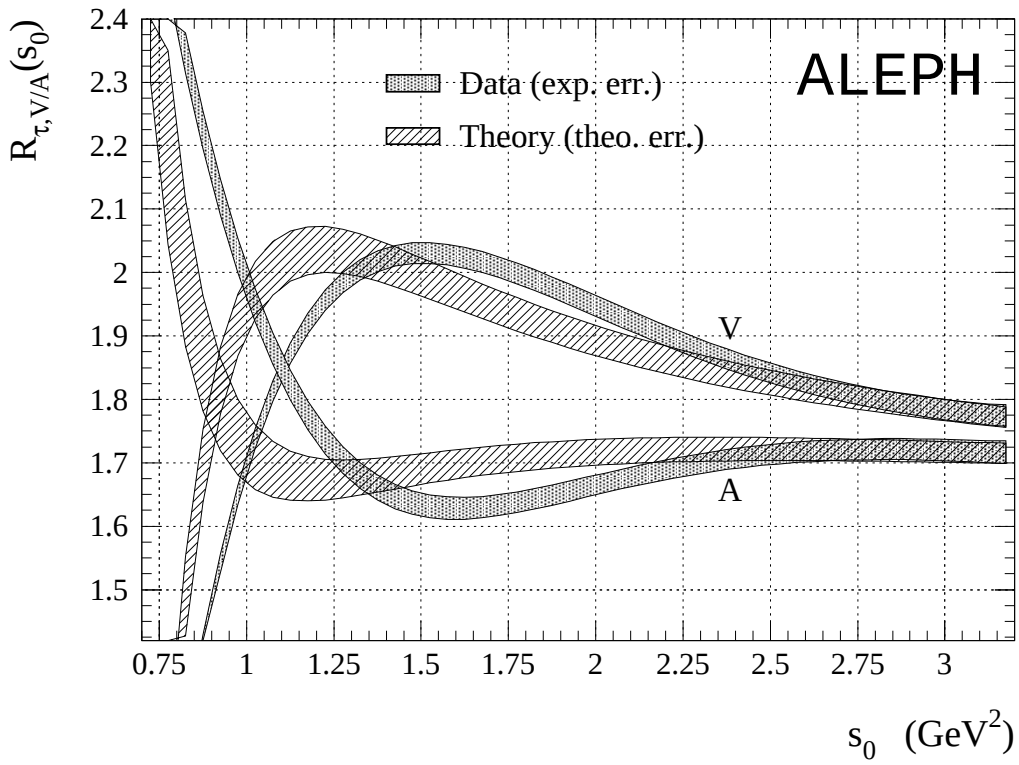

Fig. 63. *The ratios $R_{\tau,V}$ and $R_{\tau,A}$ versus the square "τ mass" s_0 for data and the theoretical prediction using the results of Table* 7.

the nonperturbative contributions are *not* contained in the theoretical error band. Figure 62 shows the plot corresponding to Fig. 61, translated into the running of $\alpha_s(s_0)$, i.e., the experimental value for $\alpha_s(s_0)$ has been individually determined at every s_0 from the comparison of data and theory. Also plotted is the four-loop RGE evolution using two and three quark flavors.

Figure 63 gives the vector and axial-vector ratios $R_{\tau,V/A}$ as a function of s_0 together with the corresponding theoretical predictions using as input the fitted parameters of Table 7. By construction, data and theory converge at m_τ^2, but the observed agreement is much less stable than in the $(V+A)$ case. As a consequence, one might question the reliability of the OPE approach at the scale m_τ^2 for vector or axial-vector only. On the other hand, the agreement of the $\alpha_s(m_\tau^2)$ values for V and A (see Table 7) may indicate that within the achieved precision, nonperturbative contributions are well absorbed by the dimension $D = 6, 8$ power terms. Nevertheless, the deviation between data and theory observed implies that

the values of the fitted parameters should depend on the spectral moments used, i.e., of the specific shape of the weighting function inserted in the integral (161).

The experimental fact that the nonperturbative contributions cancel over the whole range 1.2 GeV$^2 \leq s_0 \leq m_\tau^2$ leads to confidence that the α_s determination from the inclusive $(V+A)$ data is robust.

3.6.10 Discussion of the Determination of $\alpha_s(m_\tau^2)$

The evolution of the $\alpha_s(m_\tau^2)$ measurement from the inclusive $(V+A)$ observables is based on the Runge-Kutta integration of the differential equation of the renormalization group to N^{3}LO (Refs. 87, 107–110), and yields

$$\alpha_s(M_Z^2) = 0.1202 \pm 0.0008_{(\mathrm{exp.})} \pm 0.0024_{(\mathrm{theo.})} \pm 0.0010_{(\mathrm{evol.})}. \tag{173}$$

The last error stands for possible ambiguities in the evolution due to uncertainties in the matching scales of the quark thresholds.[110] Effects associated with the truncation of the RGE at $\mathcal{O}(\alpha_s^5)$ are small: the new N^{3}LO order[87] gives a tiny contribution of $\alpha_s(M_Z^2)_{3-\mathrm{loop}} - \alpha_s(M_Z^2)_{4-\mathrm{loop}} = 0.0003$.

The result (173) can be compared to the determination from the global electroweak fit discussed in the previous lecture. In this case, the sensitive observable is the ratio R_Z. This variable has similar advantages as R_τ, but it differs concerning the convergence of the perturbative expansion because of the much larger scale. It turns out that this determination is dominated by experimental errors with very small theoretical uncertainties, i.e., the reverse of the situation encountered in τ decays. The most recent value[111] yields $\alpha_s(M_Z^2) = 0.1206 \pm 0.0030$, in excellent agreement with Eq. (173). Both results agree with the less precise determinations from deep inelastic lepton scattering and from event shape analyses in lepton scattering and e^+e^- annihilation.[50]

Figure 64 illustrates well the agreement between the evolution of $\alpha_s(m_\tau^2)$ predicted by QCD between m_τ^2 and M_Z^2.

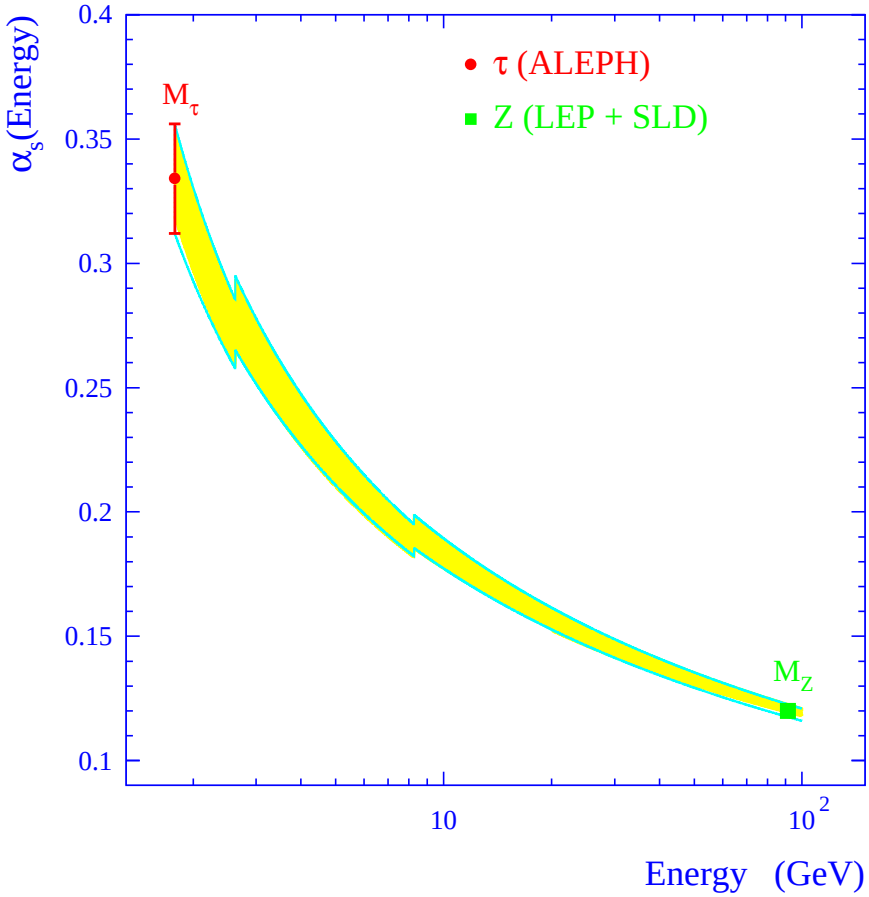

Fig. 64. *Evolution of the strong coupling measured at* (m_τ^2) *to* M_Z^2 *predicted by QCD compared to the direct measurement. The evolution is carried out at four loops, while the flavor matching is accomplished at three loops at* $2\ m_c$ *and* $2\ m_b$ *thresholds.*

3.7 Applications to Vacuum Polarization Calculations

3.7.1 Improvements to the Standard Calculations

From the studies presented above, we have learned that:

- The $I = 1$ vector spectral function from τ decays agrees with that from e^+e^- annihilation, while it is more precise for masses less than 1.6 GeV. Small CVC violations are expected at a few times 10^{-3} level[56] from radiative ρ decays and SU(2)-breaking in the π and ρ masses.
- The description of R_τ by perturbative QCD works down to a scale of 1 GeV. Nonperturbative contributions at 1.8 GeV are well below 1% in this case.

They are larger ($\sim$ 3%) for the vector part alone, but reasonably well-described by OPE. The complete (perturbative + nonperturbative) description is accurate at the 1% level at 1.8 GeV for integrals over the vector spectral function such as $R_{\tau,V}$.

These two facts have direct applications to calculations of hadronic vacuum polarization which involve the knowledge of the vector spectral function: the muon magnetic anomaly and the running of α. In both cases, the standard method involves a dispersion integral over the vector spectral function taken from the $e^+e^- \to$ hadrons data. Eventually at large energies, QCD is used to replace experimental data. Hence, the precision of the calculation is given by the accuracy of the data, which is poor above 1.5 GeV. Even at low energies, the precision can be significantly improved at low masses by using τ data.[56]

The next breakthrough comes about using the prediction of perturbative QCD far above quark thresholds, but at low enough energies (compatible with the remarks above) in place of noncompetitive experimental data.[53] This procedure involves a proper treatment of the quark masses in the QCD prediction.[107]

Finally, it is still possible to improve the contributions from data by using analyticity and QCD sum rules, basically without any additional assumption. This idea, advocated in Ref. 112, has been used within the procedure described above to still further improve the calculations.[54]

The experimental results for $R(s)$ and the theoretical prediction are shown in Fig. 65. The shaded bands depict the regions where data are used instead of theory to evaluate the respective integrals. Good agreement between data and QCD is found above 8 GeV, while at lower energies systematic deviations are observed. The R measurements in this region are essentially provided by the $\gamma\gamma 2$ (Ref. 113) and MARK I (Ref. 114) Collaborations. MARK I data above 5 GeV lie systematically above the measurements of the Crystal Ball[115] and MD1[116] Collaborations as well as the QCD prediction.

3.7.2 Muon Magnetic Anomaly

By virtue of the analyticity of the vacuum polarization correlator, the contribution of the hadronic vacuum polarization to a_μ (Fig. 66) can be calculated via the

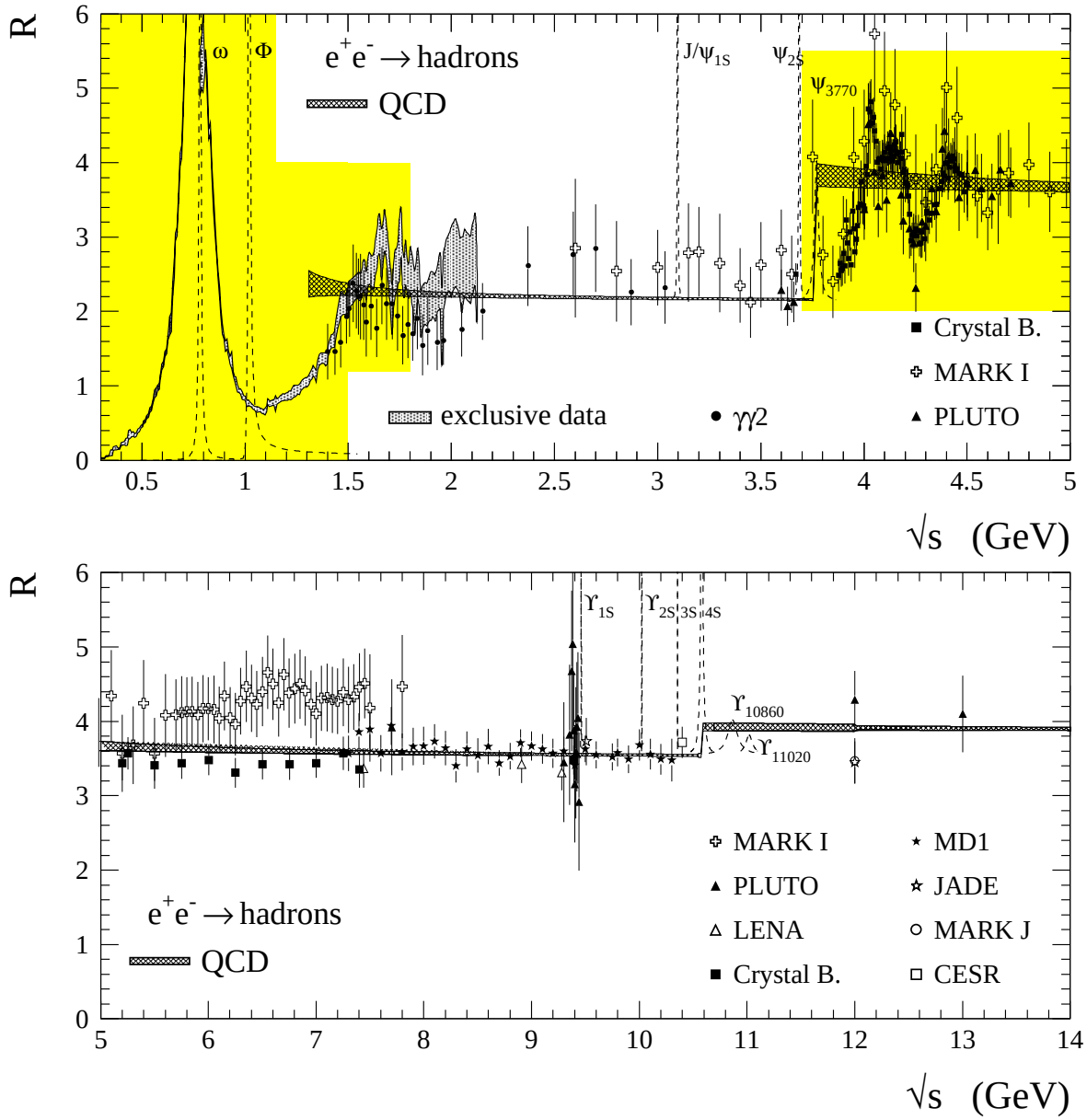

Fig. 65. *Inclusive hadronic cross section ratio in e^+e^- annihilation versus the c.m. energy $\sqrt{s}$. Additionally shown is the QCD prediction of the continuum contribution from Ref. 53 as explained in the text. The shaded areas depict regions where experimental data are used for the evaluation of $\Delta\alpha_{\rm had}(M_Z^2)$ and $a_\mu^{\rm had}$ in addition to the measured narrow resonance parameters. The exclusive e^+e^- cross section measurements at low c.m. energies are taken from DM1, DM2, M2N, M3N, OLYA, CMD, ND, and τ data from ALEPH (see Ref. 56 for detailed information).*

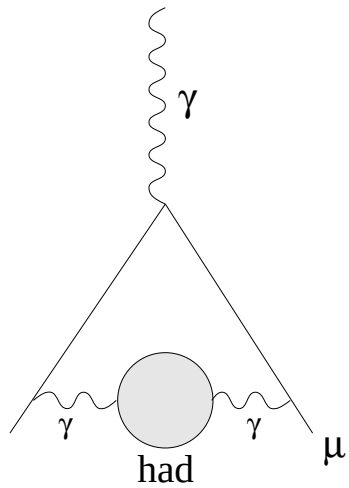

Fig. 66. *Leading order hadronic vacuum polarization contribution to a_μ.*

dispersion integral[117]

$$a_\mu^{\rm had} \;=\; \frac{1}{4\pi^3}\int\limits_{4m_\pi^2}^{\infty} ds\,\sigma_{\rm had}(s)\,K(s). \tag{174}$$

Here, $\sigma_{\rm had}(s)$ is the total $e^+e^-\to$ hadrons cross section as a function of the c.m. energy-squared s, and $K(s)$ denotes the QED kernel[118]

$$K(s) \;=\; x^2\left(2-\frac{x^2}{2}\right)+(1+x)^2\left(1+\frac{1}{x^2}\right)\left(\ln(1+x)-x+\frac{x^2}{2}\right)+\frac{(1+x)}{(1-x)}x^2\ln x, \tag{175}$$

with $x=(1-\beta_\mu)/(1+\beta_\mu)$ and $\beta=(1-4m_\mu^2/s)^{1/2}$ (see also remarks concerning the numerical stability of $K(s)$ in Ref. 71). The function $K(s)$ decreases monotonically with increasing s. It gives a strong weight to the low-energy part of the integral (174). About 91% of the total contribution to $a_\mu^{\rm had}$ is accumulated at c.m. energies $\sqrt{s}$ below 2.1 GeV, and 72% of $a_\mu^{\rm had}$ is covered by the two-pion final state which is dominated by the $\rho(770)$ resonance. The new information provided by the ALEPH two- and four-pion spectral functions can significantly improve the $a_\mu^{\rm had}$ determination.

3.7.3 Running of the Electromagnetic Coupling

In the same spirit we evaluate the hadronic contribution $\Delta\alpha(s)$ to the renormalized vacuum polarization function $\Pi'_\gamma(s)$ which governs the running of the electromagnetic fine structure constant $\alpha(s)$. For the spin 1 photon, $\Pi'_\gamma(s)$ is given

by the Fourier transform of the contraction of the electromagnetic currents $j^\mu_{\rm em}(s)$ in the vacuum $(q^\mu q^\nu - q^2 g^{\mu\nu})\,\Pi'_\gamma(q^2) \;=\; i\int d^4x\, e^{iqx}\langle 0|T(j^\mu_{\rm em}(x) j^\nu_{\rm em}(0))|0\rangle$. With $\Delta\alpha(s)$=$-4\pi\alpha\,{\rm Re}\left[\Pi'_\gamma(s)-\Pi'_\gamma(0)\right]$, one has

$$\alpha(s) \;=\; \frac{\alpha(0)}{1-\Delta\alpha(s)}, \tag{176}$$

where $4\pi\alpha(0)$ is the square of the electron charge in the long-wavelength Thomson limit. The contribution $\Delta\alpha(s)$ can naturally be subdivided into a leptonic and a hadronic part. Furthermore, at $s = M_{\rm Z}^2$ it is appropriate to separate the leading vacuum polarization contribution involving the five light quarks u, d, s, c, b from the top quark contribution since the latter cannot be calculated in the light fermion approximation.

The leading order leptonic contribution is given by

$$\Delta\alpha_{\rm lep}(M_{\rm Z}^2) = \frac{\alpha(0)}{3\pi}\sum_\ell \left(\ln\frac{M_{\rm Z}^2}{m_\ell^2} - \frac{5}{3}\right) \;=\; 314.2\times 10^{-4}. \tag{177}$$

Using analyticity and unitarity, the dispersion integral for the contribution from the light quark hadronic vacuum polarization $\Delta\alpha_{\rm had}(M_{\rm Z}^2)$ reads[119]

$$\Delta\alpha^{(5)}_{\rm had}(M_{\rm Z}^2) \;=\; -\frac{M_{\rm Z}^2}{4\pi^2\,\alpha}\,{\rm Re}\int\limits_{4m_\pi^2}^{\infty} ds\,\frac{\sigma_{\rm had}(s)}{s-M_{\rm Z}^2-i\epsilon}, \tag{178}$$

where $\sigma(s) = 16\pi^2\alpha^2(s)/s\cdot{\rm Im}\Pi'_\gamma(s)$ from the optical theorem and ${\rm Im}\Pi'_\gamma$ stand for the absorptive part of the hadronic vacuum polarization correlator. In contrast to $a_\mu^{\rm had}$, the integration kernel favors cross sections at higher masses. Hence, the improvement when including τ data is expected to be small.

The top quark contribution can be calculated using the next-to-next-to-leading order α_s^3 prediction of the total inclusive cross section ratio R from perturbative QCD[65,71]:

$$R_{\rm pert}(s) = 3\sum_f Q_f^2\left(1-\frac{4m_f^2}{s}\right)^{1/2}\left(1+\frac{2m_f^2}{s}\right)\left[1+\frac{\alpha_s}{\pi}+r_1\left(\frac{\alpha_s}{\pi}\right)^2+r_2\left(\frac{\alpha_s}{\pi}\right)^3\right], \tag{179}$$

where $r_1 = 1.9857-0.1153\,n_f$, $r_2 = -6.6368-1.2001\,n_f-1.2395(\sum_f Q_f)^2/3\sum_f Q_f^2$, and n_f is the number of involved quark flavors. The evaluation of the integral (178) with $m_{\rm top} = 175$ GeV and the running strong coupling constant fixed at $\alpha_s(M_{\rm Z}^2) = 0.121$ yields $\Delta\alpha_{\rm top}(M_{\rm Z}^2) = -0.6\times 10^{-4}$.

3.7.4 Results

Table 8 shows the experimental and theoretical evaluations of $\Delta\alpha_{\rm had}(M_{\rm Z}^2)$, $a_\mu^{\rm had}$, and $a_e^{\rm had}$ for the respective energy regimes[‡]. Experimental errors between different lines are assumed to be uncorrelated, whereas theoretical errors (except those from $c\bar{c}$ and $b\bar{b}$ thresholds, which are quark mass dominated) are added linearly.

According to Table 8, the combination of the theoretical and experimental evaluations of the integrals (178) and (174) yields the results

$$\begin{aligned}
\Delta\alpha_{\rm had}(M_{\rm Z}^2) &= (276.3 \pm 1.1_{\rm (exp.)} \pm 1.1_{\rm (theo.)}) \times 10^{-4}, \\
\alpha^{-1}(M_{\rm Z}^2) &= 128.933 \pm 0.015_{\rm (exp.)} \pm 0.015_{\rm (theo.)}, \\
a_\mu^{\rm had} &= (692.4 \pm 5.6_{\rm (exp.)} \pm 2.6_{\rm (theo.)}) \times 10^{-10}, \\
a_\mu^{\rm SM} &= (11\,659\,159.6 \pm 5.6_{\rm (exp.)} \pm 3.7_{\rm (theo.)}) \times 10^{-10},
\end{aligned} \tag{180}$$

and $a_e^{\rm had} = (187.5 \pm 1.7_{\rm (exp.)} \pm 0.7_{\rm (theo.)}) \times 10^{-14}$ for the leading order hadronic contribution to a_e. The total $a_\mu^{\rm SM}$ value includes an additional contribution from nonleading order hadronic vacuum polarization summarized in Refs. 56 and 120 to be $a_\mu^{\rm had}[(\alpha/\pi)^3] = (-10.0 \pm 0.6)\times 10^{-10}$. Also, the light-by-light scattering (LBLS) contribution has recently been reevaluated to be $a_\mu^{\rm had}[{\rm LBLS}] = (-7.9 \pm 1.5)\times 10^{-10}$ (Ref. 121). Together with the value $a_\mu^{\rm had}[{\rm LBLS}] = (-9.2 \pm 3.2)\times 10^{-10}$ (Ref. 122), we use the average $\langle a_\mu^{\rm had}[{\rm LBLS}]\rangle = (-8.5 \pm 2.5) \times 10^{-10}$, so that the total higher order hadronic correction amounts to $a_\mu^{\rm had}[(\alpha/\pi)^3 + {\rm LBLS}] = (-18.5 \pm 2.6) \times 10^{-10}$. Figures 67 and 68 show a compilation of published results for the hadronic contributions to $\alpha(M_{\rm Z}^2)$ and a_μ. Some authors give the hadronic contribution for the five light quarks only and add the top quark part separately. This has been corrected for in Fig. 67.

3.7.5 Outlook

These results have direct implications for phenomenology and ongoing experimental programs:

- We have seen in the second lecture that most of the sensitivity to the Higgs boson mass originates from the measurements of asymmetries and *in fine* from $(\sin^2\theta_W)_{eff} = \bar{s}^2$. Unfortunately, this approach is limited by the fact

[‡]The evaluation of $a_e^{\rm had}$ follows the same procedure as $a_\mu^{\rm had}$.

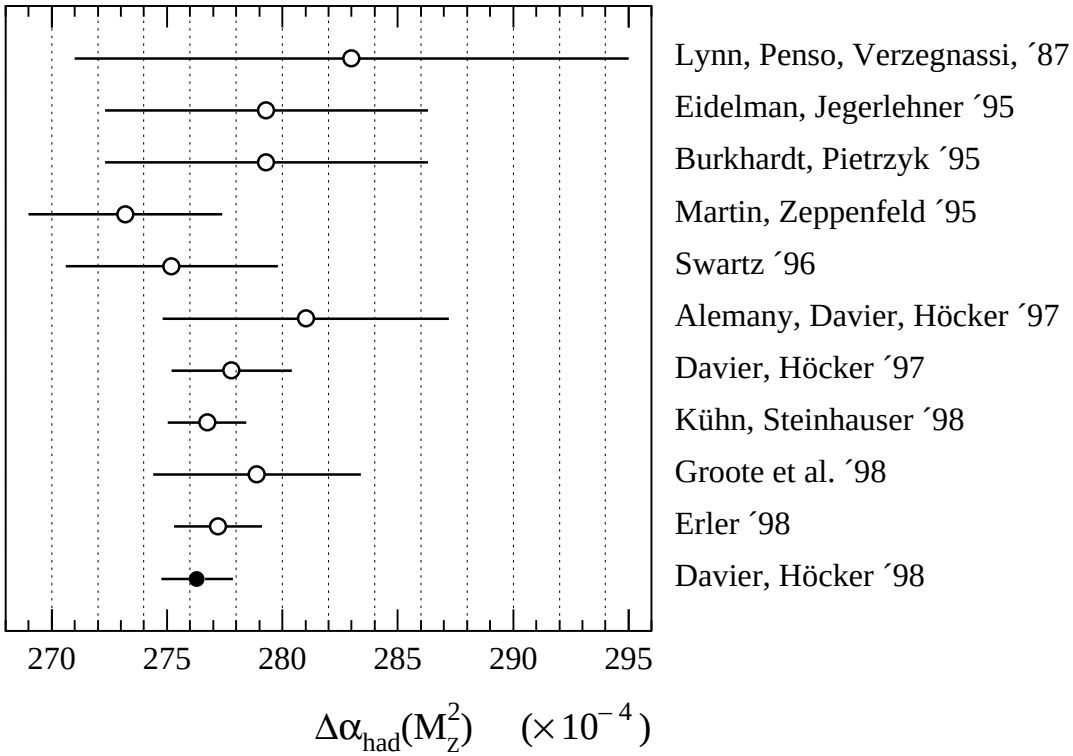

Fig. 67. *Comparison of* $\Delta\alpha_{\rm had}(M_{\rm Z}^2)$ *evaluations. The values are taken from Refs. 54, 55, 57, 72, and 125–130.*

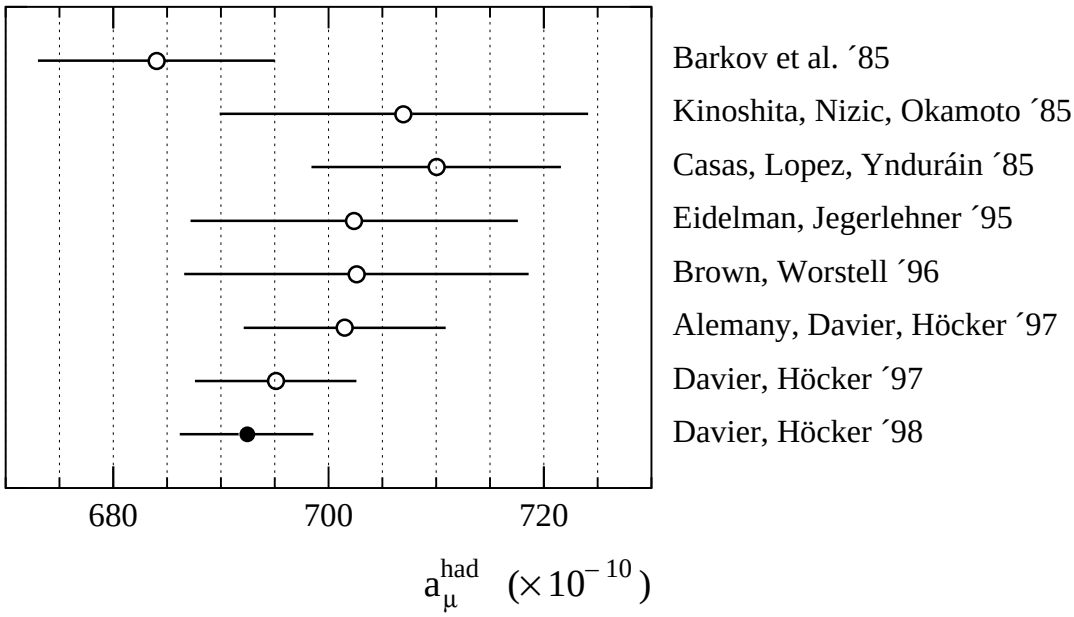

Fig. 68. *Comparison of* $a_\mu^{\rm had}$ *evaluations. The values are taken from Refs. 54, 55, 57, 72, 131–134.*

Energy (GeV)	$\Delta\alpha_{\rm had}(M_{\rm Z}^2) \times 10^4$	$a_\mu^{\rm had} \times 10^{10}$	$a_e^{\rm had} \times 10^{14}$
$(2m_\pi - 1.8)_{uds}$	$56.36 \pm 0.70_{\rm (exp.)} \pm 0.18_{\rm (theo.)}$	$634.3 \pm 5.6_{\rm (exp.)} \pm 2.1_{\rm (theo.)}$	$173.67 \pm 1.7_{\rm (exp.)} \pm 0.6_{\rm (theo.)}$
$(1.8 - 3.700)_{uds}$	$24.53 \pm 0.28_{\rm (theo.)}$	$33.87 \pm 0.46_{\rm (theo.)}$	$8.13 \pm 0.11_{\rm (theo.)}$
$\psi(1S, 2S, 3770)_c$ $+ (3.7 - 5)_{udsc}$	$24.75 \pm 0.84_{\rm (exp.)} \pm 0.50_{\rm (theo.)}$	$14.31 \pm 0.50_{\rm (exp.)} \pm 0.21_{\rm (theo.)}$	$3.41 \pm 0.12_{\rm (exp.)} \pm 0.05_{\rm (theo.)}$
$(5 - 9.3)_{udsc}$	$34.95 \pm 0.29_{\rm (theo.)}$	$6.87 \pm 0.11_{\rm (theo.)}$	$1.62 \pm 0.03_{\rm (theo.)}$
$(9.3 - 12)_{udscb}$	$15.70 \pm 0.28_{\rm (theo.)}$	$1.21 \pm 0.05_{\rm (theo.)}$	$0.28 \pm 0.02_{\rm (theo.)}$
$(12 - \infty)_{udscb}$	$120.68 \pm 0.25_{\rm (theo.)}$	$1.80 \pm 0.01_{\rm (theo.)}$	$0.42 \pm 0.01_{\rm (theo.)}$
$(2m_t - \infty)_t$	$-0.69 \pm 0.06_{\rm (theo.)}$	≈ 0	≈ 0
$(2m_\pi - \infty)_{udscbt}$	$276.3 \pm 1.1_{\rm (exp.)} \pm 1.1_{\rm (theo.)}$	$692.4 \pm 5.6_{\rm (exp.)} \pm 2.6_{\rm (theo.)}$	$187.5 \pm 1.7_{\rm (exp.)} \pm 0.7_{\rm (theo.)}$

Table 8. *Contributions to* $\Delta\alpha_{\rm had}(M_{\rm Z}^2)$*,* $a_\mu^{\rm had}$*, and* $a_e^{\rm had}$ *from the different energy regions. The subscripts in the first column give the quark flavors involved in the calculation.*

that the intrinsic uncertainty on $\alpha(M_{\rm Z}^2)$ in the standard evaluation is at the same level as the experimental accuracy on $\bar{s}^2$, as shown in Table 9. The situation has completely changed with the new determination of $\alpha(M_{\rm Z}^2)$ which does not limit anymore the extraction of the Higgs mass from accurate experimental determinations of $\sin^2\theta_{\rm W}$. As a result, the 95% C.L. upper limit on M_H has decreased from 215 to 202 GeV/c^2, even though the most probable value increased from 66 to 83 GeV/c^2. The improvement in precision is more directly appreciated on the more relevant variable log M_H with M_H in GeV/c^2 (Ref. 55):

$$\log M_H = 1.82^{+0.33}_{-0.40} \qquad [\alpha(M_Z^2) \text{ from Ref. 72}], \tag{181}$$

$$\log M_H = 1.92^{+0.24}_{-0.27} \qquad [\alpha(M_Z^2) \text{ from Ref. 55}]. \tag{182}$$

- The interest in reducing the uncertainty in the hadronic contribution to $a_\mu^{\rm had}$ is directly linked to the possibility of measuring the weak contribution. Let us write down explicitly the different parts as

$$a_\mu^{\rm SM} = a_\mu^{\rm QED} + a_\mu^{\rm had} + a_\mu^{\rm weak}, \tag{183}$$

where $a_\mu^{\rm QED} = (11\,658\,470.6 \pm 0.2) \times 10^{-10}$ is the pure electromagnetic contribution (see Ref. 133 and references therein), $a_\mu^{\rm had}$ is the contribution from

	$\Delta \sin^2\theta_{\rm eff}^{\rm lept}$
Experiment	0.00023
$\alpha(M_{\rm Z}^2)$	$0.00023 \stackrel{\text{this work}}{\Longrightarrow} 0.00005$
m_t	0.00018
Theory	0.00010
$M_{\rm Higgs}$	0.00160 [$M_{\rm Higgs}$ = 60–1000 GeV]

Table 9. *Dominant uncertainties of input values of the Standard Model electroweak fit, expressed in terms of* $\Delta \sin^2\theta_{\rm eff}^{\rm lept}$.

hadronic vacuum polarization, and $a_\mu^{\rm weak} = (15.1 \pm 0.4) \times 10^{-10}$ (Refs. 133–135) accounts for corrections due to the exchange of the weak interacting bosons up to two loops. Note that the one-loop electroweak part of $a_\mu^{\rm SM}$ with the Higgs boson contribution neglected gives $a_\mu^{\rm weak}(1\ {\rm loop}) = 19.5 \times 10^{-10}$. Taking into account fermionic and bosonic two-loop corrections reduces the electroweak contribution to the value given above. The authors of Ref. 136 considered effects from nonzero quark masses and obtained $\Delta a_\mu^{\rm weak}(2\ {\rm loop}) \simeq -(36.9 \pm 2.5) \times 10^{-11}$, which gives $a_\mu^{\rm weak} = 15.8 \times 10^{-10}$. The present value from the combined μ^+ and μ^- measurements,[137]

$$a_\mu \;=\; (11\,659\,230 \pm 85) \times 10^{-10}\ , \tag{184}$$

should be improved to a precision of at least 4×10^{-10} by a forthcoming Brookhaven experiment (BNL-E821) (Ref. 138), well below the expected weak contribution. Such a program makes sense only if the uncertainty on the hadronic term is made sufficiently small. The improvements described above represent a significant step in this direction.

3.8 Are τ Decays Standard?

For many years, several nagging problems were casting doubts on our understanding of the τ decays within the Standard Model. A recurrent pathology was the so-called "missing one-prong decay" problem. Then appeared some persistent in-

dication of a violation of universality. Both problems were rooted in experimental systematic effects and they have now disappeared thanks to precise and reliable data. In particular, the ALEPH Collaboration has measured all the important exclusive modes[61,139] and shown them to be in good agreement with the standard phenomenology.

Indeed, it is possible to describe phenomenologically the τ decay modes starting from the following ingredients:

- the measurement of τ_τ providing the total τ width;
- the universality of the $Wl\bar{\nu}_l$ couplings;
- the isospin invariance of the vector currents (CVC): hadron production through the vector coupling to W is identical to that observed in e^+e^- annihilation through the $I = 1$ electromagnetic current;
- the equality between the hadronic vector and axial-vector counterparts, slightly broken by a small QCD nonperturbative contribution;
- the Cabibbo angle and an estimate of the $SU(3)_{flavor}$ symmetry breaking, in order to compute the strange modes.

In practice, the calculation is limited by the accuracy of e^+e^- data for the modes $\tau \to \nu_\tau \pi\pi^0$ and $\nu_\tau 3\pi\pi^0$, and consequently, for the axial modes. Nevertheless, the comparison between the measured branching ratios and the calculated ones shows a good level of consistency and no significant deviation, as can be seen in Table 10.

By construction, the measured branching fractions add up to one, while this is not guaranteed for the predictions because the widths for the modes are estimated independently and turned into branching ratios through the τ total width. The theory sum is therefore a test of the global consistency of the standard description. The value obtained

$$\sum_i B_i^{standard} = (9813 \pm (41)_{\tau_\tau} \pm (156)_{e^+e^-} \pm (28)_{SU(3)} \pm (50)_{QCD})\ 10^{-4} \qquad (185)$$

is compatible with 1 within a precision of 2% dominated by uncertainties from e^+e^- data.

Within the present experimental accuracy, the τ lepton decays according to the Standard Model.

$B_X(10^{-4})$	modes $\tau \to \nu_\tau$ X	Standard Model
	ALEPH	$+ \tau_\tau$
X	* + other exp.	$+ e^+e^-$ data
e $\bar{\nu}_e$	1779 (7)*	1778 (7)
$\mu\bar{\nu}_\mu$	1732 (8)*	1729 (7)
π	1123 (16)	1090 (5)
$\pi\pi^0$	2534 (19)	2467 (70)
$\pi 3\pi^0$	118 (14)	107 (5)
$3\pi\pi^0$	418 (12)	420 (30)
6π	4 (2)	13 (2)
$\pi\pi\eta$	17 (3)*	13 (2)
$\bar{K}K^0$	19 (4)	15 (3)
$\pi\omega(\to \pi\gamma)$	17 (2)	17 (5)
$\bar{K}K\pi(V)$	21 (11)	16 (16)
$\bar{K}K\pi\pi(V)$	8 (8)	20 (20)
$A(3\pi, 5\pi, \bar{K}K\pi)$	1933 (25)	1834 (86)
$\bar{K}$	69 (3)	73 (1)
$\bar{K}\pi$	127 (9)	120 (12)
$\bar{K}\pi\pi$	67 (10)	81 (20)
$\bar{K}\pi\pi\pi$	11 (10)	20 (20)
Sum	10 000	9813 $\pm$ 171

Table 10. *Branching ratios of the τ lepton and Standard Model predictions. The labels V, A correspond to final states obtained through the vector and axial-vector currents, respectively.*

Conclusion

We have witnessed in recent years an avalanche of new and precise results in particle physics. Mostly thanks to the democratic character of e^+e^- annihilation and the generosity of the Z boson, properties of leptons have been studied with great accuracy. The net result is somewhat disappointing as the Standard Theory is still undisputed and many of the old questions remain unanswered. Nevertheless, much progress has been achieved. The number of quark and lepton families has profound consequences for particle physics and cosmology. The agreement between the indirect and direct determinations of the top quark mass is a test of the electroweak theory at the level of its quantum fluctuations. Starting from almost nowhere, the mass of the Higgs boson is found to lie in a band close to the W and Z masses. Finally, much progress has been achieved in testing QCD, especially in the transition region between the hadrons and the asymptotic regime, thanks to our universal τ lepton.

Acknowledgments

I wish to thank my friends at SLAC for their warm hospitality and for the perfect atmosphere created at the Summer Institute. A special thought to David Leith who invested much to make this School so unique.

References

[1] L. Michel, Proc. Phys. Soc. A **63**, 514 (1950).

[2] W. Fetscher, Phys. Lett. B **140**, 117 (1984);
J. Carr *et al.*, Phys. Rev. Lett. **51**, 627 (1983).

[3] CHARM II Collaboration, D. Geiregat *et al.*, Phys. Lett. B **247**, 131 (1990).

[4] S. Derenzo, Phys. Rev. **181**, 1854 (1969);
J. Carr *et al.*, Phys. Rev. Lett. **51**, 627 (1983);
H. Burkard *et al.*, Phys. Lett. B **150**, 242 (1985);
H. Burkard *et al.*, Phys. Lett. B **160**, 343 (1985).

[5] W. Fetscher *et al.*, Phys. Lett. B **173**, 102 (1986).

[6] M. Davier, L. Duflot, F. LeDiberder, and A. Rougé, Phys. Lett. B **306**, 411 (1993).

[7] ALEPH Collaboration, D. Buskulic *et al.*, Phys. Lett. B **346**, 379 (1995).

[8] CLEO Collaboration, J. P. Alexander *et al.*, Phys. Rev. D **56**, 5320 (1997).

[9] ARGUS Collaboration, H. Albrecht *et al.*, Z. Phys. C **58**, 61 (1993); ARGUS Collaboration, H. Albrecht *et al.*, Phys. Lett. B **349**, 576 (1995).

[10] Particle Data Group, R. M. Barnett *et al.*, Phys. Rev. D **54**, 1 (1996).

[11] M. A. B. Bég, R. V. Budny, R. Mohapatra, and A. Sirlin, Phys. Rev. Lett. **38**, 1252 (1977).

[12] ARGUS Collaboration, H. Albrecht *et al.*, Phys. Lett. B **337**, 383 (1994); ARGUS Collaboration, H. Albrecht *et al.*, Phys. Lett. B **341**, 441 (1995).

[13] CLEO Collaboration, R. Ammar *et al.*, Phys. Rev. Lett **78**, 4686 (1997).

[14] L3 Collaboration, M. Acciari *et al.*, Phys. Lett. B **377**, 313 (1996).

[15] W. Marciano and A. Sirlin, Phys. Rev. Lett. **61**, 1815 (1988).

[16] W. Marciano and A. Sirlin, Phys. Rev. Lett. **71**, 3629 (1993); R. Decker and M. Finkemeier, Phys. Lett. B **334**, 199 (1994).

[17] BES Collaboration, J. Z. Bai *et al.*, Phys. Rev. D **53**, 20 (1996).

[18] DELCO Collaboration, W. Bacino *et al.*, Phys. Rev. Lett. **41**, 13 (1978).

[19] ARGUS Collaboration, H. Albrecht *et al.*, Phys. Lett. B **292**, 221 (1992); CLEO Collaboration, R. Balest *et al.*, Phys. Rev. **47**, R3671 (1993).

[20] ALEPH Collaboration, D. Buskulic *et al.*, Phys. Lett. B **297**, 432 (1992); DELPHI Collaboration, P. Abreu *et al.*, Phys. Lett. B **302**, 356 (1993).

[21] ALEPH Collaboration, D. Décamp *et al.*, Phys. Lett. B **279**, 411 (1992).

[22] ALEPH Collaboration, R. Barate *et al.*, Z. Phys. C **74**, 387 (1997).

[23] Y. S. Tsai and A. C. Hearn, Phys. Rev. **140**, 721 (1965).

[24] ALEPH Collaboration, R. Barate *et al.*, Phys. Lett. B **414**, 362 (1997).

[25] P. Weber, Nucl. Phys. B (Proc. Suppl. C) **55**, 107 (1997).

[26] M. Davier, Nucl. Phys. B (Proc. Suppl. C) **40**, 395 (1995).

[27] G. Czapek *et al.*, Phys. Rev. Lett. **70**, 17 (1993).

[28] D. I. Britton *et al.*, Phys. Rev. D **49**, 28 (1994).

[29] P. Chankowski, R. Hempfling, and S. Pokorski, Phys. Lett. B **333**, 403 (1994).

[30] CDF Collaboration, F. Abe *et al.*, Phys. Rev. Lett. **79**, 357 (1997).

[31] S. L. Glashow, Nucl. Phys. **22**, 579 (1961);
S. Weinberg, Phys. Rev. Lett. **19**, 1264 (1967);
A. Salam, in *Proceedings of the Eighth Nobel Symposium*, edited by N. Svartholm (Wiley Interscience, N.Y., 1968), p. 367.

[32] J. Alitti *et al.*, UA2 Collaboration, Phys. Lett. B **276**, 354 (1992).

[33] J. V. Allaby *et al.*, CHARM Collaboration, Z. Phys. C **36**, 611 (1987);
A. Blondel *et al.*, CDHS Collaboration, Z. Phys. C **45**, 361 (1990).

[34] A. Sirlin, Phys. Rev. D **22**, 971 (1980);
W. J. Marciano and A. Sirlin, Phys. Rev. D **22**, 2695 (1980); D **29**, 75 and 945 (1984).

[35] N. Cabibbo and R. Gatto, Phys. Rev. **124**, 1577 (1961);
F. A. Berends and G. J. Kommen, Phys. Lett. B **63**, 432 (1976).

[36] M. Veltman, Nucl. Phys. B **123**, 89 (1977).

[37] M. Consoli and W. Hollik, "Physics at LEP," edited by G. Altarelli, R. Kleiss, and C. Verzegnassi, CERN 89-08 (Sept. 1989) and references therein.

[38] "A combination of preliminary LEP and SLD electroweak measurements and constraints on the Standard Model," CERN PPE/97-154 (1997).

[39] K. Assamagan *et al.*, Phys. Rev. D **53**, 6065 (1996).

[40] ALEPH Collaboration, Phys. Lett. B **349**, 585 (1995);
EPJ C **2**, 3, 395 (1998).

[41] R. Cowsik and J. McClelland, Phys. Rev. Lett. **29**, 669 (1972).

[42] C. Albajar *et al.*, UA1 Collaboration, Phys. Lett. B **198**, 271 (1987);
R. Ansari *et al.*, UA2 Collaboration, Phys. Lett. B **186**, 440 (1987).

[43] W. Ford *et al.*, MAC Collaboration, Phys. Rev. D **33**, 3472 (1986);
C. Hearty *et al.*, ASP Collaboration, Phys. Rev. Lett. **58**, 1711 (1987);
H. J. Behrend *et al.*, CELLO Collaboration, Phys. Lett. B **215**, 186 (1988).

[44] G. Steigman *et al.*, Phys. Lett. B **176**, 33 (1986);
J. Ellis *et al.*, Phys. Lett. B **167**, 457 (1986).

[45] G. Danby *et al.*, Phys. Rev. Lett. **9**, 36 (1962).

[46] K. Abe *et al.*, SLD Collaboration, Phys. Rev. Lett. **73**, 25 (1994).

[47] K. Abe *et al.*, SLD Collaboration, Phys. Rev. Lett **78**, 2075 (1997).

[48] G. Crawford, *Rencontres de Moriond* (March 1998).

[49] D. Abbaneo, *Rencontres de Moriond* (March 1998).

[50] M. Davier, *Rencontres de Moriond* (March 1998).

[51] M. Jones, *Rencontres de Moriond* (March 1998).

[52] G. Degrassi *et al.*, Phys. Lett B **418**, 209 (1998).

[53] M. Davier and A. Höcker, Phys. Lett. B **419**, 419 (1998).

[54] M. Davier and A. Höcker, "New results on the hadronic contributions to $\alpha(M_Z^2)$ and $(g-2)_\mu$," Report LAL 98-38 (May 1998).

[55] C. Paus (LEPEWWG), private communication (1998).

[56] R. Alemany, M. Davier, and A. Höcker, Europ. Phys. J. C **2**, 123 (1998).

[57] E. Braaten, S. Narison, and A. Pich, Nucl. Phys. B **373**, 581 (1992).

[58] A. Pich, Nucl. Phys. B **39**, 326 (Proc. Suppl.) (1995).

[59] R. Barate *et al.* (ALEPH Collaboration), Z. Phys. C **76**, 15 (1997).

[60] R. Barate *et al.* (ALEPH Collaboration), Report CERN PPE/98-012 (1998), to be published in Europ. Phys. J.

[61] D. Buskulic *et al.* (ALEPH Collaboration), Z. Phys. C **70**, 579 (1996).

[62] D. Buskulic *et al.* (ALEPH Collaboration), Z. Phys. C **74**, 263 (1997).

[63] P. L. Campana (for the ALEPH Collaboration), "Branching fractions for modes involving kaons," talk given at the TAU'96 Conference, Colorado (1996).

[64] H. Albrecht *et al.* (ARGUS Collaboration), Phys. Lett. B **185**, 223 (1987).

[65] L. R. Surguladze and M. A. Samuel, Phys. Rev. Lett. **66**, 560 (1991);
S. G. Gorishny, A. L. Kataev, and S. A. Larin, Phys. Lett. B **259**, 144 (1991).

[66] A. Pais, Ann. Phys. **9**, 548 (1960).

[67] J. H. Kühn and A. Santamaria, Z. Phys. C **48**, 445 (1990).

[68] A. Dobado, M. J. Herrero, and T. N. Truong, Phys. Lett. B **235**, 134 (1990).

[69] G. J. Gounaris and J. J. Sakurai, Phys. Rev. Lett. **21**, 244 (1968).

[70] J. Gasser and U. G. Meissner, Nucl. Phys. B **357**, 90 (1991).

[71] S. Eidelman and F. Jegerlehner, Z. Phys. C **67**, 585 (1995).

[72] K. Huber and H. Neufeld, Phys. Lett. B **357**, 221 (1995).

[73] J. Gasser and H. Leutwyler, Phys. Rep. **87**, 77 (1982).

[74] L. P. Chen and W. Dunwoodie (for the MARK III Collaboration), in *Proceedings of Hadron-91* (World Scientific, 1992), p. 100.

[75] J. Bijnens and P. Gosdzinsky, Phys. Lett. B **388**, 203 (1996).

[76] T. Das, V. S. Mathur, and S. Okubo, Phys. Rev. Lett. **19**, 895 (1967).

[77] S. R. Amendolia *et al.* (NA7 Collaboration), Nucl. Phys. B **277**, 168 (1986).

[78] S. Weinberg, Phys. Rev. Lett. **18**, 507 (1967).

[79] T. Das, G. S. Guralnik, V. S. Mathur, F. E. Low, and J. E. Young, Phys. Rev. Lett. **18**, 759 (1967).

[80] J. F. Donoghue and E. Golowich, Phys. Rev. D **49**, 1513 (1994).

[81] E. Braaten, Phys. Rev. Lett. **60**, 1606 (1988).

[82] S. Narison and A. Pich, Phys. Lett. B **211**, 183 (1988).

[83] E. Braaten and C. S. Li, Phys. Rev. D **42**, 3888 (1990).

[84] K. G. Wilson, Phys. Rev. **179**, 1499 (1969).

[85] F. Le Diberder and A. Pich, Phys. Lett. B **286**, 147 (1992).

[86] K. G. Chetyrkin and A. Kwiatkowski, Z. Phys. C **59**, 525 (1993).

[87] S. A. Larin, T. van Ritbergen, and J. A. M. Vermaseren, Phys. Lett. B **400**, 379 (1997).

[88] A. A. Pivovarov, Sov. J. Nucl. Phys. **54**, 676 (1991).

[89] M. A. Shifman, A. L. Vainshtein, and V. I. Zakharov, Nucl. Phys. B **147**, 385, 448, 519 (1979).

[90] C. Becchi, S. Narison, E. de Rafael, and F. J. Yndurain, Z. Phys. C **8**, 335 (1981);
D. J. Broadhurst, Phys. Lett. B **101**, 423 (1981);
S. C. Generalis, J. Phys. G **15**, L225 (1989).

[91] D. J. Broadhurst and S. C. Generalis, Phys. Lett. **165**, 175 (1985).

[92] F. Le Diberder and A. Pich, Phys. Lett. B **289**, 165 (1992).

[93] M. Davier, Nucl. Phys. B (Proc. Suppl. C) **55**, 395 (1997).

[94] S. M. Chen, in *Proceedings of the QCD97 Conference* (Montpellier, July 1997).

[95] A. L. Kataev and V. V. Starshenko, Mod. Phys. Lett. A **10**, 235 (1995); Nucl. Phys. B **39**, 312 (Proc. Suppl.) (1995).

[96] P. M. Stevenson, Phys. Rev. D **23**, 2916 (1981).

[97] F. Le Diberder, Nucl. Phys. B **39**, 318 (Proc. Suppl.) (1995).

[98] A. L. Kataev (private communication).

[99] P. A. Rączka, Phys. Rev. D **57**, 6862 (1998).

[100] G. Grunberg, Report CPTH-PC510-0597 (1997).

[101] G. Altarelli, P. Nason, and G. Ridolfi, Z. Phys. C **68**, 257 (1995).

[102] M. Beneke and V. M. Braun, Phys. Lett. B **348**, 513 (1995); P. Ball, M. Beneke, and V. M. Braun, Nucl. Phys. B **452**, 563 (1995).

[103] M. Neubert, Report CERN-TH-7524-94 (1994); Nucl. Phys. B **463**, 511 (1996).

[104] C. N. Lovett-Turner and C. J. Maxwell, Nucl. Phys. B **452**, 188 (1995).

[105] C. J. Maxwell and D. G. Tonge, Nucl. Phys. B **481** (1996); Report DTP-97-30 (1997).

[106] D. Buskulic *et al.* (ALEPH Collaboration), Phys. Lett. B **307**, 209 (1993).

[107] K. G. Chetyrkin, B. A. Kniehl, and M. Steinhauser, Phys. Rev. Lett. **79**, 2184 (1997).

[108] K. G. Chetyrkin, B. A. Kniehl, and M. Steinhauser, Nucl. Phys. B **510**, 61 (1998).

[109] W. Bernreuther and W. Wetzel, Nucl. Phys. B **197**, 228 (1982);
W. Wetzel, Nucl. Phys. B **196**, 259 (1982);
W. Bernreuther, talk given at the Workshop on QCD at LEP, Aachen, Germany 1994, PITHA-94-31 (1994).

[110] G. Rodrigo, A. Pich, and A. Santamaria, Phys. Lett. B **424**, 367 (1998).

[111] D. Reid, *Rencontres de Moriond* (March 1998).

[112] S. Groote, J. G. Körner, N. F. Nasrallah, and K. Schilcher, "QCD Sum Rule Determination of $\alpha(M_{\rm Z})$ with Minimal Data Input," Report MZ-TH-98-02 (1998).

[113] C. Bacci *et al.* ($\gamma\gamma 2$ Collaboration), Phys. Lett. B **86**, 234 (1979).

[114] J. L. Siegrist *et al.* (MARK I Collaboration), Phys. Rev. D **26**, 969 (1982).

[115] Z. Jakubowski *et al.* (Crystal Ball Collaboration), Z. Phys. C **40**, 49 (1988); C. Edwards *et al.* (Crystal Ball Collaboration), SLAC-PUB-5160 (1990).

[116] A. E. Blinov *et al.* (MD-1 Collaboration), Z. Phys. C **49**, 239 (1991); A. E. Blinov *et al.* (MD-1 Collaboration), Z. Phys. C **70**, 31 (1996).

[117] M. Gourdin and E. de Rafael, Nucl. Phys. B **10**, 667 (1969).

[118] S. J. Brodsky and E. de Rafael, Phys. Rev. **168**, 1620 (1968).

[119] N. Cabibbo and R. Gatto, Phys. Rev. Lett. **4**, 313 (1960); Phys. Rev. **124**, 1577 (1961).

[120] B. Krause, Phys. Lett. B **390**, 392 (1997).

[121] M. Hayakawa and T. Kinoshita, Phys. Rev. D **57**, 465 (1998).

[122] J. Bijnens, E. Pallante, and J. Prades, Nucl. Phys. B **474**, 379 (1996).

[123] B. W. Lynn, G. Penso, and C. Verzegnassi, Phys. Rev. D **35**, 42 (1987).

[124] H. Burkhardt and B. Pietrzyk, Phys. Lett. B **356**, 398 (1995).

[125] A. D. Martin and D. Zeppenfeld, Phys. Lett. B **345**, 558 (1995).

[126] M. L. Swartz, Phys. Rev. D **53**, 5268 (1996).

[127] J. H. Kühn and M. Steinhauser, "A theory driven analysis of the effective QED coupling at $M_{\rm Z}$," MPI-PHT-98-12 (1998).

[128] J. Erler, "$\overline{\rm MS}$ Scheme Calculation of the QED Coupling $\hat{\alpha}(M_Z)$," UPR-796-T, 1998.

[129] L. M. Barkov *et al.* (OLYA, CMD Collaboration), Nucl. Phys. B **256**, 365 (1985).

[130] T. Kinoshita, B. Nižić, and Y. Okamoto, Phys. Rev. D **31**, 2108 (1985).

[131] J. A. Casas, C. López, and F. J. Ynduráin, Phys. Rev. D **32**, 736 (1985).

[132] D. H. Brown and W. A. Worstell, Phys. Rev. D **54**, 3237 (1996).

[133] A. Czarnecki, B. Krause, and W. J. Marciano, Phys. Rev. Lett. **76**, 3267 (1995); Phys. Rev. D **52**, 2619 (1995).

[134] T. V. Kukhto, E. A. Kuraev, A. Schiller, and Z. K. Silagadze, Nucl. Phys. B **371**, 567 (1992).

[135] R. Jackiw and S. Weinberg, Phys. Rev. D **5**, 2473 (1972).

[136] S. Peris, M. Perrottet, and E. de Rafael, Phys. Lett. B **355**, 523 (1995).

[137] J. Bailey *et al.*, Phys. Lett. B **68**, 191 (1977).
F. J. M. Farley and E. Picasso, "The muon $(g-2)$ experiments," advanced series on directions in high-energy physics–Vol. 7, *Quantum Electrodynamics*, edited by T. Kinoshita (World Scientific, 1990).

[138] B. Lee Roberts, Z. Phys. C **56**, 101 (Proc. Suppl.) (1992).
See, also, "http://www.phy.bnl.gov/g2muon/home.html".

[139] D. Buskulic *et al.* (ALEPH Collaboration), Z. Phys. C **70**, 561 (1996).